CALCIUM PHOSPHATE GLASSES AND GLASS-CERAMICS FOR MEDICAL APPLICATIONS

François de Mestral, B. Eng.

A Thesis Submitted to the Faculty of Graduate Studies and Research as Partial Fulfilment of the Requirements for the Degree of Master of Engineering.

Department of Mining and Metallurgical Engineering
McGill University
MONTREAL, Que.
CANADA

June 1986

UNIVERSITÉ McGILL

FACULTÉ DES ÉTUDES AVANCÉES ET DE LA RECHERCHE

Date _____

NOM DE L'AUTEUR: _____

DÉPARTEMENT: _____ GRADE: _____

TITRE DE LA THÈSE: _____

_____

_____

1. Par la présente, l'auteur accorde à l'université McGill l'autorisation de mettre cette thèse à la disposition des lecteurs dans une bibliothèque de McGill ou une autre bibliothèque, soit sous sa forme actuelle, soit sous forme d'une réproduction. L'auteur détient cependant les autres droits de publications. Il est entendu, par ailleurs, que ni la thèse, ni les longs extraits de cette thèse ne pourront être imprimés ou reproduits par d'autres moyens sans l'autorisation écrite de l'auteur.

2. La présente autorisation entre en vigueur à la date indiquée ci-dessus à moins que le Comité exécutif du conseil n'ait voté de différer cette date. Dans ce cas, la date différée sera le _____

_____

Signature de l'auteur

Adresse permanente:

_____

_____

_____

_____

Signature du doyen si une date figure à l'alinéa 2.

(English on reverse)

TABLE OF CONTENTS

ENGLISH ABSTRACT ---------- iv

RESUME FRANCAIS ---------- v

LIST OF FIGURES ---------- vi

LIST OF TABLES ---------- ix

ACKNOWLEDGEMENTS ---------- xi

CHAPTER 1. INTRODUCTION ---------- 1

1.1 Biomaterials ---------- 2

1.2 Objectives of the Study ---------- 4

CHAPTER 2. BIOMATERIALS AND THEIR DRAWBACKS ---------- 5

2.1 Selection Criteria ---------- 6
2.1.1 Medical Criteria ---------- 6
2.1.2 Mechanical Criteria ---------- 7

2.2 Current Biomaterials ---------- 13
2.2.1 Metallic Alloys ---------- 13
2.2.2 Polymers ---------- 15
2.2.3 Bone Cement ---------- 16
2.2.4 Ceramics ---------- 18

CHAPTER 3. CALCIUM PHOSPHATE CERAMICS ---------- 24

3.1 Calcium Phosphate Ceramics ---------- 25
3.1.1 Properties of Calcium Phosphate Ceramics ---------- 27

3.2 Calcium Phosphate Glass-Ceramics ---------- 29
3.2.1 Crystallization Behavior above T_g ---------- 29
3.2.2 Crystallization Behavior below T_g ---------- 30
3.2.3 Unidirectional Crystallization ---------- 33

CHAPTER 4. MATERIAL AND EXPERIMENTAL PROCEDURE ---------- 35

4.1 Starting Materials ---------- 36
4.1.1 Calcium Phosphate Powder ---------- 36
4.1.2 Additive Powders ---------- 37

4.2 Sample Preparation ---------- 39
4.2.1 Drying and Melting ---------- 39
4.2.2 Casting ---------- 41

4.3 Differential Scanning Calorimetry ---------- 46

4.4 Crystallization ---------- 48
4.4.1 Unidirectional Crystallization ------- 49

4.5 Ceramography ---------- 51

4.6 Strength Measurements ---------- 53
4.4.1 Flexural Strength ---------- 53
4.4.2 Statistical Treatement of Data ------- 55

4.7 Fracture Toughness Measurements ---------- 58
4.5.1 Vickers Indentation Technique -------- 58
4.5.2 Single Edge Notched Beam Technique --- 61

4.8 Tribological Study ---------- 63

CHAPTER 5. RESULTS AND DISCUSSION ---------- 66

5.1 Crystallization ---------- 67
5.1.1 DSC Study ---------- 67
5.1.2 Random Crystallization ---------- 76
5.1.3 Unidirectional Crystallization -------- 84

5.2 Glass and Glass-Ceramic Strength ---------- 88
5.2.1 Glass Strength ---------- 88
5.2.2 Glass-Ceramic Strength ---------- 93
5.2.3 Bulk Nucleated Glass-Ceramics --------- 96
5.2.4 Strengthening Agent ---------- 100

5.3 Fracture Toughness ---------- 105
5.3.1 Indentation Technique ---------- 105
5.3.2 Notched Beam Technique ---------- 112

5.4 Tribological Study ---------- 115

CHAPTER 6. CONCLUSIONS ---------- 118

6.1 Calcium Phosphate Glass-Ceramics ---------- 119

6.2 Calcium Phophate Glasses ---------- 120

CHAPTER 7. SUGGESTIONS FOR FURTHER WORK ---------- 122

REFERENCES ---------- 125

APPENDIX 1 ---------- 129

Abstract

Despite their excellent biocompatibility, the use of calcium phosphate ceramics and glass-ceramics in the medical area is limited to non-load bearing applications because of their poor mechanical properties.

The poor strength of the glass-ceramic ($CaO/P_2O_5 = 1$), e.g. 70 MPa, arises from the fact that only surface nucleation takes place thus generating a fibrous structure perpendicular to the surface. Three types of glasses and glass-ceramics were studied: a) pure calcium phosphate, randomly and unidirectionally crystallized, b) calcium phosphate with additions of a nucleating agent (ZrO_2), and c) calcium phosphate with additions of a strengthening agent (Al_2O_3).

Unidirectional crystallization is an effective strengthening mechanism typically increasing the flexural strength by up to 600 %. However, the slow rate of crystallization as well as the sensitivity of the process to experimental conditions may limit its commercial applicability. Small additions of the nucleating agent, ZrO_2, enables bulk rather than surface nucleation to be achieved. However, the strength of the glass-ceramic is not improved. Additions of the strengthening agent, Al_2O_3, increases the fracture toughness of the glass significantly, e.g. by 70 %, but does not affect the strength of the glass-ceramic.

Calcium phosphate glasses seem to be more promising biomaterials than the glass-ceramics, since they exhibited superior mechanical properties.

Résumé

Malgré l'excellente biocompatibilité des céramiques à base de phosphate de calcium, leur usage dans des applications médicales impliquant des contraintes élevées est resté limité en raison de leur manque de résistance mécanique.

La faible résistance à la flexion (70 MPa) du verre-céramique (rapport molaire CaO/P_2O_5=1) est dû au mode de cristallisation. En effet, les germes ne se développant qu'en surface, les cristaux croissent vers le centre de l'éprouvette, créant ainsi une structure fibreuse hautement anisotropique. Trois techniques de renforcement de ce matériau ont été étudiées: a) par croissance unidirectionnelle des cristaux, b) par l'addition d'un agent de germination (ZrO_2), et c) par l'addition d'un agent modificateur de réseau (Al_2O_3).

La cristallisation unidirectionnelle augmente la résistance à la flexion d'environ 600%. Toutefois, ce procédé n'aurait que des applications industrielles limitées, puisque très lent et d'une mise en oeuvre difficile. Bien que favorisant la formation de germes à l'intérieur du materiau, l'oxyde de zircone n'augmente pas sa résistance à la flexion. Si l'addition d'oxyde d'aluminium augmente la ténacite à la rupture du verre, il n'influence que peu les propriétés du verre-céramique.

De manière générale, les propriétés du verre sont supérieures à celles du verre-céramique; il est donc possible de conclure que ce verre semble être un biomateriau prometteur.

LIST OF FIGURES

Figure 1:	Total hip prosthesis with a metallic femoral part and a high density polyethylene pelvic part [13].	8
Figure 2:	a: Fixation plate used to stabilize a femoral fracture. b: Bone resorption (arrow) at the previous location of the fixation plate [12].	9
Figure 3:	Femoral part of an alumina hip prosthesis designed to minimize bending moments [30].	19
Figure 4:	$CaO-P_2O_5$ system phase diagram.	26
Figure 5:	Temperature range where unidirectional crystallization can occur [32].	34
Figure 6:	DSC curve showing the water dissociation behavior for the calcium phosphate powder.	37
Figure 7:	Four-point bend specimen and the boron nitride mold.	43
Figure 8:	Sample for fracture toughness measurements using the notched beam technique.	45
Figure 9:	Example of a DSC plot determinig the glass transition and the crystallization peak temperatures.	47
Figure 10:	Apparatus designed for unidirectional crystallization.	49
Figure 11:	Temperature profile in the tube furnace for different hot zone temperatures.	50
Figure 12:	Microstructure of a calcium phosphate glass-ceramic obtained by alumina polishing.	52
Figure 13:	Stress distribution in a a) 3-point bending specimen, b) 4-point-bending specimen, and c) tensile specimen.	55
Figure 14:	Vickers indentation technique a) crack length at the indentation corners, b) half penny like crack.	59
Figure 15:	Test configuration for the fracture toughness determination using a single edge notched beam.	62

Figure 16: Schematic of a rotating pin on reciprocating plate wear apparatus. 64

Figure 17: Arrhenius plot for the determination of the crystallization activation energy of calcium phosphate glass above T_g. 71

Figure 18: Nucleation rate versus temperature curves: a) ideal situation [43] b) case of 1% ZrO_2 calcium phosphate glass. 75

Figure 19: Surface nucleation in calcium phosphate glass, with fan-like crystals around the nucleation centre. 77

Figure 20: Calcium phosphate glass-ceramic showing large fan-like crystals due to a small number of nuclei. 78

Figure 21: Calcium phosphate glass ceramic showing crystal bundles growing towards the centre of the specimen arising from a large number of nuclei. 79

Figure 22: Calcium phosphate crystal fibrils grown at 570 °C for 15 hours. 80

Figure 23: Crystal fibres arising from one nucleus crossing the complete section of a four point bending sample. 81

Figure 24: Calcium phosphate crystals grown at 650 °C showing extensive inter-needle porosity. 82

Figure 25: Calcium phosphate crystal fibre grown at 650 °C interrupted by porosity. 83

Figure 26: Fracture surface of an unidirectional fibre. The axis of growth is perpandicular to the surface. 85

Figure 27: Little fibrils growing parallel one another. The axis of growth is in the plane of the page. 85

Figure 28: Particle size distribution of silica sand used for sandblasting specimens. 89

Figure 29: Weibull moduli determination for the a) annealed specimens and b) annealed + sand-blasted specimens. 90

Figure 30: Fracture surface of a calcium phosphate glass-ceramic bending specimen showing the interfibre fracture behavior. 9,

Figure 31: Crack progressing perpadicular to the fibre axis in a calcium phosphate glass-ceramic crystallized at 650¢°C. 95

Figure 32: Characteristic fibrous structure of surface nucleation in pure calcium phosphate glass. 96

Figure 33: Addition of 1% zirconia enhanced bulk rather than surface nucleation (fracture surface). 97

Figure 34: 1% zirconia calcium phosphate glass showing a glassy layer on the crystallization defect surface (fracture surface). 97

Figure 35: 1% zirconia calcium phosphate glass-ceramic densely crystallized (fracture surface). 99

Figure 36: 1% zirconia calcium phosphate glass-ceramic showing micropores of approximatly 0.5 μm in size (fracture surface). 100

Figure 37: 2% alumia calcium phosphate glass-ceramic showing crystal fibres grown from the surfacetowards the centre of the specimen. 102

Figure 38: 2% alumina calcium phosphate glass-ceramic fibres (fracture surface). 103

Figure 39: Microporosity in 2% alumina calcium phosphate glass-ceramic (fracture surface). 104

Figure 40: Vickers indentation in a calcium phosphate glass-ceramic (load 20 kg). 105

Figure 41: Vickers indentation in a calcium phophate glass showing a well-developed crak system (load 2 kg). 106

Figure 42: Fracture surface below a Vickers indentation illustrating the half-penny like crack (load 2 kg). 107

Figure 43: Variation of fracture toughness with indenter load for a 1% zirconia calcium phosphate glass. 108

Figure 44: Typical crack geometry for indenter load >= 3 kg. 109

Figure 45: Effect of additions of alumina to calcium phosphate glass on the fracture toughness and the hardness. 112

Figure 46: Fracture surface of a calcium phosphate glass-ceramic notched beam. 114

Figure 47 : Wear behavior of UHMWPE pins tested on Vitallium, alumina and calcium phosphate glass under a 9 MPa stress and in saline solution. 116

LIST OF TABLES

Table I: Elastic Modulus Comparison Between Bone and Different Common Biomaterials. 8

Table II: Strength and Fracture Foughness Comparison Between Bone and Different Common Biomaterials. 11

Table III: Tribological Properties of a Natural Joint Compared with Artificial Prostheses 12

Table IV: Common Metallic Alloys for Artifitial Joint Prostheses. 14

Table V: Typical Composition of Bioglasses. 20

Table VI: Physical Property Comparison Between Natural Tooth and a Calcium Aluminophosphate Glass-Ceramic 23

Table VII: Mechanical Properties of a Calcium Phosphate Ceramic Under Dry and Wet Conditions. 28

Table VIII: Impurity Level in the Calcium Phosphate Powder. 36

Table IX: Characteristics of the Zirconia Powder Used as a Nucleating Agent. 39

Table X: Characteristics of the Alumina Powder Used as a Strengthening Agent. 39

Table XI: Weight Losses During the Drying and the Melting of 10 g of $CaH_4(PO_4)_2.H_2O$. 40

Table XII: Glass Transition and Crystallization Peak Temperatures of Calcium Phosphate Glasses Doped with Alumina and Zirconia. 68

Table XIII: Flexural Strength and Weibull Modulus for Calcium Phosphate Glass Specimens. 91

Table XIV: Flexural Strength and Weibull Modulus for Calcium Phosphate Glass-Ceramic Specimens. 93

Table XV: Flexural Strength and Weibull modulus for Calcium Phosphate Glass and Glass-Ceramic Samples with 1% ZrO_2 addition. 98

Table XVI: Flexural Strength and Weibull Modulus for 2% Alumina Calcium Phosphate Glass and Glass-Ceramic Samples. 101

Table XVII: Fracture Toughness Determined by Vickers Indentation Technique on As-Polished Samples (load 2 kg). 110

Table XVIII: Fracture Toughness Determined by Vickers Indentation Technique - on Annealed Glass Samples (load 2 kg). 110

Table XIX: Single Edge Notched Beam Fracture Toughness for Pure Calcium Phosphate Materials. 113

Acknowledgements

The author wishes to thank particularly Professor R.A.L. Drew for his guidance and advice.

All my colleagues in the ceramics group are gratefully acknowledged for providing such a pleasant working atmosphere during my time with them.

Kind thanks go to M. Knoepfel and B. Grondin for their technical assistance.

R. Makhoul, A, Merklein and especially D. Oelberg are acknowledged for the construction of the wear testing apparatus and for the testing of the different materials. The Vitallium and the polyhetylene were kindly furnished by Mr. P. Higham from Howmedica, Inc.

Appreciation is extended to Professor Altounian from the Physics Departement for the use of the DSC.

Et finalement, qu' Yvonne trouve ici l'expression de toute ma gratitude pour son soutien tout au long de notre séjour à Montréal.

Chapter 1

INTRODUCTION

1.1 Biomaterials

The term "biomaterial" is used for any type of material which is employed as an artificial organ in the human body. The variety of biomaterials is very extensive since they are used in such complex prostheses as artificial hearts as well as for quite simple implants such as plastic pipes for replacement of small sections of blood vessels. The biomaterials to be discussed in this thesis will be limited to materials used in the locomotor system for load bearing joint prostheses.

The most commonly used biomaterials for knee or hip prostheses are metallic alloys [1], e.g. Co-Cr, stainless steel and Ti-Al-V alloys for the femoral component, and High Density / Ultra High Molecular Weight Polyethylene [2] for the tibial and pelvic components, respectively. However, these materials are only satisfactory for short term joint replacement [3], since they tend to loosen or corrode after a few years service in the highly stressed and corrosive environment of the human body.

These problems have led physicians and material engineers to look for other suitable biomaterials. An obvious direction was ceramics. High Density - High Purity Alumina was chosen because of its excellent corrosion resistance, good tribological and mechanical properties [4]. However, together with low fatigue resistance and brittleness, the attachment of the prosthesis still remains a problem [5].

Since bone is an apatite material composed of calcium, phosphorus and organic tissue, materials from the calcium-phosphate system were investigated. Calcium phosphate ceramics (molar $CaO/P_2O_5 > 1.6$) are already used as non-load bearing components of the skeleton [6], e.g. for the maxillo-facial reconstructive surgery. This biomaterial is perfectly biocompatible and even bioactive, which means that bone grows into the pores of the prosthesis and the minerals of the implant are then used by the body to generate new, living and mature bone, i.e. by chemical resorption of the prosthesis [7]. However, the poor mechanical properties of calcium phosphate ceramics make it impossible to use as a bulk prosthesis in a load bearing joint.

Ceramics produced by the "glass-ceramic" process usually exhibit higher toughness than sintered materials. Starting with a glass, it is possible to produce very fine grains by suitable heat treatement involving a nucleation stage and a crystal growth stage with a consequent improvement in mechanical properties.

Calcium phosphate glass-ceramics (molar $CaO/P_2O_5 < 1.6$) are already used in dental applications and in some experimental joint prostheses [8]. Although they have good casting characteristics, their strength is still not sufficient to allow their use in the locomotor system.

1.2 Scope of the Study

The purpose of this work was to study the mechanical properties of calcium phosphate glasses and glass-ceramics to determine their suitability for load bearing medical applications, e.g. hip or knee joint prostheses.

Three types of material were investigated: a) pure calcium phosphate glasses and glass-ceramics, randomly and unidirectionaly crystallized, b) glasses and glass-ceramics with additions of a nucleating agent, i.e. ZrO_2, and c) glasses and glass-ceramics with additions of a strengthening agent, i.e. Al_2O_3.

These glasses and glass-ceramics were characterised in terms of modulus of rupture (4-point bend strength) and fracture toughness (Vickers indentation and notched beam techniques). A tribological study was also conducted for the most promising material and a comparison with conventional biomaterials was made.

Chapter 2 is a literature survey of biomaterials which are used in load bearing joint prostheses in the locomotor system and Chapter 3 deals with the current knowledge of calcium phosphate ceramics and glass-ceramics.

Chapter 2

BIOMATERIALS AND THEIR DRAWBACKS

2.1 Selection Criteria for Biomaterials

2.1.1. Medical Criteria

A biomaterial has to meet both medical [9] and mechanical [10] requirements. The most important medical criteria are the biocompatibility and the corrosion behavior.

The biocompatibility is a critical parameter because if the biomaterial is not perfectly biocompatible the attachment of the prosthesis becomes a problem and furthermore the immune system of the body may react against the material thus leading to tissue inflammation, necrosis, or even to the rejection of the prosthesis [11].

The corrosion resistance is also very important since the body fluid is saline and has a pH of approximately 7.3. Slight variations of pH within the human body can generate small galvanic cells in metal alloys which can lead to preferential corrosion and leaching of toxic ions into the human body. This provokes tissue inflammation and eventually, rejection of the implant.

2.1.2 Mechanical Criteria

From a materials science point of view, the most important requirements for a biomaterial are:

a) Ease of Fabrication
b) Suitable Young's Modulus
c) Strength and Toughness
d) Fatigue Resistance
e) Tribological Properties

a) Ease of Fabrication

This is an important criterion because a load bearing joint prosthesis typically has a moderately complex shape (Figure 1); furthermore, for each implant design several sizes have to be available since each patient has a different joint configuration. Therefore, materials which are easy to cast or deform are preferentially chosen.

b) Suitable Young's Modulus

An ideal biomaterial should have a Young's modulus very similar to that of bone [12]. Table I gives the Young's moduli for some typical biomaterials currently used in orthopaedics.

Figure 1: Total hip prosthesis with a metallic femoral part and a high density polyethylene pelvic part [13].

Table 1: Elastic Modulus Comparison Between Bone and Different Common Biomaterials

MATERIAL	YOUNG'S MODULUS [GPa]
Cortical bone	14-24
Bone cement	0.6
Stainless steel	190
Ti-Al-V alloy	118
Polyethylene	0.5
Alumina	400

A large elastic modulus mismatch between the prosthesis and the bone can have dramatic consequences. The internal fixation plate used to stabilise a long bone fracture (e.g. a femoral fracture) provides a good example of this problem [12]. These plates are usually screwed to the two parts of the bone so that the fracture site is under compression (Figure 2a). If the plate is not stiff enough, the parts of the bone are allowed to move, and hence, the union will never occur. But if the Young's modulus of the plate is too high, large stress shielding through the plate will occur. Therefore, since living bone reacts to external stresses, if no demand is placed on it, the bone will tend to disappear. Hence, the hard and strong cortical bone next to the fixation plate will be replaced by soft and weak cancellous bone (Figure 2b). This will lead to a high risk of refracturing the bone after removal of the plate.

a: b:

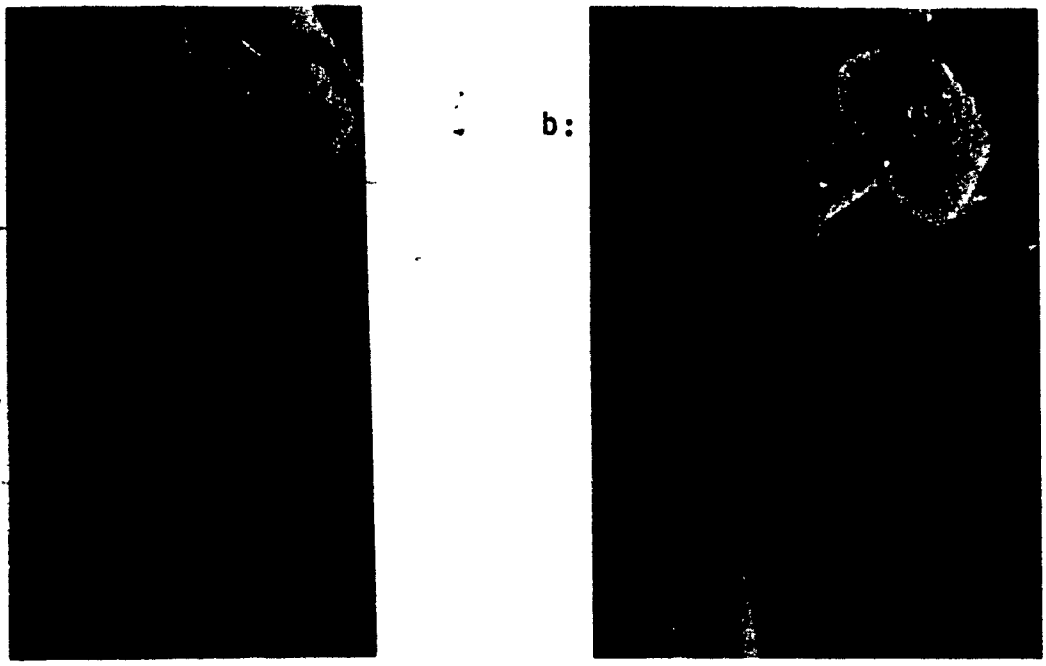

Figure 2: a: Fixation plate used to stabilize a femoral fracture. b: Bone resorption (arrow) at the previous location of the fixation plate [12].

Another effect of a high elastic modulus mismatch between the bone and the implant material is the high stress it can induce at the bone-implant interface. Under constant stress, bone is likely to deform more than the metallic prosthesis thus creating an interface problem. This may lead to loosening of the prosthesis within a short period of time [12].

c) Strength and Toughness

In the locomotor system, load bearing joint prostheses are highly stressed [14], e.g. the total reaction on a hip joint when a man is standing very quietly on one leg is three times his body weight, this value reaches five when he is walking and is over ten when he is going upstairs or downstairs. And since the space available for the implant is quite small, the stress level in a hip joint during these activities is very high, e.g. a) maximum contact bearing stress of 15 MPa and b) an estimate of the stress in the part of the prosthesis submitted to the maximum bending moment is 130 MPa.

In Table II the ultimate tensile strength and the fracture toughness of the same biomaterials currently used in orthopaedic surgery are given. This Table shows that the ultimate tensile strength of cortical bone is rather low and the low K_{1c} value indicates that it fractures in a brittle manner. But here again bone is a living material which can accommodate minor structural deterioration and heal, but this is obviously not possible for a biomaterial. Therefore, an

ideal biomaterial should have a much higher tensile strength and toughness than cortical bone.

Table II: Strength and Fracture Toughness Comparison Between Bone and Different Common Biomaterials

MATERIAL		Fracture Stress [MPa]	K_{1c} [MPa $m^{1/2}$]
Cortical bone		60-170	2-6
Bone cement		70	1
Stainless steel		660	20-100
Ti-Al-V alloy		880	70
Polyethylene		50	10-20
Alumina	tension	400	4-5
	compression	4000	

d) Fatigue Resistance

The fatigue resistance under stress and corrosion of a biomaterial should be very high. It was estimated that a knee-joint of a normal middle-aged North American adult has to withstand about 1.2×10^6 cycles per year. Hence the conventional fatigue limit, i.e. 10^7 cycles, is reached within eight years.

e) Tribological Properties

Since the coefficient of friction and the wear rate of a natural joint are very low (Table III), it is essential that the pair of biomaterials have similar characteristics [4]. A high coefficient of friction will be responsible for a difficult and painful motion and for loosening of the prosthesis. Tissue inflammation, necrosis and prosthesis loosening could be some of the consequences of poor tribological properties.

Table III : Tribological Properties of a Natural Joint Compared with Artificial Prostheses

	Coeff. of Friction	Wear Rate [mm/year]
Joint Articulation	0.01	none (regeneration)
Metal-Polyethylene	0.1-0.2	0.1-0.2
Ceramic-Ceramic	0.1-0.05	0.1-0.01

In a metal to polyethylene prosthesis, the initial coefficient of friction and wear rate are very low because of the highly polished surfaces, i.e. polished to 0.05 μm. However, the polyethylene component is quickly damaged and, hence, the wear product keeps increasing when in service. The body immune system is capable of accommodating a small amount of polyethylene wear debris but as soon as the wear rate becomes too high, debris accumulation occurs and an adverse

reaction takes place resulting in tissue inflammation and necrosis.

From a tribological point of view, a ceramic-ceramic configuration is more favorable. The initial coefficient of friction and wear rate are quite low, and they drop to an even lower value after a short "run-in" period. Furthermore, since ceramics are more bioinert than polyethylene, all the wear products can easily be accommodated [15].

2.2 Current Biomaterials

The most popular biomaterials used for hip and knee prostheses are metallic alloys, alumina and polyethylene. Metals and alumina are used for the femoral part in both the knee and the hip prostheses where a material with a high strength is required. High Density / Ultra High Molecular Weight Polyethylene is the conventional counterface material since it acts as a shock absorber and results in a satisfactory coefficient of friction when used in conjunction with metallic alloys or ceramics.

2.2.1 Metallic alloys

Table IV gives the composition of some typical metallic alloys used as biomaterials [1]. All these alloys were chosen

because of their high strength, toughness, relatively low density and good corrosion resistance.

Table IV : Common Metallic Alloys for Artificial Joint Prostheses.

ALLOY	TYPICAL COMPOSITION (wt %)		
Stainless steel	18% Cr	14% Ni	3% Mo
Cast Co-Cr-Mo	28% Cr	2% Ni	6% Mo
Wrought Co-Cr	20% Cr	10% Ni	15% W
Wrought Ti-Al-V	6% Al	4% V	

Their corrosion resistance arises from the passive oxide film on the surface of the implant. However, the weakness of this passive film can lead to the failure of the prosthesis, since the slightest disruption of this surface layer causes preferential corrosion to occur.

In the sixties the metal-metal combinations were widely used. However, high coefficients of friction leading to high wear rates were encountered. It was very difficult for the body to cope with the wear product because most metals except Fe, Al and Ti are toxic. Therefore loosening and even rejection of the prostheses were very common and they had to be replaced frequently [1].

In a metal to plastic implant only the polyethylene part is affected by wear. However, this wear product is much less

toxic and the human body can easily accommodate the wear debris. The coefficient of friction in such an implant is quite low during the early years of service, but increases with time (Table III). The wear rate follows the same trend, so that the "wearing out" of the plastic component is to be expected within about ten years [3].

By far the greatest problem in total joint replacement surgery is still the attachment of the prosthesis. This is usually achieved by using bone cement. The problems of bone cement will be discussed in detail later, but the introduction of a second interface, and hence another elastic modulus mismatch, increases further the problems already described in section 2.1.2.

Another method for attaching the prostheses is to allow bone ingrowth into a porous layer on the surface of the implant. But since for every metallic alloy there is at least one element which is not completely biocompatible, this process is very slow. However, some progress has been made with a porous coating of pure titanium [16].

2.2.2 Polymers

In order to have a material capable of absorbing shock without damaging the surrounding bone as well as to obtain a low coefficient of friction, various polymers have been tested, e.g. acrylic materials, nylon, and fluon [3]. These

were employed as a part of a multicomponent implant, i.e. the pelvic part of hip prostheses or the tibial part of knee prostheses. These polymers were chosen because of their good biocompatibility in non-load bearing implants, e.g. pipes for small sections of blood vessel. However, they were not found suitable for load bearing joint prostheses for three reasons: a) gross shape deformations under loading, b) high wear rate and c) poor biocompatibility under high stress conditions.

The surgeon Charnley made the fortunate choice of High Density / Ultra High Molecular Weight Polyethylene [2]. This polymer, used in conjunction with metal, has a low coefficient of friction and gives satisfactory clinical results. However two important problems remain: a) the increasing wear rate with time and b) the attachment of the implant. The high wear rate has to be taken into account when the prosthesis is designed, i.e. by increasing the thickness of the polyethylene part beyond the required shock absorbing capability. Thus, the loosening of the implant usually precedes the "wearing out" of the polyethylene component. The loosening of the prosthesis is to be expected since the fixation is achieved by using bone cement as discussed below.

2.2.3 Bone Cement

Bone cement is used for the fixation of metallic and polymeric prostheses. The cement is first cast into a cavity machined in the bone. The implant is then forced into the

cement and held in place until hardening of the cement is achieved. Today, only self-curing acrylic cements are employed, which are composed of a mixture of methyl methacrylate (MMA) and polymethyl methacrylate (PMMA) [17]. However, several problems still occur with the use of these acrylic cements.

First the success of the attachment depends mainly on the skill of the surgeon, since he has only a short time (e.g. about five minutes) to achieve the correct location of the implant. Secondly, during the curing phase, the high temperature generated requires the use of an efficient cooling system, otherwise all the surrounding tissues would be burned. Thirdly, instead of only one interface (bone-prothesis) the use of bone cement introduces two interfaces: bone-bone cement and bone cement-prostheses. This means that the elastic modulus mismatch is also doubled (Table I), thus, worsening the problems described in 2.1.2.

Finally, the introduction of bone cement into the bone can be immediately followed by a drastic drop in the blood pressure. There are even several cases where a cardiac arrest followed by the death of the patient have been reported [18].

2.2.4 Ceramics

The different problems such as corrosion, wear rate, biocompatibility, but more particularly, the bonding of the prosthesis have led physicians and material engineers to search for other suitable biomaterials.

Apart from bone cement, there are three other ways of bonding an implant to bone. (a) By hard tissue ingrowth into a porous layer of the protheses; this requires a perfectly inert biomaterial (e.g. pure titanium and alumina) [19]. (b) By chemical reaction between the implant and bone; here the material not only has to be biocompatible, but also bioactive to chemicaly react with bone (e.g. SiO_2-CaO-Na_2O glasses) [20]. (c) By material resorption; in this case the material has a composition so similar to that of the bone that it is decomposed and used for the formation of new bone (e.g. porous CaO-P_2O_5 ceramic) [21]. Usually the implant has a porous layer to increase the reactive surface.

a) Alumina

Nowadays, the only ceramic used in orthopaedics is high density- high purity alumina [4]. This ceramic has excellent tribological properties since it starts with a very low coefficient of friction of 0.1 and a wear rate of 0.1 mm/year and these values drop to 0.05 and 0.01 respectively after a short "run-in" period. The special mechanical characteristics

of alumina, i.e. tensile strength = 400 MPa, compressive strength = 4000 MPa, fracture toughness = 4 MPa $m^{1/2}$, as well as the fact that satisfactory bone ingrowth only occurs in areas where stresses are transmitted, require a special implant design (Figure 3).

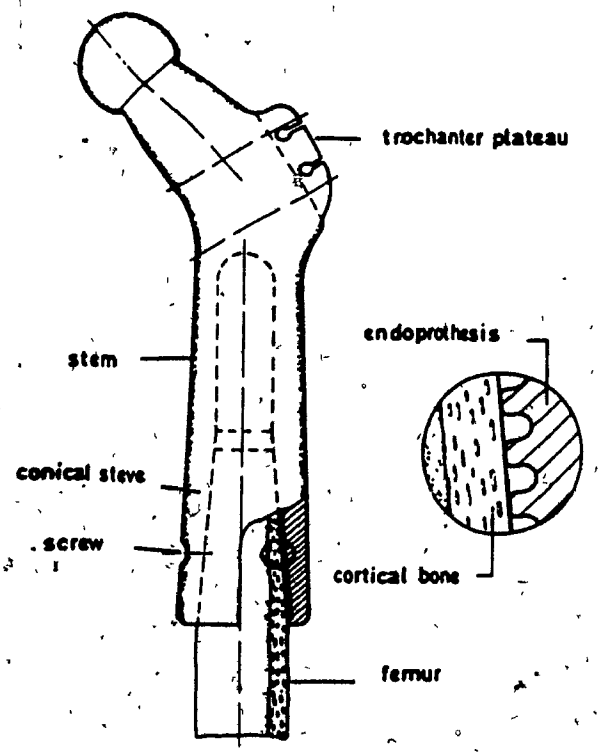

Figure 3: Femoral part of an alumina hip prosthesis designed to minimize bending moments [30].

Although it gives satisfactory results [5], alumina is still not the ideal biomaterial. Some of the problems include: a) a high elastic moduli mismatch (400 GPa for alumina against 17 GPa for bone), b) its inherent brittleness, c) the low fatigue resistance and d) the slowness and inhomogeneity of bone ingrowth.

b) Bioglass

Hench et al. [20] developed bioglasses which, by chemical reaction, achieve a very strong attachment to bone. Typical compositions are given in Table V.

Table V: Typical Composition of Bioglasses

Material	Composition in Weight Percent					
	SiO_2	P_2O_5	CaO	Na_2O	CaF	B_2O_3
45S5	45	6	24.5	24.5	-	-
45S5F	43	5.7	11.7	23.4	16.3	-
45BS5	40	6	24.5	24.5	-	5

This direct bond is obtained without the use of a porous structure, hence retaining the strength of these materials. The strength of the bond is promoted by the dissolution of calcium and phosphorus ions in the slightly acid body fluid, which promotes the precipitation of hydroxyapatite in bone. The rate at which the bonding occurs, as well as its strength, are not dependent upon the Ca/P ratio or the microstructural state. This means that it is possible to modify the physical properties of the material (e.g. by crystallizing the glass) without changing the biological behavior.

The strength of this bond is excellent, since after only

28 weeks, fracture would occur preferentially in the surrounding bone, leaving the interface and the ceramic compound intact.

c) Calcium phosphate ceramics

Since calcium sulphate (Gypsum) was successfully used as bone substitute last century [22], there is a growing interest in ceramics based on biological salts. Because bone is composed of calcium, phosphorus and organic tissues (mainly collagen), calcium phosphate ceramics have received considerable attention [23]. Calcium phosphate ceramics exhibit a very high biocompatibility since neither encapsulation nor rejection of the material occurs [6]. A tight bond between the implant and bone is quickly developed.

Densely sintered ceramics do not exhibit a measurable biodegradation rate (resorption). A comparative animal study seems to indicate that the presence of both pores and impurities favors the resorption of the material [23]. It is, therefore, possible to achieve different degradation rates varying from negligible to 10% or more per month.

Resorption occurs in two steps. First powder particles are isolated from the ceramic body by physio-chemical dissolution of the neck of the sintered particles. These particles are then ingested by the surrounding cells and tranformed into new living bone. It is obvious that the pore

size is a critical parameter for controlling resorption rate since the more available surface area , the more physio-chemical action.

The mechanical properties of calcium phosphate ceramics depend strongly upon the porosity of the sample. For the dense ceramic, compressive strengths of 500 MPa and tensile strengths of 100 MPa have been reported [24]. It exhibits substantial slow crack growth and low fracture toughness (e.g. $K_{1c} = 1$ MPa $m^{1/2}$).

It seems possible to overcome these general ceramic drawbacks by prestressing the implant in compression [25]. Such prestressed implants are already successfully used as load bearing tooth prostheses and they seem to show promise as joint prostheses.

d) Calcium Phosphate Glass-Ceramics

The poor mechanical properties of calcium phosphate ceramics has stimulated research in glass-ceramics where fine grained ceramics are obtained by controlled crystallization of suitable glasses [8,21].

In France, Pernot et al. investigated the porous form of such a glass-ceramic [21,26]. For a bioinert material like alumina, the minimum size of the interconnection between pores has to be about 100 μm to allow satisfactory bone ingrowth. They produced porous calcium phosphate glass-ceramics using

the "foaming agent" technique. The resorption characteristics of this material allowed for a reduction in the interconnection diameter to about 15 μm without lowering the bone ingrowth properties, and hence led to an improvement in the mechanical properties.

Dense calcium phosphate glass-ceramics are under investigation in Japan [27]. Their biological behavior is excellent, since it was shown in an animal study that after only 6 weeks a tight bond was developed between bone and the ceramic while a control titanium implant (the most biocompatible metal) was still loose. They were found highly suitable for the manufacture of artifical teeth since their mold filling characteristics are excellent and their mechanical properties are very similar to that of natural tooth (Table VI) [8].

Table VI: Physical Property Comparison Between Natural Tooth and a Calcium Aluminophosphate Glass-Ceramic

	MOR [MPa]	Hardness [GPa]
Natural tooth	142	3.6
Glass-ceramic	116	3.8

A hardness similar to that of natural tooth is highly desirable for a dental biomaterial because materials harder than tooth enamel (like conventional dental porcelain) would wear away the tooth by abrasion.

Chapter 3

CALCIUM PHOSPHATE CERAMICS

3.1 Calcium Phospnate Ceramics

Under normal cooling conditions in the calcium phosphate system, crystalline ceramic formation occurs above 55 molar percent calcium oxide. This concentration corresponds to the eutectic point between monobasic and dibasic calcium phosphate (Figure 4).

Most of the studies in the biomedical field were conducted on ceramics having a Ca/P ratio varying from 1.5 to 1.7 (CaO/P_2O_5 = 3 to 3.4), i.e. close to the tribasic calcium phosphate composition. The former will undergo a phase transformation from apatite to beta-whitlockite at 800 ^{o}C, while the latter will remain in the apatite form [6]. The three most important processes used for the production of such ceramics are : a) slip casting and sintering, b) cold pressing and sintering, and c) hot pressing.

Slip casting involves the casting of a slurry composed of calcium phosphate powder, water and proper deflocculating agent into a plaster mold. The water is removed by capillary action, leaving the so-called "green" body. After drying, the compact is fired at the appropriate sintering temperature (usually 2/3 of the melting temperature in degree kelvin).

Cold pressing of the dry powder can be carried out either in a conventional uniaxial press or preferentially in an isostatic press. Compaction of the powder is achieved with pressures of up to 500 MPa. The resulting compact body is then

heated at the sintering temperature for a suitable period of time.

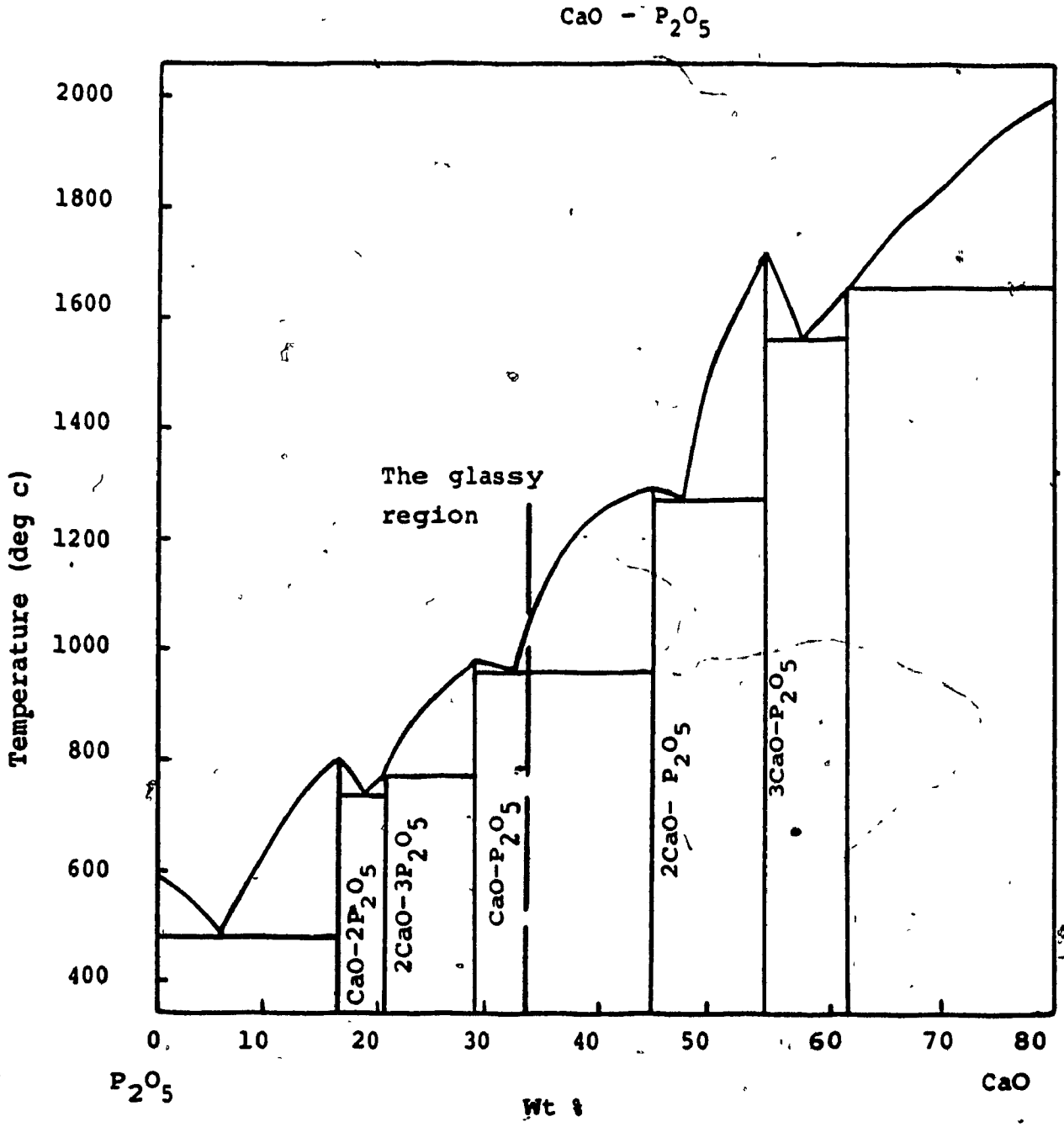

Figure 4: $CaO-P_2O_5$ system phase diagram.

Hot pressing is a complex technique where compaction and sintering of the powder occur simultaneously. Although it is an expensive process limited to simple shapes, improved mechanical properties can be achieved.

3.1.1 Properties of Calcium Phosphate Ceramics

A careful determination of the mechanical properties of dense calcium phosphate ceramics was carried out by de With et al. [24]. The starting material was a calcium phosphate powder having an Ca /P ratio of 1.64, a specific surface area of 85 m^2/g and 50% of the grains below 1 μm. This powder was first pressed uniaxially in a die at 5 MPa and then isostatically compacted at 100 MPa. The resulting green body was subsequently sintered at 1450 K for 6 hours in a moist atmosphere, achieving a density of 98% theoretical. This ceramic was characterized in terms of elastic modulus, bend strength, fracture toughness and slow crack growth under dry and wet conditions. Results are listed in Table VII.

The mechanical properties decreased significantly when tested under wet conditions. However ageing for three weeks in aqueous solutions containing biologically active components (proteins and cells) has no effect on the properties of samples carefully dried prior to testing. Therefore it was concluded that even though the presence of water does not degrade the material, the fracture behavior is greatly

affected by moisture.

Table VII: Mechanical Properties of a Calcium Phosphate Ceramic Under Dry and Wet Conditions.

	dry	wet
Elastic Modulus, GPa	116	
Modulus of Rupture, MPa	103	92
Fracture Toughness, MPa $m^{1/2}$	1.33	0.88
Slow Crack Growth Coeff., n (see Appendix 1)	32	14

Although this ceramic has satisfactory short term mechanical characteristics, the low value of n indicates that a substantial slow crack growth would cause deterioration in these properties with time, i.e. static fatigue. Furthermore this decrease would be more pronounced under in vitro conditions than in dry atmosphere. This ceramic is therefore a doubtful candidate for the highly stressed environment of load bearing joint prostheses.

3.2 Calcium Phosphate Glass-Ceramics

3.2.1 Crystallization Behavior Above T_g

In the calcium phosphate system, glass formation occurs up to 55 molar percent CaO. Abe [28] extensively studied the crystallization behavior of the monobasic calcium-orthophosphate glass. Its glass transition temperature was found to be close to 510 ^{o}C. The crystallization kinetic study of the glass at temperature close to 800 ^{o}C gave the following results :

1) The major crystalline phase was beta calcium metaphosphate with a small amount of metastable gamma calcium metaphosphate present. This gamma phase transforms into the beta phase if sufficient time is given.

b) The activation energy of nucleation and crystallization of the beta phase was found to be the same (about 115 kcal/mol). Since this energy is comparable to that of the P-O-P bond energy, it was thought that crystal growth occurs by breaking and rearranging the chain pattern at the glass-crystal interphase [29].

c) The nucleation activation energy of the metastable gamma phase was estimated to be larger than that of the stable beta phase.

3.2.2 Crytallization Behavior Below T_g

It is usually accepted that glasses do not crystallize at, or below, their glass transition temperature T_g, because the thermal energy is too small to break and reform the glass network, and also the rate of ionic diffusion is slow. However, Abe et al. [29] found two groups of phosphate glasses, (a) $Be(PO_3)_2$, $Ca(PO_3)_2$, $Sr(PO_3)_2$, $Ba(PO_3)_2$ which crystallize both below and above T_g, and (b) $Mg(PO_3)_2$, $Ni(PO_3)_2$, $NaPO_3$ which only crystallize above T_g. The first metaphosphate series (a) has a chain-like structure in both the glass and the crystalline state, whereas the later (b) has a chain structure in the glass and ring morphology in the crystalline state.

The glass transition temperature for the monobasic calcium metaphosphate glass was found to be close to 490 ^oC from thermal expansion curves, with variations depending on the heating rate. The corresponding viscosity was 10^{14} Pa s. Nucleating at the surface, the crystals which form at a temperature as low as 420 ^oC, have a typical hemispherulitic shape. The surface remains covered by a glassy layer approximately 20 μm thick except at the nucleation site. These hemispherulites can reach several millimeters in size and are composed of fibrils about 0.8 μm in diameter.

The activation energy of crystal growth was found to be 30 kcal/mol for crystallization below T_g which is a low value

compared to that above T_g (110 kcal/mol). This indicates that the crystallization mechanism in the two cases is basically different. For crystallization below T_g, it is thought that the structure of the glass and crystal are similar. Although the molecular chains follow a completely random path in the glass, the crystal contraction (around 3%) induces a high stress at the glass-crystal interface, thus straightening and ordering the glass chains. This crystallization mechanism requires only a small amount of energy with little atomic rearrangement, since it does not involve the breaking and the reforming of bonds. This stress-induced crystallization mechanism explains the presence of the glassy layer. Any stress applied to this thin glassy layer (20 μm) will result in its deformation rather than to chain straightening.

The structure and the phases present in crystals grown below T_g (e.g. 420 ^{o}C) are the same as those grown above (e.g. 800 ^{o}C), i.e. hemispherulites composed mainly of beta calcium phosphate with a small amount of the metastable gamma phase. The crystal growth rate around the glass transition temperature for this $CaO-P_2O_5$ glass is surprisingly high. Equation (1) is roughly valid for network glasses having the same chemical composition as the growing crystal.

$$V \eta / \Delta T = 1.6667 \cdot 10^{-5} \quad N/m\ K \qquad (1)$$

with V : crystal growth rate, m/s

η : viscosity, Pa s

ΔT : degree of undercooling , K
(from the melting temperature)

Usually, at temperatures close to T_g, this equation leads to crystal growth rate of several microns per hundred years. However, at T_g, this calcium phosphate glass crystallizes at a rate as high as 10 μm/min, which corresponds to:

$$V_n / \Delta T = 16.667 \text{ N/m K.}$$

The growth rate seems to be dependent on the thickness of the glass sample [30]. The critical thickness (where the growth rate jumps from 1-2 to 20-25 μm/min) was found to be about 1 mm at 560 °C and 2 mm at 540 °C. It is believed that this critical thickness is determined by competition between the rate of relaxation of the induced tension in the molecular chains at the glass-crystal interface and the crystal growth rate at a given temperature.

Although the crystal growth rate is not affected by the presence of water, the number of nucleation sites is proportional to the partial vapor pressure of water in the atmosphere. The incubation time also decreases as the vapor pressure increases [29].

3.2.3 Unidirectional Crystallization

Another interesting characteristic of $CaO-P_2O_5$ glass is its ability to crystallize along the direction of applied stress [30]. A fine glass rod was obtained by stretching it three times its original length at a temperature slightly above T_g (i.e. 540 ^oC). When this specimen was heated at 510 ^oC under no load, crystallization occurred in the elongation direction at a rate ten times faster than that of a hemispherulite. This high rate is due to the orientation of the glass molecular chains in the stretching direction, thus providing an easy path for crystal growth.

This characteristic is used to produce unidirectionaly crystallized samples [31,32]. One end of the rod is heated at about 600 ^oC until random crystallization takes place. The rod is then pulled through a thermal gradient of 30 $^oC/cm$ around T_g at a rate equal to the crystal growth rate (e.g. 20 $\mu m/min$). The crystals grow unidirectionaly from the high temperature region to the low one. The driving forces are (a) the stress induced by the thermal gradient and (b) the stress induced at the glass-crystal interface.

The temperature range where unidirectional crystallization can occur depends on the composition of the glass (Figure 5). This range is quite wide for a molar ratio of CaO/P_2O_5, R = 0.94, but becomes very narrow for R >= 1.

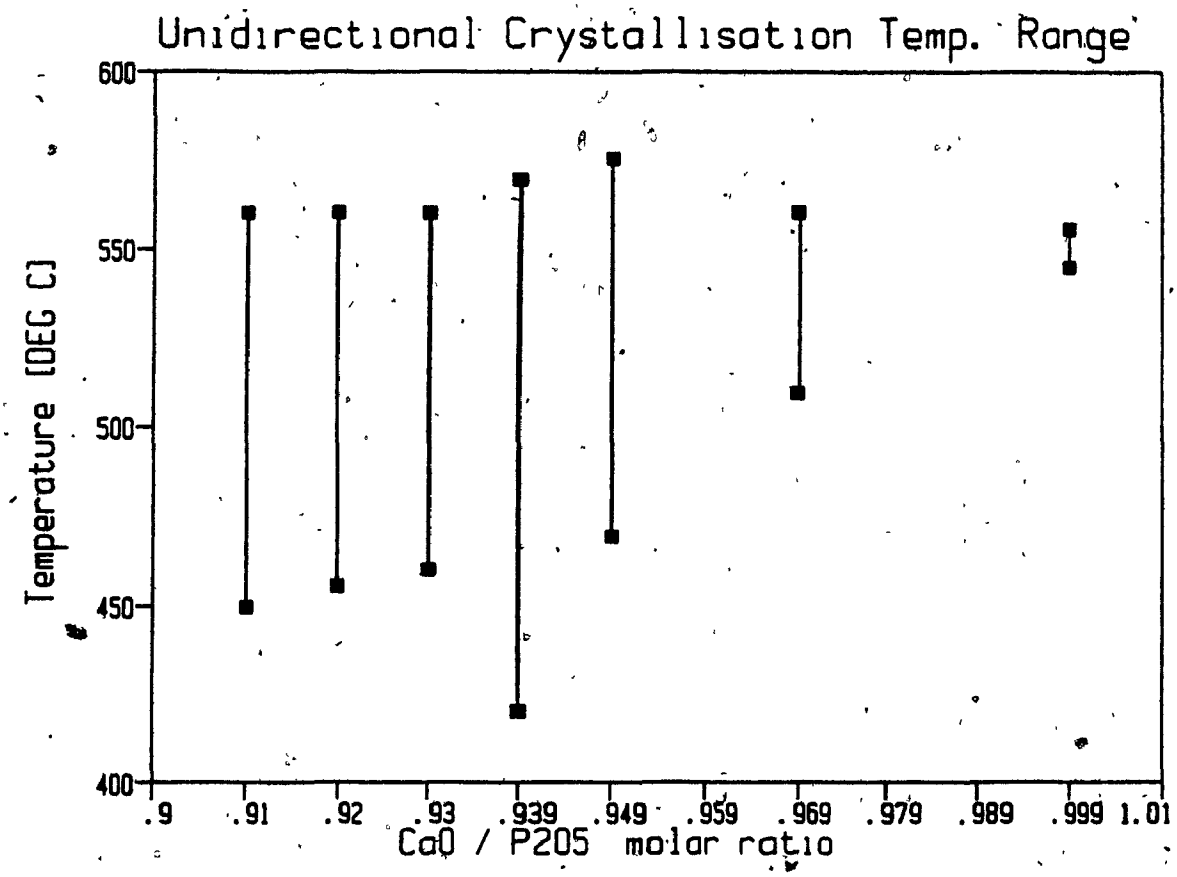

Figure 5: Temperature range where unidirectional crystallization can occur (from [32]).

The strength was improved from 50 MPa for a randomly crystallized calcium phosphate glass-ceramic to 600 MPa for a unidirectional one. The maximum strength was found for a molar ratio of 0.94 (i.e. 640 MPa). The fracture toughness was also greatly improved since instead of shattering like conventional ceramics, the glass-ceramic fractured in step-like fashion, as each bundle of crystalline fibres broke. The cracks tended to propagate in the direction of the fibre axis breaking the cohesion between them.

Chapter 4

MATERIAL AND EXPERIMENTAL PROCEDURE

4.1 Starting Materials

4.1.1 Calcium Phosphate Powder

Purified grade calcium phosphate powder, in the form of $CaH_4(PO_4)_2.H_2O$, was purchased from BDH Chemicals. The major impurities are given in Table VIII.

Table VIII: Impurity Level in the Calcium Phosphate Powder.

chloride	< 0.005 %
sulfate	< 0.05 %
iron	< 0.015 %

Since it is a hydrated powder, a differential scanning calorimeter (DSC) run was performed to determine the water dissociation temperatures (Figure 6). The three main endothermic peaks characteristic of water loss occured at 150, 270 and 310 ^{o}C. Water dissociation is completed above 450 ^{o}C.

X-ray diffraction analysis indicated that the powder was composed mainly of alpha $Ca_3(PO_4)_2$, with large peaks characteristic of combined water of crystallization.

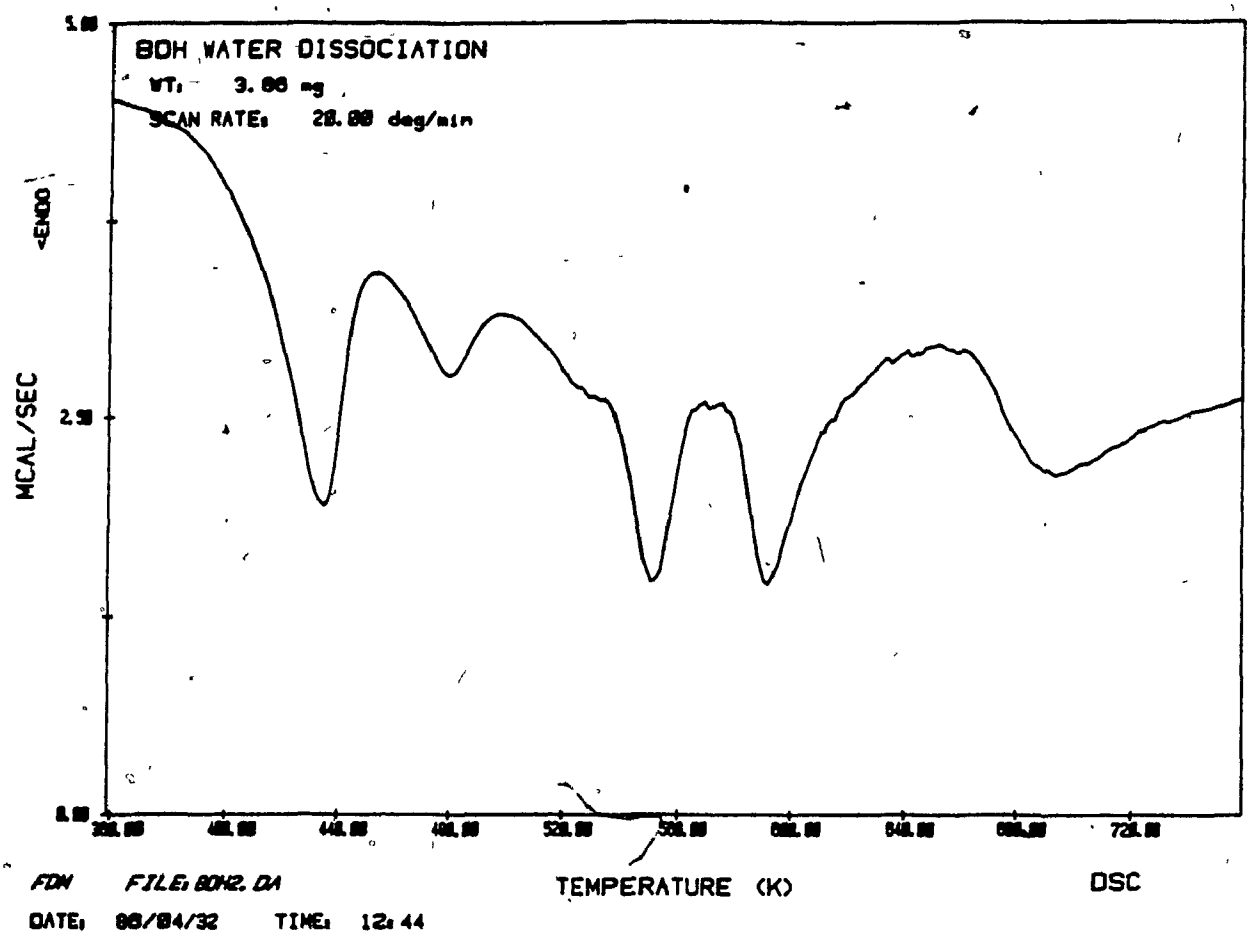

Figure 6: DSC curve showing the water dissociation behavior for the calcium phosphate powder.

4.1.2 Additive Powders

Two additions were made to calcium phosphate to investigate their affect on a) the nulceation and b) the strengthening; they were ZrO_2 and Al_2O_3 respectively.

a) Nucleating Powder

In pure calcium phosphate glass only surface nucleation

occurs and, hence, during crystallization a fibrous structure is developed. The addition of a nucleating agent that would promote bulk nucleation rather than surface nucleation was investigated in order to produce a fine grained structure.

Conventional nucleating agents used in the glass-ceramic industry are: phosphorus pentoxide (P_2O_5), titanium oxide (TiO_2), and zirconium oxide (ZrO_2). Phosphorus pentoxide was immediately excluded since phosphorus is one of the main glass constituents. Titanium oxide could not be dissolved in the glass even at 1600 ^{o}C. Titanium ions could also be introduced in the glass by dissolving titanium phosphate. However, it was considered too expensive at $20 / gram. Therefore, zirconium oxide was chosen as the nucleating agent.

The specifications of the zirconia powder are given in Table IX. One weight percent of zirconia dissolves in stoichiometric calcium phosphate glass (Ca/P = 0.5) at 1230 ^{o}C, whereas the dissolution temperature for 2% zirconia is over 1500 ^{o}C. Therefore, the nucleation behavior of calcium phosphate glass with an addition of only one weight percent of zirconia was investigated. The appropriate amount of zirconia was added to the starting calcium phosphate powder, carefully mixed, dried and melted at 1250 ^{o}C; no significant increase of the viscosity of the melt was noted. The glass was poured into a mold preheated at 560 ^{o}C and annealed at this temperature for 10 minutes. Half the resulting glass samples were crystallized at 650 ^{o}C for 12 to 16 hours.

Table IX: Characteristics of the Zirconia Powder Used as Nucleating Agent.

Impurities: 0.9 SiO_2, 0.3 Al_2O_3, 0.2 TiO_2, 0.06 Fe_2O_3 Wt %

Mean Grain Size: 1.5 μm

Specific Surface Area: 4.2 m^2/g

b) Strengthening Powder

Alumina was added to calcium phosphate glass to modify the glass network and promote the formation of stronger bonding, i.e. Al-PO_4 bonds, and also increase the strength of the bonding between the crystal fibres. The characteristics of the alumina powder used are given in Table X. The appropriate amount of alumina was added to the starting powder, e.g 1.6 g Al_2O_3 for 100 g of $CaH_4(PO_4)_2.H_2O$, mixed, dried and melted at 1200 °C. The glass was cast into a mold preheated at 580 °C, and then annealed at this temperature.

Table X: Characteristics of the alumina powder used as a strengthening agent.

Impurities: 0.04 Na_2O, 0.06 SiO_2, 0.04 Fe_2O_3, 0.04 CaO, 0.04 B_2O_3 Wt %

Mean Crystal Size: 11 μm

Specific Surface Area: <1 m^2/g

4.2 Sample Preparation

4.2.1 Drying and Melting

Since phosphorus pentoxide is an unstable material (pure P_2O_5 begins to sublime around 300 ^oC and melts at 560 ^oC), the weight losses occurring at different melting temperature were monitored (see Table XI). Ten grams of powder were dried for 16 hours at 115 ^oC to ensure no loss of P_2O_5. The batch was then heated at 1000 ^oC to remove all the water of crystallization and then reheated at 1000, 1100, 1200, 1300, and 1400 ^oC for 20 minutes in each case. The sample was carefully weighed between each increment of temperature rise. After the first heating at 1000 ^oC there were no P_2O_5 losses, since the theoretical weight loss due to water should be 21.43 % and a weight loss of only 20.24 % was measured, this meant that some water had dissolved in the glass (1.19 %).

Table XI: Weight Losses During the Drying and the Melting of 10 g of $CaH_4(PO_4)_2.H_2O$.

Temperature [oC]	Weight Losses in 20 Minutes [g]	[%]
1000	1.4701	20.24
1000	0.0014	0.02
1100	0.0057	0.07
1200	0.0229	0.29
1300	0.0662	0.83
1400	0.1544	1.96

Serious losses of P_2O_5 during melting of a glass batch were observed at T >= 1300 °C (0.83 wt% after 20 min). Therefore, a melting temperature of 1200 °C was chosen. To check if such a melting temperature would result in high phosphorus pentoxide losses, a batch of glass, having a molar ratio of CaO/P_2O_5 = 0.9, was made by adding 6 ml of 85% phosphoric acid (H_3PO_4) to 100 g of calcium phosphate powder. After careful drying, this batch was melted at 1200 °C, weighed and then reheated at this temperature for one hour. A weight loss of only 0.2 % was measured. Therefore, it was decided that 1200 °C was the optimum melting temperature for these glasses.

A DSC study showed that complete dissociation of the water occurred below 450 °C (Figure 6). Hence, the powder was carefully dried at 500 °C in a platinum crucible since no other material could withstand this temperature without reacting with the powder. A small layer of powder, about 1 cm thick, was dried at a time to avoid the formation of a dry crust at the top of the crucible which would prevent any further dehydration of the underlying powder. The crucible was then charged into an air furnace at 1200 °C for one hour.

4.2.2 Casting

Two types of samples were prepared: a) four-point bend samples and b) fracture toughness samples.

a) Four-point bend samples

Since crystallization is a time consuming operation, especially unidirectional crystallization, the option of making large samples that could be machined to give a number of specimens of suitable size after crystallization was first investigated. A square graphite mold of dimensions 15 mm X 15 mm X 80 mm was designed. However, the quality of the graphite used did not allow for proper annealing of the samples since mold degradation occurred at temperatures below T_g. This resulted in samples which contained high residual stresses. Since this glass has the property to crystallize towards the stress direction [30], the crystals followed the isothermal curves left during the cooling of the sample. Furthermore, since nucleation occurs only at the surface of the specimen, crystals grow towards the centre of the sample in a fibrous form, leaving an anisotropic texture. This means that the measured flexural strength would not only depend on the chemical composition but also on the location of the specimen. Therefore, this method of sample preparation was abandoned.

Round specimens, 5 mm in diameter and 80 mm in length, were then made (Figure 7) using a boron nitride (BN) mold. Since the coefficient of thermal expansion of BN from 0 to 1000 ^{o}C is negligible, on cooling, the glass sample shrinks away from the mold, facilitating specimen removal. As BN is completely inert up to 1400 ^{o}C, it is possible to anneal the sample for a long period of time or even to crystallize it in

the mold. Therefore, BN is the ideal mold material.

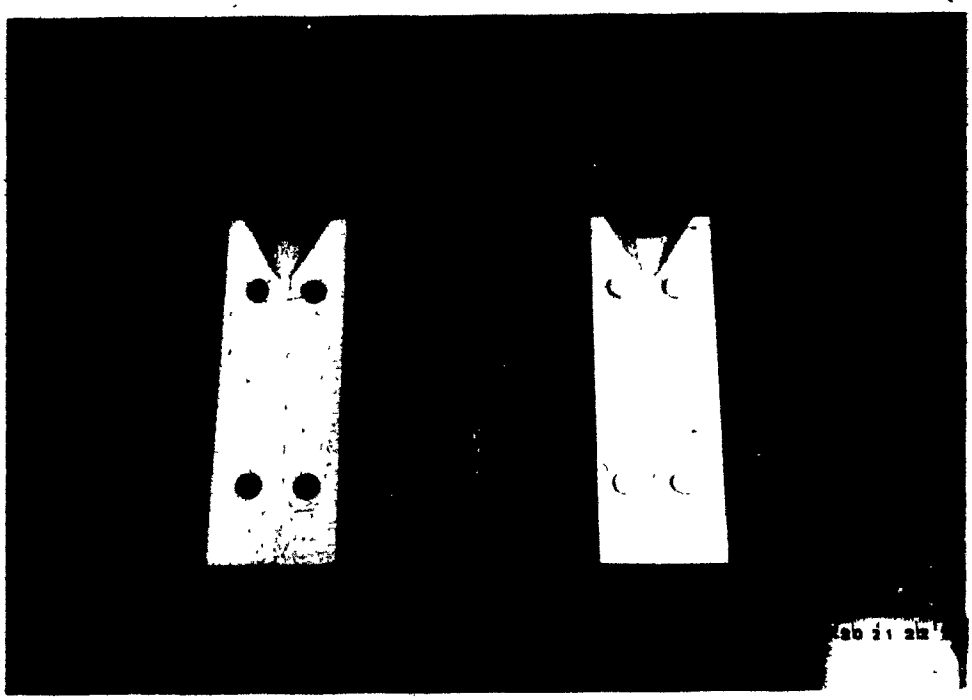

Figure 7: Four-point bend specimen and the boron nitride mold.

To obtain good mold-filling characteristics, the glass batch had to be heated at 1200 ^{o}C, or above, in order to achieve a low melt viscosity. Lower melting temperatures would result in the freezing of the glass before it reached the bottom of the mold. The mold was preheated in a furnace slightly above the glass transition temperature. After the pouring of the glass, the mold was placed back in the furnace for 10 minutes for annealing. The mold was then removed and left to cool to room temperature. The resulting samples had a smooth surface and low residual stress.

The cooling rate is a critical parameter in calcium phosphate glass casting. Too high, a cooling rate is

responsible for two undesirable effects: a) a wavy pattern is generated at the specimen surface, probably due to preferential shrinkage following the random molecular chain path and, b) gas bubble formation. The gas is thought to be a mixture of phosphorus pentoxide and hydrogen. The bubble formation is also favored by the large length to diameter ratio of the samples. Although, there is molten glass available at the top of the mold, during freezing the centre of the rod becomes too viscous to flow. Therefore, any further shrinkage of the glass at the centre will result in bubble formation.

On the other hand, too slow a cooling rate would give sufficient time for nucleation and crystallization to occur, which must be avoided at this stage. The cooling rate can easily be varied by changing both the melting temperature and the mold temperature. A melting temperature of 1200 ^{o}C with a preheated mold around T_g was found to be a good compromise although gas bubble formation was reported in 40 % of the specimens produced. These could not be used for strength testing and had to be discarded and remelted.

b) Fracture toughness samples

Samples for fracture toughness measurements using the notched beam technique were machined according to the ASTM E399 standard (Figure 8); they had a size of 15 mm X 30 mm X

80 mm. Since boron nitride is an expensive material, high quality graphite was chosen for of this large mold. As high quality graphite does not oxidize significantly below 600 ^{o}C, it was suitable for containing the sample during annealing. The coefficient of thermal expansion of graphite being lower than that of calcium phosphate glass, meant that a split mold was not even necessary to enable easy removal of the specimen after annealing.

The glass was melted at 1200 ^{o}C and poured into a mold preheated slightly above the glass transition temperature. The mold was then left for 15 min in the furnace before it was furnace cooled to 300 ^{o}C and then removed. This procedure was very satisfactory, since the samples were perfectly annealed and bubbles were almost never present.

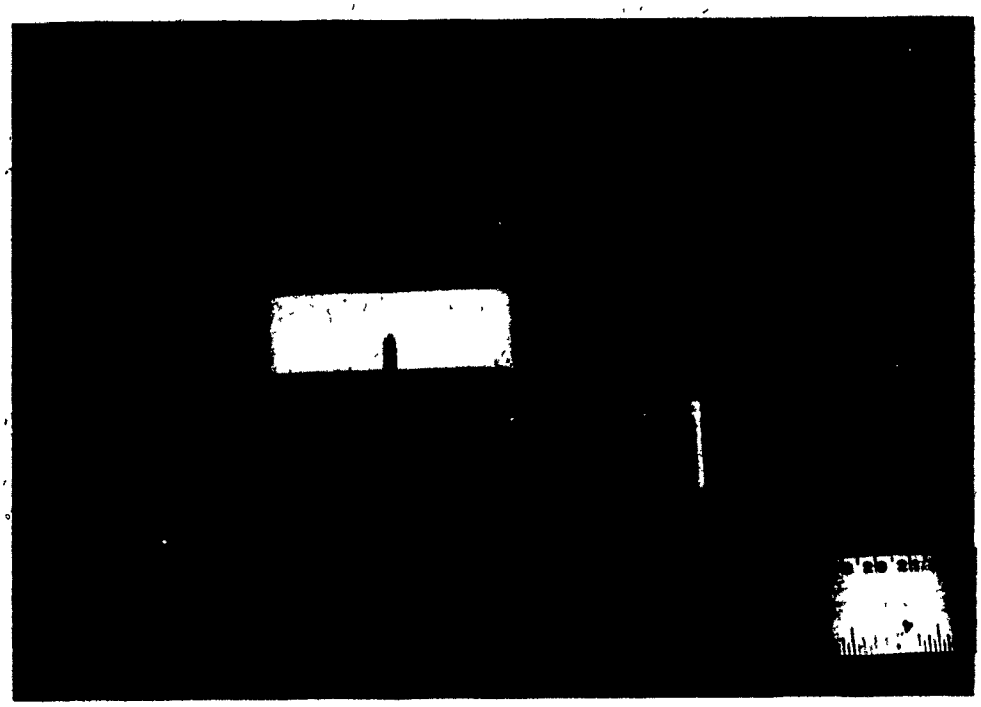

Figure 8: Sample for fracture toughness measurements using the notched beam technique.

The top surface of the specimen was rounded and this face was ground down to the required dimension. The V-notch was machined on the ground face so that the stress due to grinding would not influence fracture toughness measurements.

4.3 Differential Scanning Calorimetry

A Differential Scanning Calorimeter (DSC) is an improved Differential Thermal Analysis apparatus (DTA). A DTA only measures the temperature increase or decrease involved in a chemical or physical change or in a phase transformation, whereas a DSC is capable of measuring the actual amount of heat it has to furnish to maintain both the reference sample and the test sample at the same temperature during the tranformation. Therefore, it gives the energy involved in such a tranformation. Although the use of a DSC is much simpler than the one of a DTA, its major drawback is that it is not possible to reach temperatures above 727 ^{o}C (1000 K).

The DSC experiments were carried out on a Perkin Elmer DSC-2 in graphite crucibles under nitrogen atmosphere. Initially small bulk samples lying on a graphite powder bed were used in order to reproduce more closely the conditions of a real bulk cast piece, i.e. low specific surface area. However, the poor thermal contact between the sample and the sensor-lead to enormous peak temperature offsets (of the order of 50 ^{o}C) and to very poor data reproducibility. Therefore, glass powder was used for all the following experiments. Prior

to testing, each glass sample was ground and sieved either through No. 100 and 120 sieves or through No. 70 and 100 sieves. The resulting powders had a size distribution between 125 and 150 μm, and 150 and 212 μm respectively. Each test was usually carried out with a heating rate of 10 °C/min and with 10 to 30 mg of glass powder.

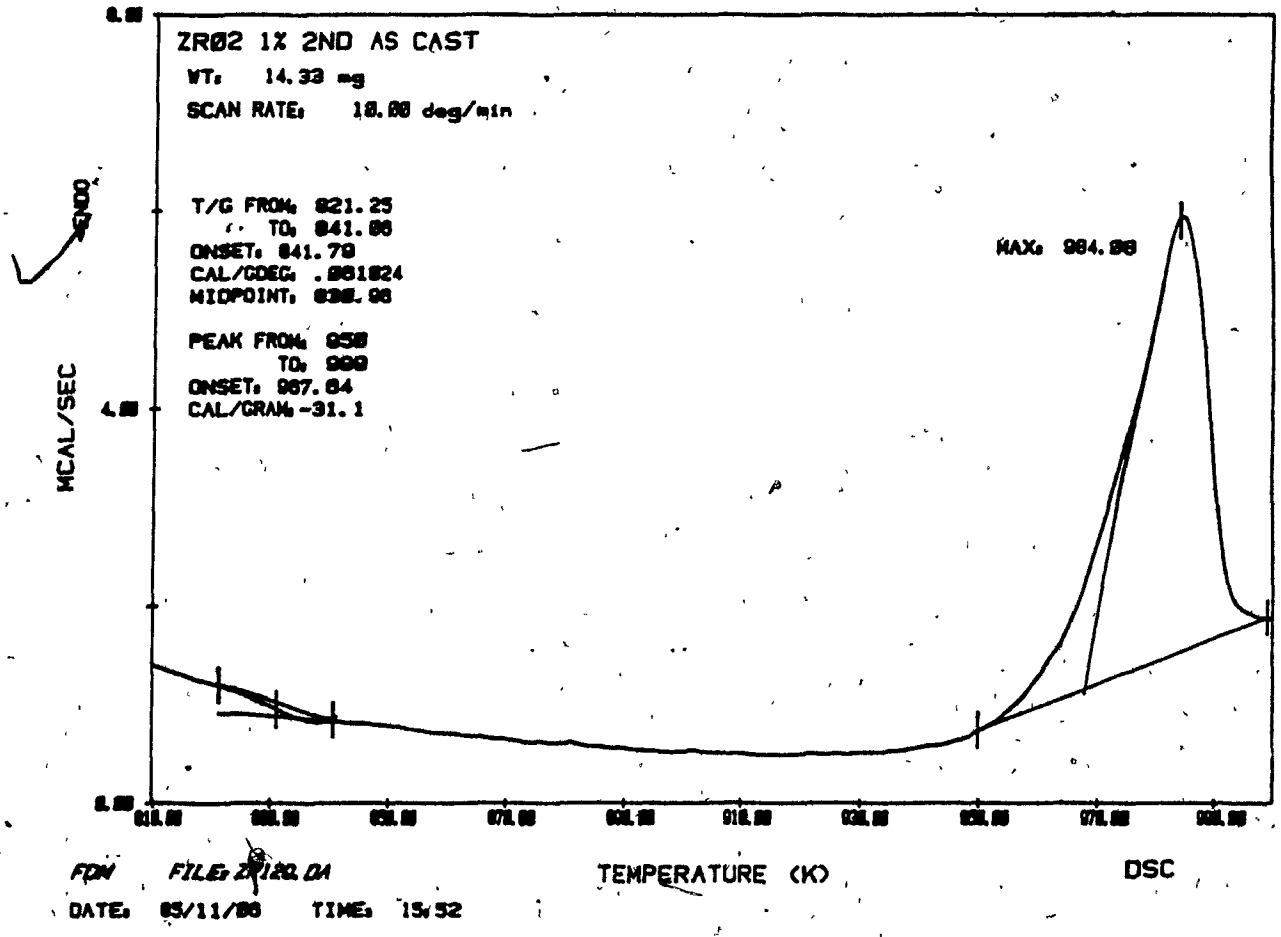

Figure 9: Example of a DSC plot determining the glass transition and the crystallization peak temperatures.

The DSC was calibrated using potassium chromate, K_2CrO_4. The melting temperature was found to be 954.6 K instead of 943.7 K. Hence, a temperature shifting of -11 ^{o} was performed on every measure. On the other hand, the calibration of the latent heat of fusion was 8.13 cal/gram compared with a true value of 8.5 cal/gram.

Figure 9 gives a typical example of a DSC curve. The glass transition temperature is determined by a small endothermic deviation arising from the internal stress relaxation. The large exothermic peak is characteristic of crystallization. The area under the peak represents the energy lost by the material during the transformation to the more stable crystalline state.

4.4 Crystallization

The specimens for 4-point bend testing were crystallized at temperatures ranging from 550 to 700 ^{o}C for 12-16 hours. They were placed in BN tubes having twice the glass rod diameter. Since the crystallization temperature was higher than the glass transition temperature, the samples had time to deform before crystallizing. Therefore, the resulting glass-ceramic samples had an elliptical shape.

However, since the shape of the beams for the fracture toughness determination is important, these were crystallized in a stainless steel mold. The mold had to be coated with BN

to avoid reaction of the glass with the steel. The specimens were nucleated at 650 ^{o}C for 1/2 hr and then crystallized for 16 hours at 570 ^{o}C.

4.4.1 Unidirectional Crystallization

One of the special characteristics of calcium phosphate glass is that it tends to crystallize towards the stress direction [30]. As discussed earlier, Abe et al. showed that it was possible to grow unidirectional crystal fibres from one end of a glass rod to the other by passing it through a thermal gradient [31,32].

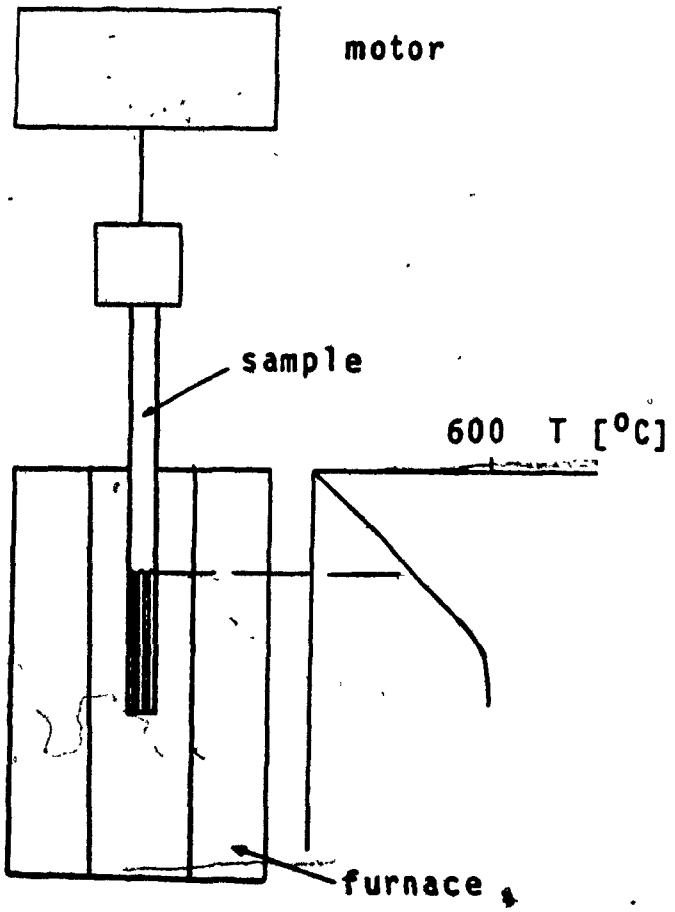

Figure 10: Apparatus designed for unidirectional crystallization.

An apparatus designed for unidirectional crystallization was built (Figure 10). The sample advance system was composed of a 1/10 HP electrical motor turning at 1530 RPM, a variable reducer ranging from 13 to 120 RPM, a worm gear having a 335/1 reducing ratio and a thread advancing at 0.5 mm/revolution. This gave an advance speed which was variable from 20 to 200 μm/min. The glass rod was pushed through a vertical tube furnace. The thermal gradient could be varied by changing the setting of the hot zone as illustrated in Figure 11.

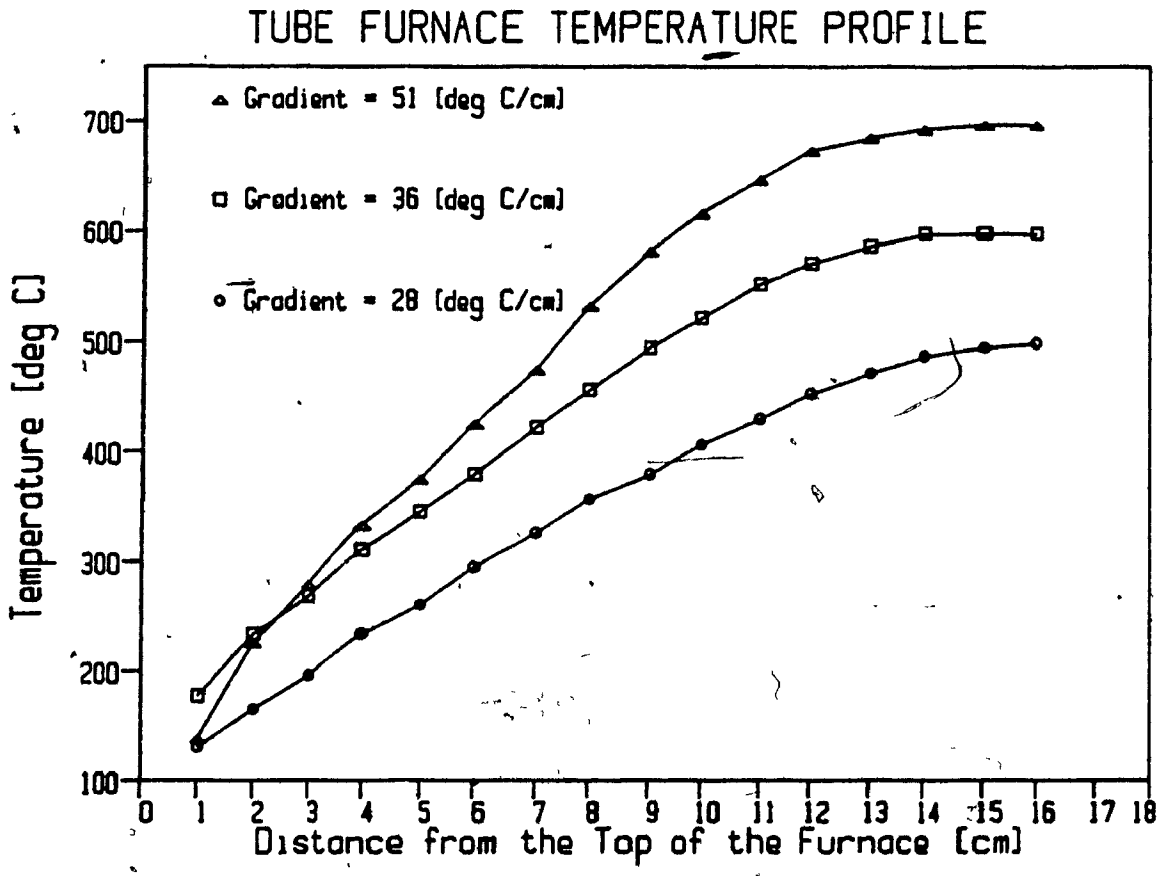

Figure 11: Temperature profile in the tube furnace for different hot zone temperatures.

The tip of the glass rod was first held at 650 °C until random crystallization took place, i.e. 30 minutes. The tip was then moved to the location corresponding to 450 °C and the advance system was turned on. This location depended on the setting of the furnace and, therefore, on the thermal gradient used.

The length of the specimens was 80 mm. Since the advance speed was set at 20 μm/min, 67 hours were necessary to achieve the complete crystallization of the sample. Furthermore, since unidirectional crystallization occurs somewhere between 450 and 560 °C (see section 3.2.3), time had to be given for the sample to reach the appropriate growing temperature. Therefore, the running time for each sample was 84 hours, i.e. three and a half days.

4.5 Ceramography

For conventional light microscopy, samples were ground using 120, 240, 400, and 600 grid silicon carbide paper. After ultrasonic cleaning, the samples were polished with 6 and 1 μm diamond paste. Different etching techniques were attempted, i.e. hot or cold hydrochloric acid, hydrofluoric acid, phosphoric acid or $HF-H_3PO_4$ mixtures, and high temperature etching, e.g. 700 °C for 30 min. None of these techniques resulted in preferential etching to reveal the microstructure.

Instead of diamond paste, alumina (5, 0.3, 0.05 μm) on a

thick soft cloth was tried. Alumina acted, at the same time, as a polishing agent and an etching agent. In fact the more the crystal fibre was perpendicular to the polished surface, the better it resisted abrasion. Similary, the more parallel to the polished surface the fibre was, the easier it was abraded away and hence, the microstructure was revealed (Figure 12). In order to ensure that the microstructure obtained was not due to the presence of a second phase, a microhardness profile of the sample was made. No correlation between the hardness scatter and the microstructure could be seen, confirming that the microstructure was only dependent on the crystal fibre orientation.

Figure 12: Microstructure of a calcium phosphate glass-ceramic obtained by alumina polishing.

Scanning electron micrographs were taken of fracture surfaces. The sides of the gold coated specimens were covered with silver paint and low acceleration voltages were used to avoid charging. The number on the left hand side of the scanning electron micrographs represent the length of the bar in microns.

4.4 Strength Measurements

4.4.1 Flexural Strength

Tensile testing is normally not used for the determination of the mechanical strength of ceramics [33]. The main reasons are the high fabrication cost of the tensile specimens and the requirement for extremely good alignment of the load train during testing. Poor alignment induces a bending moment, increasing the stress level on one side of the sample. Any flaw present on this face acts as a stress concentration factor and fracture of the specimen will originate at this flaw. Therefore, a large uncertainty is introduced in the measured strength.

Because of these problems, the characterization of a ceramic strength in bending is very common. The flexural strength or modulus of rupture (MOR) is measured either under three point or four point bending. The bend strength is calculated using the general flexure stress formula:

$$MOR = P\ a\ c\ /\ I \qquad (2)$$

where: P= failure load, N

a= distance from the supporting edge to the loading edge, mm

c= distance from the neutral axis to the surface in tension, mm

I= moment of inertia, mm^4

The advantages are that testing is quick and easy and the sample geometry is simple, i.e. square, rectangular or circular rod of uniform cross-sectional area. The severe limitation to this method is that the MOR depends on the size and the geometry of the specimen and whether 3-point or 4-point bending is used. The stress distributions in the different sample configurations are illustrated in Figure 13.

Although the volume of material under maximum stress is larger in the 4-point test than in the 3-point test, the best configuration for the stress distribution is the tensile test. The complete volume of the sample is under uniform tensile stress (provided the alignment is perfect). Therefore, the probability that the fracture will occur at the largest flaw is 100 %.

Since the equipment required to perform an accurate unfaxial tensile test is not commercialy available for ceramic testing, strength determination using the 4-point bending technique was chosen. A loading apparatus was built for

circular specimens, with 15 mm and 50 mm for the inner and outer spans, respectively; this is according to the ASTM standard C-158. All the strength data were collected using circular samples, 5 mm in diameter by 80 mm in length.

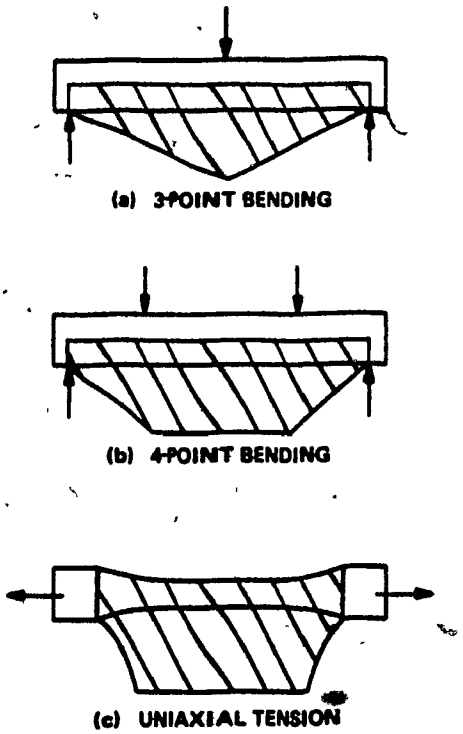

Figure 13: Stress distribution in a) 3-point bending specimen, b) 4-point bending specimen, and c) tensile specimen.

4.4.2 Statistical Treatment of Data

Ceramic strength measurements require an approach which takes into account both the flaw and stress distribution. The most commonly used method is Weibull's statistical approach [34] characterizing the scatter of the measurements and so determining the degree of confidence of the measured stress.

It is based on the "weakest link" theory which assumes that a given volume of ceramic under uniform stress will fail at the most severe flaw. With this condition, the probability of failure can be described by:

$$P_f = 1 - \exp f(S) \qquad (3)$$

where P_f = probability of failure

S = modulus of rupture

Weibull proposed an empirical relation for f(S). Since a better relationship to statistically describe the scatter in experimental data has not yet been found, it is still widely used and is as follows:

$$f(S) = -((S - S_u) / S_0)^m \qquad (4)$$

where S = measured stress

S_u = stress below which the probability of failure is 0

S_0 = stress at which the probability of failure is 0.632

m = Weibull modulus

The Weibull modulus (m) is the parameter that describes the flaw distribution and thus, the scatter of the data; the lower the Weibull modulus, the higher the scatter. Due to subcritical slow crack growth problems in ceramics, S_u is often set at zero.

Experimentaly, the probability of failure (P_f) is associated with the measured strength, and can be calculated using:

$$P_f = n / N+1 \qquad (5)$$

with: n = the ranking of the sample

N = the total number of samples tested

The Weibull modulus, m, can then be determined by plotting ln ln $(1/(1-P_f))$ versus ln (S). The resulting plot should be a straight line of slope, m.

The accuracy of the Weibull modulus is determined by the number of specimens tested. Due to the large scatter of the measured strength, large number of samples have to be tested. A Weibull modulus determined with 10 bend samples will have an accuracy of $\pm$40% [35]. To decrease this value to $\pm$10%, 300 samples should be tested.

Weibull reports a value of m=3 for the measurements of the yield strength of a steel [34]. This low value indicates a very substantial scatter. Such a low Weibull modulus is perfectly acceptable for the measurements of the yield strength of a steel since, even if this stress is exceeded, failure of the sample will not occur. This is not true in the case of ceramics. If the stress applied to a ceramic sample reaches the order of magnitude of the measured strength,

dramatic failure of the sample is likely to occur. Since the probability for such a failure to occur is inversely proportional to the Weibull modulus, high Weibull moduli are required for the strength measurements of ceramics, i.e. greater than 10.

4.5 Fracture Toughness Measurments

4.5.1 Vickers Indentation Technique

Development of radial cracks around Vickers indentation in brittle materials has long been noticed. The cracks were first regarded as a nuisance to effective hardness measurements. However, in 1962, Palmqvist [36] showed that this was not the case, and that it was even possible to empirically correlate the fracture toughness of a material to the crack length. More recent studies [37,38] developed a theory describing the crack propagation under a sharp indenter and related it to the fracture toughness. The advantages of such a technique are: a) many tests can be performed on a small sample not suitable for conventional fracture toughness tests, and b) the ease, simplicity and short time required for testing.

The fracture mechanics analysis is based on the propagation of a penny-like crack (Figure 14) which forms

below the indenter. The general complexity of the elastic/plastic contact field description [38] led to the development of semi-empirical models relating the fracture toughness, K_c, the hardness, H, the crack length, c, the indentation diagonal, a, the constraint factor, $\emptyset$, (about 3 for Vickers indenter), Poisson's ratio, v, the friction between the indenter and the material, u, and the plastic zone radius, R_y [39].

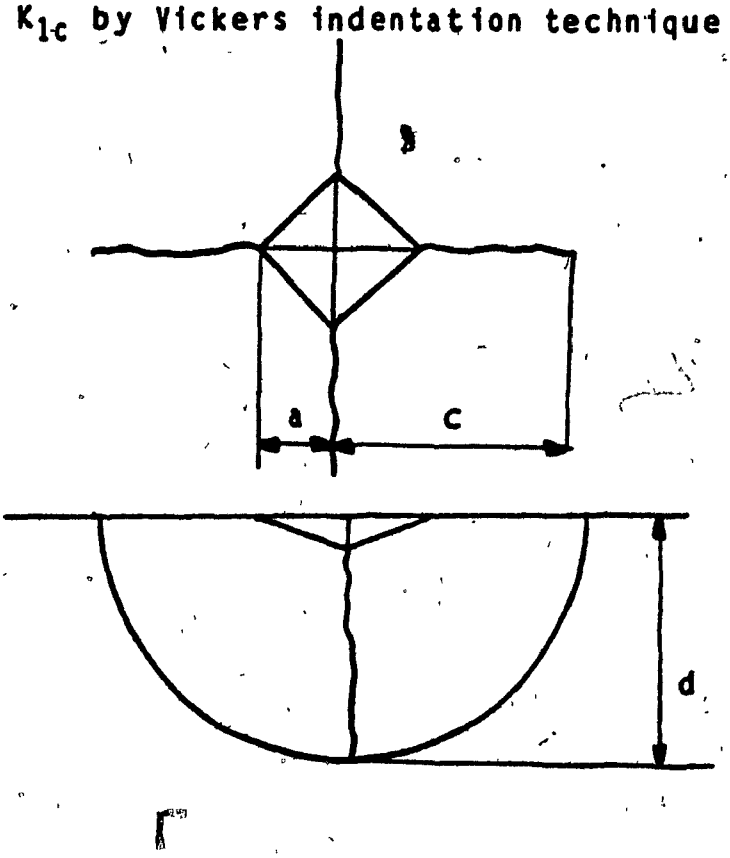

Figure 14: Vickers indentation technique a) crack length at the indentation corners b) half penny like crack.

Initial experimental studies indicated that the fracture toughness was strongly dependent on the ratio c/a, but was not affected by v and u. A correction taking into account the residual stresses left by the indenter and the plastic zone had to be introduced in terms of hardness to elastic modulus ratio, H/E. The following relation [39] was obtained:

$$K_c \, \emptyset \, / \, H \, a^{1/2} = 0.45 \, (c/a)^{-3/2} \, (H \, / \, \emptyset \, E)^{0.4} \qquad (6)$$

Evans [37] has further rationalized this argument and has obtained a more precise relation by using a polynomial curve fitting:

$$\log [(K_c \, \emptyset \, / \, H \, a^{1/2}) \, (H \, / \, \emptyset \, E)^{0.4}] = \qquad (7)$$
$$-1.59 - 0.34 \, X - 2.02 \, X^2 + 11.23 \, X^3 - 24.97 \, X^4 + 16.32 \, X^5$$

where $X = \log (c/a)$

Two conditions have to be fulfilled for this technique to be valid: a) a half penny-like crack has to be developed so that the crack length, c, is representative of the crack depth, d; b) the c/a ratio has to be greater than 2 to ensure that the crack crosses the plastic deformation zone. Residual stresses at the surface of the specimen, i.e. due to machining or fast cooling rates, are known to seriously affect the fracture toughness measurement. Evans [39] estimated the precision of a fracture toughness determined by Vickers indentation technique to be within 10 % if the elastic modulus

and, therefore, $(H/\emptyset E)^{0.4}$ is known and within 40 % if it is not known. A study of silicon carbide [40] indicated a value which was 30 % lower for the Vickers indentation technique compared to the value obtained by the single edge notched beam technique, SENB, even if the elastic modulus was known.

In the present study, specimens used for the fracture toughness determination were annealed, ground and then carefully polished down to 0.05 μm alumina. Some of the specimens were tested, annealed, and retested to determine the effect of the residual surface stresses left by the polishing.

4.5.2 Single Edge Notched Beam Technique

Fracture toughness (K_{1c}) determination using the single edge notched beam technique was carried out. The specimens were tested in 3-point bending according to standard ASTM E399; an illustration of the test configuration is given in Figure 15. The main requirements of this standard are:

a) The thickness of the specimen, B, and the notch plus crack length should both be larger than $2.5\ (K_{1c}/MOR)^2$.

b) A fatigue crack should be generated at the tip of the notch. The notch plus crack length should be between 0.45 and 0.55 times the width of the specimen, W.

c) A load-displacement curve has to be monitored to determine the load to be used for the fracture toughness calculation. It also determines the validity of the test.

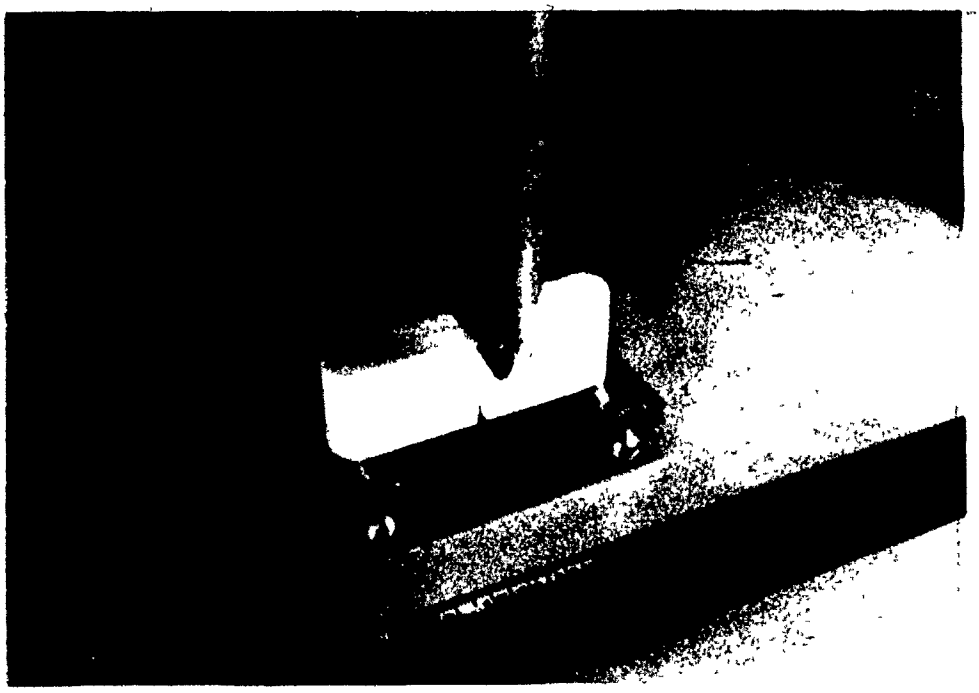

Figure 15: Test configuration for the fracture toughness determination using a single edge notched beam.

The fracture toughness, K_{1c}, is calculated using the following relationship:

$$K_{1c} = (P_q \; S \; / \; B \; W^{3/2}) \; f(a/W) \qquad (8)$$

where:

$$f(a/W) = \frac{3(a/W)^{1/2}[1.99-(a/W)(1-a/W)(2.15-3.93a/W+2.7a^2/W^2)]}{2(1+2a/W)(1-a/W)^{3/2}}$$

and K_{1c} = Fracture toughness, MPa $m^{1/2}$

P_q = Suitable load, N

S = Span between the loading and support edge, m

B = Thickness of the specimen, m

W = Width of the specimen, m

a = notch + fatigue crack length, m

The suitable load is usually 0.2% yield load for metals; since there is usually no yielding in ceramics, the breaking load is used.

4.6 Tribological Study

The coefficient of friction in a healthy synovial joint is very low, i.e. 0.01. This an essential requirement for the bearing of a joint prosthesis since it dissipates less muscular energy and minimizes the reaction stresses at the bone-prosthesis interface. The wear rate should also be as low as possible since adverse biological reactions may result as a consequence of a modest amount of wear debris.

A hip joint is subjected to a very complex system of loading, movement and environmental conditions [45]. Although joint simulators have been developed, it is essential to be able to determine the tribological behavior of any potential biomaterials so that only the more promising combinations undergo the more rigorous examination provided by the simulation technique. Many simplified apparatus have been built for this reason, e.g. disk on flat, annulus on flat, pin on disk, and pin on flat; they are reviewed by K. Wright [46].

In a study involving a Co-Cr-Mo pin on a ultra high molecular weight polyethylene (UHMWPE) disk [47], it was noticed that the wear tracks were parallel to one another when the pin was stationary, and randomly oriented and similar

to that observed in a hip prosthesis with a rotating pin. Therefore, it was decided to built a wear apparatus with a rotating pin on a reciprocating plate (Figure 16).

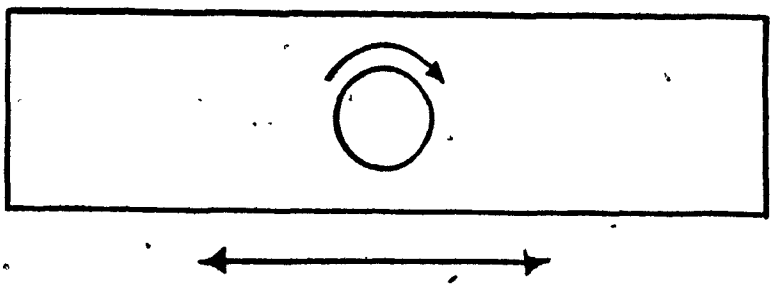

Figure 16: Schematic of a rotating pin on a reciprocating plate.

A reciprocating plate rather than a rotating disk was chosen because it reproduces more closely the alternate motion of a hip joint. It was also more convenient to produce long rectangular counterfaces than circular ones. The sliding distance was 50 mm and the plate was reciprocating at 1 cycle/s. The load on the pin was 250 N, corresponding to a contact stress of 9 MPa. This stress is higher than the mean contact stress in a hip joint, i.e. 5 MPa, but is still reasonable since, during walking, the peak stress reaches 15 MPa [46]. The pin was also rotating at 1 cycle/s. The tests were carried out in saline solution, i.e. 3.7 g of iodized salt in 500 ml water.

Three different combinations of materials were tested: a) UHMWPE - Co-Cr alloy (Vitallium), b) UHMWPE - high density alumina, and c) UHMWPE - calcium phosphate glass. The pin material was always polyethylene. The pin, the Vitallium and the glass were polished down to 0.05 um using alumina polishing powder. The alumina was polished down to 1 um with diamond paste. The pins were presoaked overnight to avoid water absorption and weighed regularly to determine the wear losses. The three material combinations were tested for up to 70×10^5 cycles.

Chapter 5

RESULTS AND DISCUSSION

5.1 Crystallization Study

The crystallization behavior of the different glasses was first studied using a Differential Scanning Calorimeter (DSC). The glass transition and the crystallization peak temperatures, as well as the activation energy were determined. An attempt to define the optimum nucleation temperature was also carried out by DSC.

Bulk samples were used to determine the maximum nucleation temperature and the optimum crystal growth temperature. The resulting microstructures will be discussed.

5.1.1 DSC Study

5.1.1.1 Glass Transition and Peak Crystallization Temperatures

The effects of the addition of a third phase to calcium phosphate glass on the glass transition and the crystallization peak temperature were investigated by DSC. Alumina (Al_2O_3) and zirconia (ZrO_2) were added as a strengthening phase and a nucleating phase, respectively; the results are listed in Table XII.

The glass transition temperature found for the calcium phosphate glass having a molar ratio Ca/P=0.5 (i.e CaO/P_2O_5 = 1) is significantly higher than that found by Abe et al. [29].

There are two reasons which can be given to explain this discrepency. First, the difference in techniques used to determine T_g, since Abe used thermal expansion curves. Secondly, the fact that, in this technique, the value of T_g is dependent on the heating rate. Abe reports a value of T_g of 510 ^oC (compared to 550 ^oC in the present study) with the indentical heating rate of 10 ^oC/min. Yamamoto [41] made a systematic study of the determination of the glass transition temperature for nine commercial glasses using viscometric and DTA techniques. T_g values determined by DTA were always consistantly 10-35 ^oC higher than those determined by the viscometric technique. Therefore, the discrepencies in T_g's observed here and in other studies are within the expected range when comparing the two different techniques.

Table XII: Glass Transition and Crystallization Peak Temperatures of Calcium Phosphate Glasses Doped with Alumina and Zirconia.

Material	Glass Transition ^oC	Crystallization Peak ^oC
Ca/P=0.5	550	665
1% ZrO_2	548	702
1% Al_2O_3	547	697
2% Al_2O_3	551	712
5% Al_2O_3	570	761

Furthermore, for glasses of the phosphate group, T_g is lowered by the presence of residual hydrogen or hydroxyl groups [42]. Therefore, the glass prepared in this study may have less combined water than the one prepared by Abe et al..

The glass transition temperature is the temperature at which molecular motion becomes sufficient to allow stress relaxation to occur. Addition of small amounts of Al_2O_3 or ZrO_2 (e.g up to 2 wt %) did not change T_g. This indicates that the structure and bonding in the glass are not altered significantly by these levels of addition and so do not change the thermal properties and viscosity of the glass. For higher percentages of alumina, the increase of T_g could indicate that Al_2O_3 is affecting the structure of the glass by introducing stronger and more stable bonds. In fact, according to the ternary phase diagram, additions of Al_2O_3 to calcium phosphate promote the formation of the Al_2O_3-P_2O_5 compound, which has a higher melting point (1450 ^oC) than CaO-P_2O_5 (980 ^oC).

On the other hand, the crystallization peak temperature always increased in the presence of Al_2O_3 or ZrO_2 even for small additions (< 5 Wt %). This could be explained by the fact that alumina as well as zirconia are very stable oxides which tend to increase the stability of the glass. Therefore, the activation energy necessary to crystallize the glass should be higher. The gradual increase in the crystallization peak temperature with an increasing presence of additives indicates that the more stable the glass is, the more thermal energy is required for crystallization to take place.

5.1.1.2 Activation Energy

The activation energy of a phase transformation is defined by the Arrhenius equation:

$$V = V_0 \exp(-Q / R T) \quad (9)$$

with: V = crystal growth rate, μ/min

V_0 = constant, μ/min

Q = activation energy, cal/mole

R = gas constant (1.98 cal/mole K)

T = absolute temperature, K

Taking the natural logarithm of equation (9) gives:

$$\ln(V) = \ln(V_0) - Q / R T \quad (10)$$

From equation (10), by plotting the logarithm of the crystal growth rate, V, versus the inverse of the absolute temperature, 1/T, a straight line is obtained, with the slope representing the activation energy Q.

Pure calcium phosphate glass was ground and sieved to obtain a size distribution between 150 and 212 μm. Isothermal DSC runs were made at 640, 650, 660 and 677 °C. To determine the crystal growth rate, the following assumptions were made:

a) all the powder particles were spheres having a diameter of 181 μm,

b) nucleation occurred only at the surface of the particle,

c) the crystal growth rate was constant throughout the experiment,

d) at the crystallization peak time, one quarter of the diameter was crystallized.

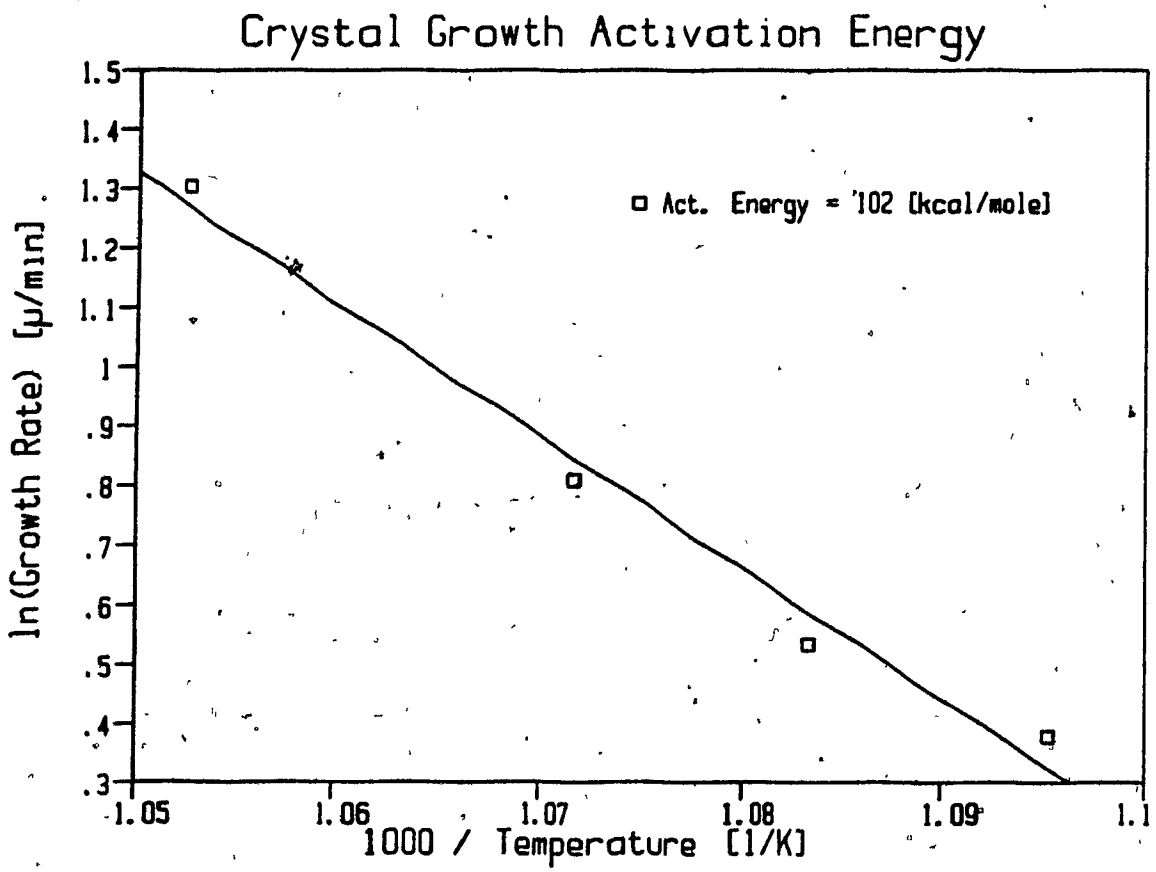

Figure 17: Arrhenius plot for the determination of the crystallization activation energy of calcium phosphate glass above T_g.

The activation energy for crystal growth above the glass transition temperature was found to be 102 kcal/mole (Figure 17). This value is in good agreement with that found by Abe et al. [29]. Since this value is similar to the energy needed to break the phosphorus-oxygen bond, it is thought that crystallization occurs by breaking and rearranging these atomic bonds.

5.1.1.3 Optimum Nucleation Temperature

The determination of the optimum nucleation temperature in silicate glasses using DTA curves has been demonstrated by Marotta et al. [43]. The total number of nuclei per unit volume is equal to the sum of nuclei formed during the DTA run (N_h), nuclei formed during a previous nucleation heat treatment (N_n) and the number of heterogeneous bulk nuclei (N_c). Using the Johnson-Mehl-Avrami equation [48,49] describing nucleation and crystal growth, it is possible to show that if the DTA runs are carried out on samples with the same specific surface area and at the same heating rate, the sum of nuclei formed during the DTA run is constant. For a previously nucleated sample, it is described by equation (11).

$$\ln (N_o + N_n) = (Q / R T_p) + K \qquad (11)$$

with: N_o = number of nuclei formed during the DTA run

N_n = number of nuclei formed during previous heat treatment

T_p = crystallization peak temperature for a nucleated sample, K

Q = activation energy, cal/mole

R = gas constant, cal/mole K

K = constant

For an as-quenched sample (N_n=0) equation (11) becomes:

$$\ln (N_o) = (Q / R T_{pq}) + K \qquad (12)$$

with: T_{pq} = crystallization peak temperature for an as-quenched sample

From (11) and (12) the following equation can be obtained:

$$\ln ((N_o + N_n) / N_o) = (Q/R) \quad (1/T_p - 1/T_{pq}) \qquad (13)$$

It is possible to assume that N_n is much greater than N_o since the glass is quenched and only surface nuclei are generated during the nucleation heat treatment. The number of nuclei, N_n, is related to the length of the nucleation period, t, by:

$$N_n = I\ t^b \qquad (14)$$

with: I = the rate of nucleation

b = a parameter related to the nucleation mechanism

Hence, if all the samples having the same specific surface area, are held the same time at the nucleation temperature and are submitted to the same heating rates, the following approximate equation can be obtained from (13) :

$$\ln I = (Q / R) (1/T_p - 1/T_{pq}) + K' \qquad (15)$$

where K' is a constant.

So, by plotting $(1/T_p - 1/T_{pq})$ versus the temperature of nucleation, T_n, a bell-type curve is obtained, with the maximum indicating the optimum nucleation temperature (see Figure 18a).

Calcium phosphate glass was quenched into a small cold boron nitride mold and subsequently ground and sieved to achieve a particle size distribution between 100 and 125 μm. Three DSC runs on as-quenched specimens were performed to precisely determine the crystallization peak temperature, T_{pq}. The other samples were brought rapidly to the different nucleation temperatures (ranging from 520 °C to 610 °C) with a heating rate of 80 °C/min to minimize the formation of nuclei during heating. They were held at this temperature for 1 hour and then a DSC run was performed with a heating rate of 10 °C/min.

Two series of experiment were made: a) twelve samples of pure calcium phosphate and b) nine samples with an addition of one percent of zirconium oxide. Both resulted in the type of curves shown in Figure 18b.

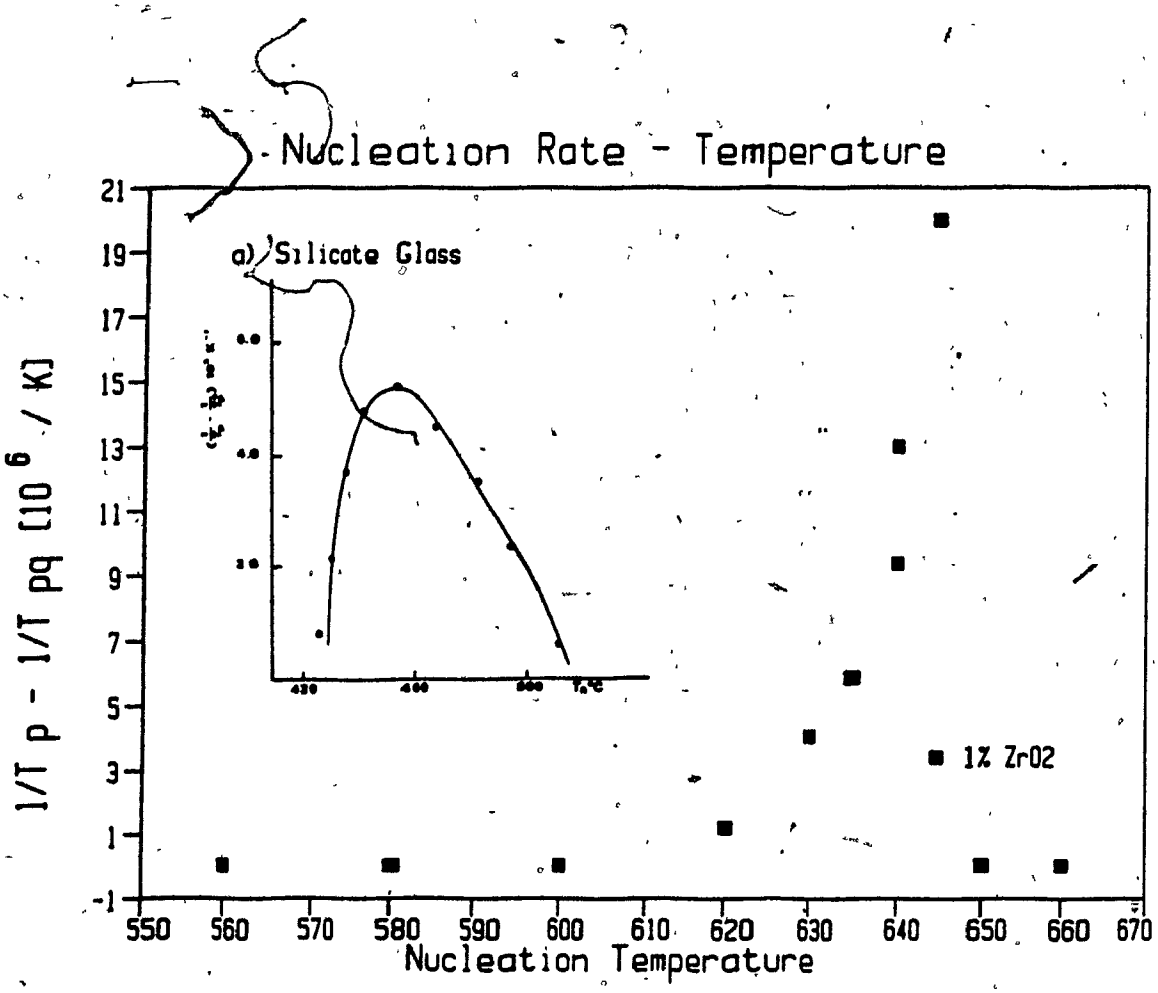

Figure 18: Nucleation rate versus temperature curves: a) ideal situation [43] b) calcium phosphate glass containing 1% ZrO_2.

The type of curve obtained in Figure 18b is due to the fact that it was not the nucleation rate that was being measured but rather the progressive crystallization of the sample which was occurring during the so-called "nucleation period". This glass has the property of crystallizing at, or even below, the glass transition temperature. Therefore, instead of forming nuclei only, partial crystallization of the particles also occurred. This behavior was further reflected by the decrease of energy involved in crystallization during

the DSC runs. The more crystalline the sample became during the nucleation period, the less driving force was available for crystallization during the actual crystallization run.

Since both significant nucleation and crystal growth can occur within the same range of temperature, it is concluded that the technique to determine the optimum nucleation temperature by thermal analysis is not applicable to calcium phosphate glasses.

5.1.2 Random Crystallization

5.1.2.1 Nucleation

To study the nucleation behavior, calcium phosphate ($Ca(PO_4)_2$) glass was melted at 1100 ^{o}C and poured into a cold boron nitride mold. The resulting glass samples were held at different nucleation temperatures, ranging from 550 to 700 ^{o}C for 10 minutes. The nucleated samples were then placed in a furnace at 540 ^{o}C for 18 hours for crystallization. This low temperature was chosen to avoid the formation of new nuclei during the crystallization heat treatment. A thin layer was then removed from each of the resulting glass-ceramic specimens which were subsequently polished with 0.05 μm alumina. The removed layer was found to be less than 0.5 mm in thickness. This procedure allowed observation of the

microstructure and estimation of the number of the nucleation sites.

Figure 19 shows that nucleation only occurs at the surface of the specimens. If the number of nuclei per unit area is small, every growing crystal has time to develop in every direction around it before being arrested due to impingement on another growing crystal; the result is the formation of hemispherulitic crystals. Therefore, by removing a small layer at the surface, it is possible to observe the radial growth of the crystal from the nucleation centres. This is shown in Figure 20. The size of the crystals is related to the number of nuclei; the larger the diameter of the fan-like crystal, the fewer the number of nuclei formed during heat treatment.

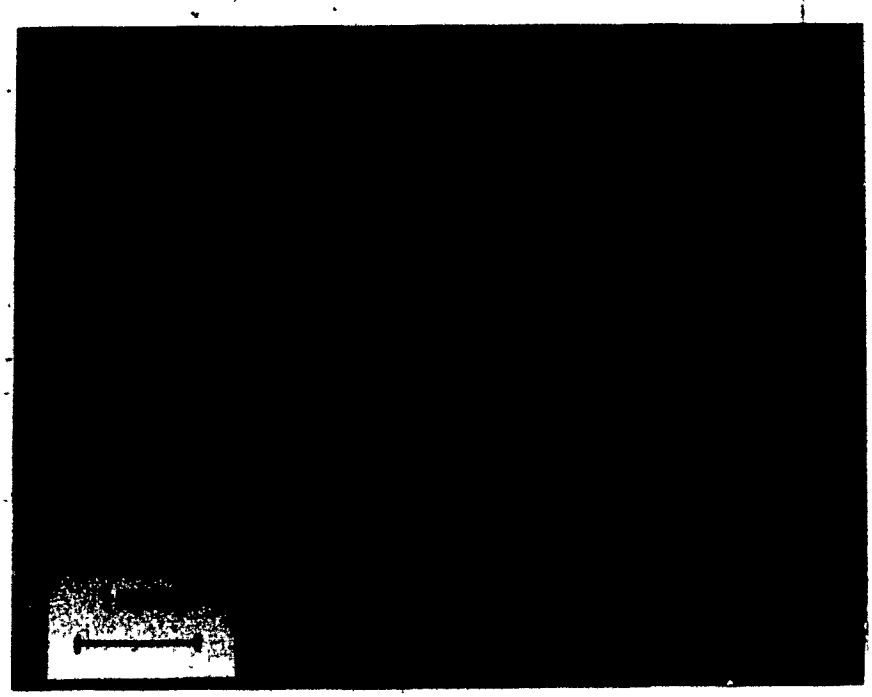

Figure 19: Surface nucleation in calcium phosphate glass, with fan-like crystals around the nucleation centre.

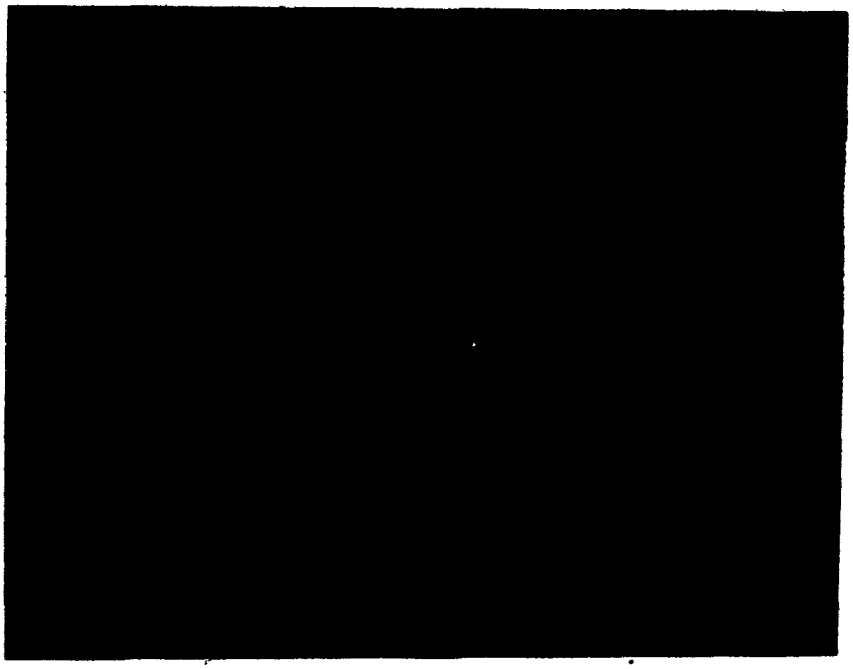

Figure 20: Calcium phosphate glass-ceramic showing large fan-like crystals due to a small number of nuclei. (nucleation: 570 ^{o}C /10 min; crystallization: 540^{o}C/18 hours).

If the number of nuclei per unit area is large, the growing crystal will not have time to grow radially since it will be rapidly blocked by the adjacent growing crystals. The only remaining free path for growth is towards the centre of the specimen. Hence, each crystal fibre bundle perpendicular to the surface is associated with one nucleation site (see Figure 21). The size of these bundles is also related to the number of nuclei; so, the smaller the bundles, the higher the nucleation rate during the heat treatment.

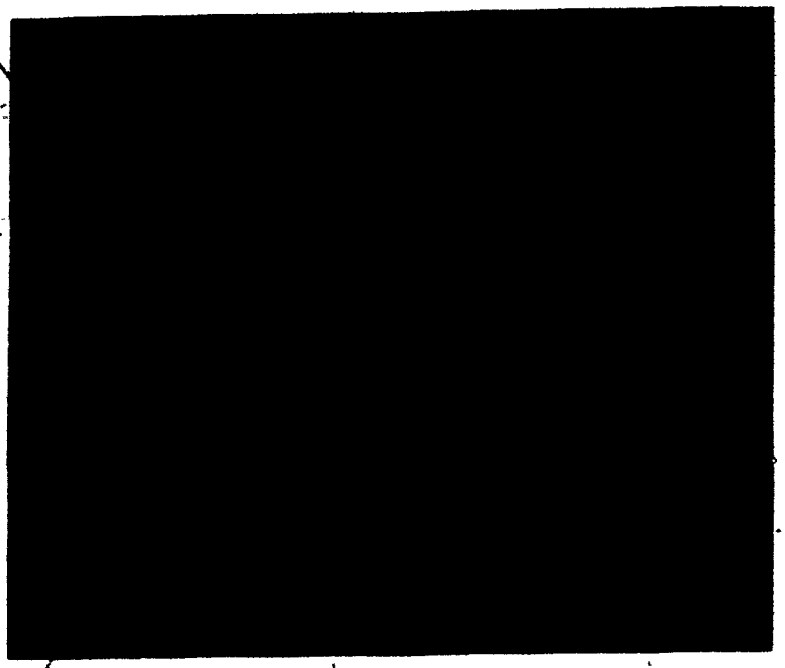

Figure 21: Calcium phosphate glass ceramic showing crystal bundles growing towards the centre of the specimen arising from a large number of nuclei. (nucleation: 650 °C; crystallization: 540 °C).

The optimum nucleation conditions were found to be in the temperature range of 630 to 670 °C. Above 670 °C the crystal growth rate is very high, so that as soon as a nucleus is formed, a large crystal is quickly developed. Hence, the surface is rapidly crystallized with the result that any further nucleation is arrested. Below 630 °C the nucleation rate is too slow to form many nuclei so that during the crystallization heat treatment, large fan-like crystals are developed. With a decreasing number of nuclei, the size of the fibre bundles increases up to the point where they start to turn into fan-like crystals (see Figure 20). Since all the samples were maintained at each of the nucleation temperatures

for the same time , i.e. 10 minutes, it is possible to conclude that the optimum nucleation rate is between 630 and 670 ^{o}C.

5.1.2.2 Crystallization

The major phase present in the glass-ceramic is beta calcium phosphate. Small peaks characteristic of the metastable gamma phase can be seen on the X-ray pattern. This gamma phase tends to disappear if the heat treatment is sufficiently long.

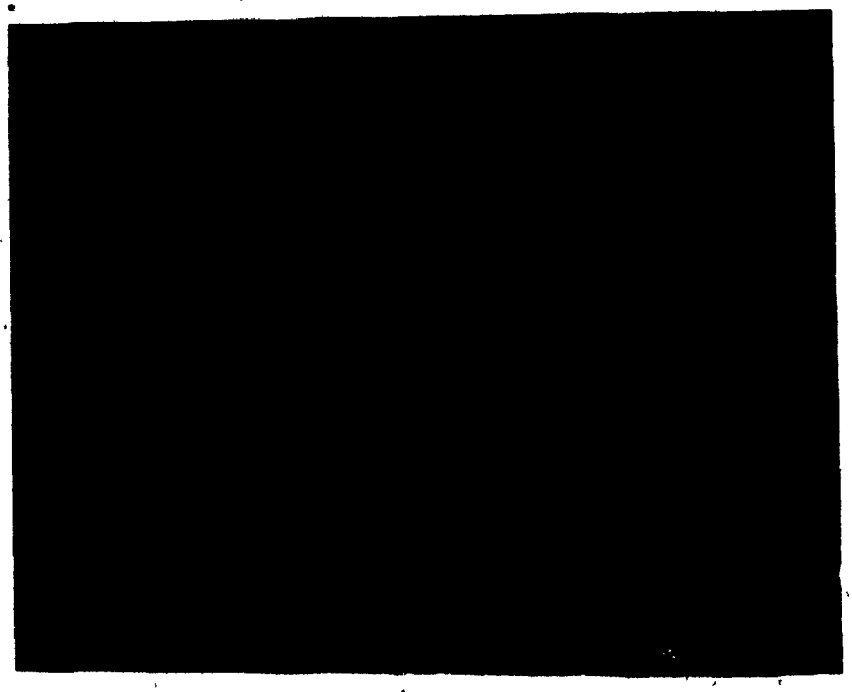

Figure 22: Calcium phosphate crystal fibrils grown at 570 ^{o}C for 15 hours.

The crystals grown close to T_g, i.e. 570 ^{0}C, have a typical fibrous structure. Figure 22 shows that hundreds of little fibrils, about 1 μm in diameter, grow parallel to one another to form fibre bundles. Since nucleation only takes place at the surface of the specimen, the growing crystal bundles first form a hemispherulite. The crystals growing parallel to the surface are then restrained by the growth of adjacent crystals. The bundles growing perpendicular to the surface keep growing until they cross the complete section of the specimen, as illustrated in Figure 23, or meet a growing crystal originating from the opposite surface.

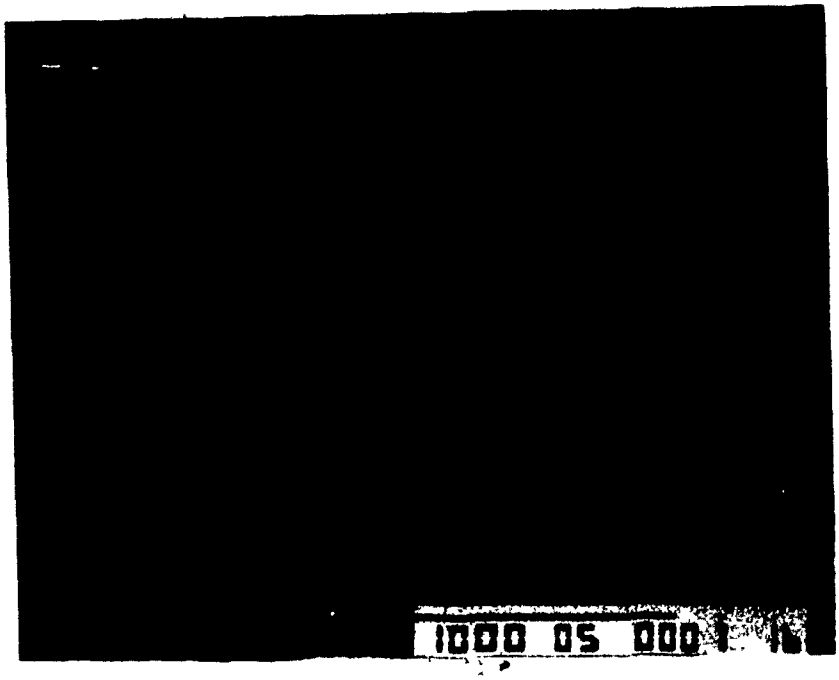

Figure 23: Crystal fibres arising from one nucleus crossing the complete section of a four point bending sample (fracture surface, T_c = 570 ^{0}C for 15 hours).

If a high crystallization temperature (with respect to the glass transition temperature, i.e. 550 ^{o}C) of 650 ^{o}C is employed, excessive deformation of the sample occurs because of the rapid decrease in viscosity of the glass at temperatures above T_g. The crystallization of the surface creates a rigid shell which stops any further deformation, but since the crystal is more dense than the glass, pores must form to compensate for the shrinkage (see Figure 24). The pores are usually situated on the edge of the fibres, thus decreasing the inter-fibre cohesion. They also tend to block the uniform growth of the fibres, thus generating a structure composed of small needle-like crystals as shown in Figure 25; this results in a significant loss of strength in the glass-ceramic (see Section 5.2.2).

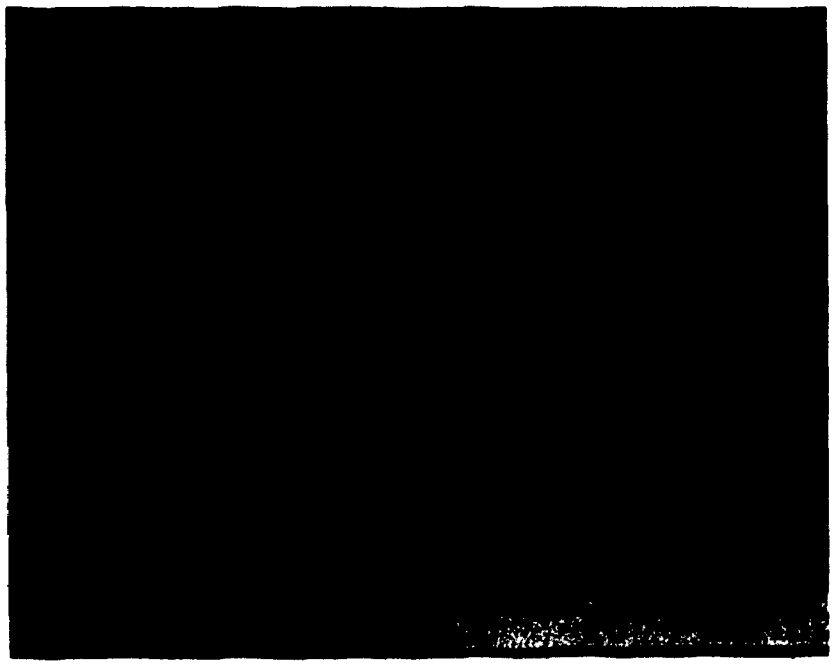

Figure 24: Calcium phosphate crystals grown at 650 ^{o}C showing extensive inter-needle porosity (fracture surface).

The glass-ceramic crystallized at a temperature close to the glass transition temperature, e.g. 570 °C, does not exhibit such porosity. This could be explained in terms of viscosity. Around T_g, the viscosity of the glass is still very high; hence, even if the ceramic is denser than the glass, the glass is too viscous to flow and to allow pore formation. At T_g + 100 °C, the viscosity has drastically been decreased so that the glass can easily flow to allow pore formation. This process is also favored by the fact that the glass density is higher at T_g than at T_g + 100 °C. Therefore, the difference in volume between the glass and the crystal becomes smaller and the driving force for pore formation decreases.

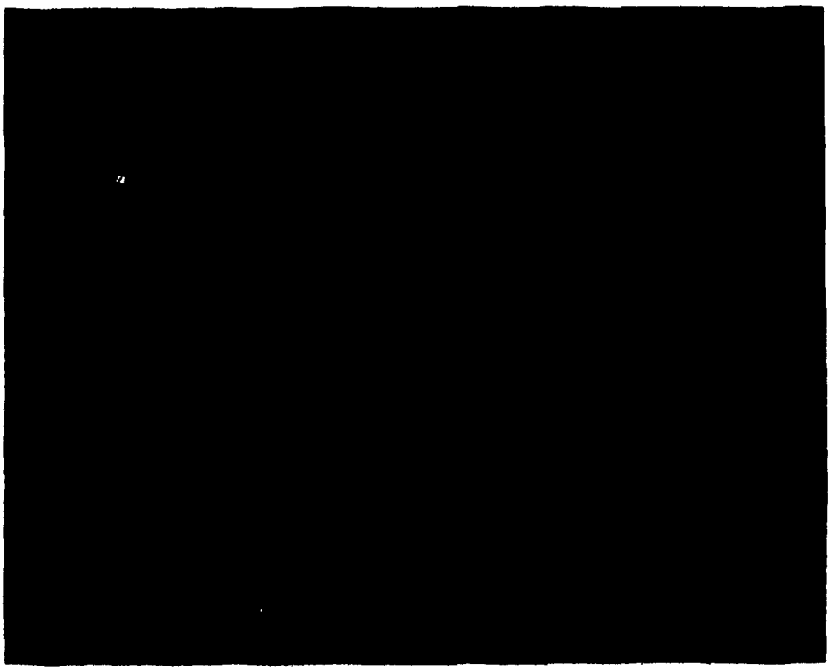

Figure 25: Calcium phosphate crystal fibre grown at 650 °C interrupted by porosity (fracture surface).

5.1.3 Unidirectional Crystallization

Unidirectional crystal fibres were grown using a thermal gradient of 30 ^{o}C/cm (with hot zone of 550 ^{o}C) and an advance speed of 20 μm/min; the microstructure is shown in Figure 26. The unidirectional crystal growth occurs from the high temperature to the low temperature regions of the furnace. Each fibre is composed of several hundreds of fibrils (about one micron in diameter), all growing parallel to one another (Figure 27). The thermal gradient tends to straighten the molecular chains in the glass giving an easy path for the growth of crystal fibres. This process is also favored by the stress induced at the glass-crystal interface [31]. This stress arises from the difference in density of the glassy and the crystalline phases.

The two major problems with unidirectional crystallization are the long time required to crystallize a relatively small sample (84 hours for a 80 mm sample), and the sensitivity of the process to the experimental conditions, i.e maintaining a sufficiently steep thermal gradient without having too high a temperature that could induce surface nucleation.

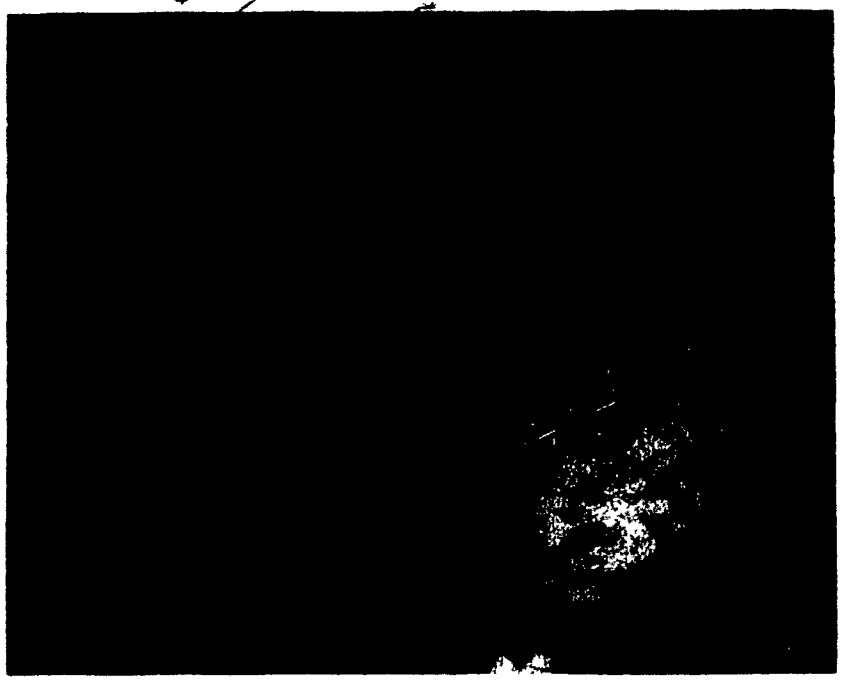

Figure 26: Fracture surface of a unidirectional fibre. The axis of growth is perpandicular to the surface.

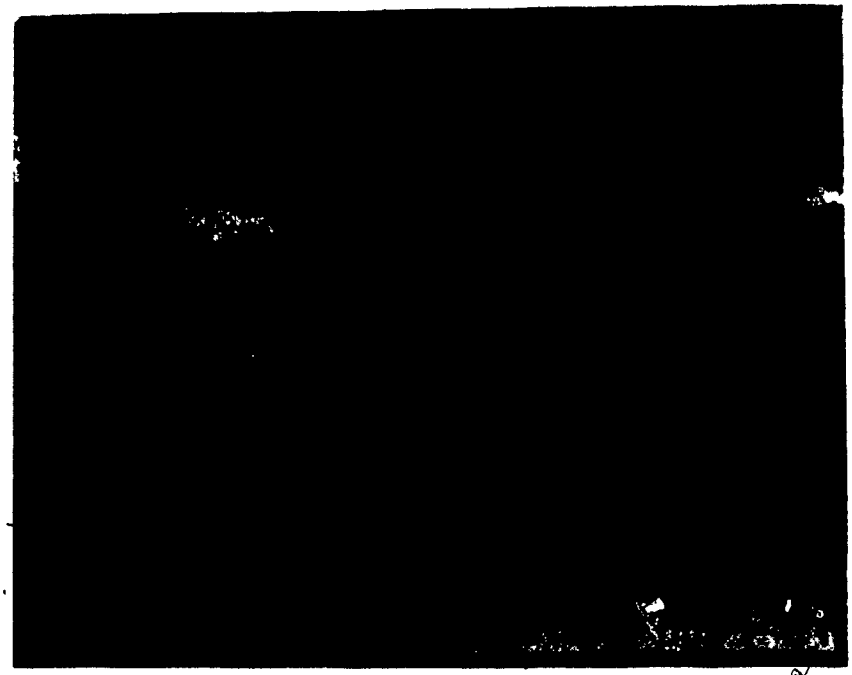

Figure 27: Unidirectional fibre showing small fibrils growing parallel one another. The axis of growth is in the plane of the page.

The temperature range where unidirectional crystallization occurs depends strongly on the chemical composition of the sample. Abe et al. [32] showed that this temperature range is from 540 to 560 ^{o}C for a molar ratio of CaO/P_2O_5 = 1 and from 450 to 560 ^{o}C for a molar ratio of 0.9. Infact, with a glass having a ratio of 1, unidirectional crystals greater than 10 mm were never obtained in the present study. However, for glass having a ratio of 0.9, crystals up to 40 mm in length were produced.

Several explanations are suggested for the poor success of the unidirectional crystallization experiments: (a) it is difficult to avoid the formation of new nuclei on the surface of the specimen in front of the glass-crystal interface since both nucleation and crystallization can occur within the same temperature range. Any crystal growing in front of this interface will cause the unidirectional fibre to stop when it reaches the newly nucleated surface crystal. (b) Each advance speed corresponds to a very narrow temperature range where unidirectional crystallization can occur. So any variation of the temperature in the furnace could cause this critical temperature to lag behind the crystal front, arresting unidirectional crystal growth. (c) Correspondingly, if the crystal growth rate is slower than the advance speed, the glass-crystal interface will progress towards the higher temperature region where the thermal gradient becomes lower. Therefore, the driving force for crystallization is decreased, at the same time lowering the crystal growth rate. This

process continues until unidirectional crystallization is completely stopped and is replaced by random crystallization. (c) Any variation of the advance speed (e.g. due to a line voltage drop) would also interfere with unidirectional crystallization.

More successful unidirectional crystallization might be achieved by having a linear thermal gradient up to the centre of the furnace. The driving force would be constant and the furnace could, therefore, be set at the actual crystallization temperature. This way, any nucleation of the specimen during the heat treatement could be avoided.

5.2 Glass and Glass-Ceramic Strength

The modulus of rupture of pure calcium phosphate glass was first determined and then the effect of crystallization on the mechanical properties was investigated.

5.2.1 Glass Strength

The elastic modulus of the glass was determined using the ultrasonic technique. However, this method was not used for the glass-ceramic since it is only valid for isotropic materials. The Young's modulus of the glass was found to be 57 $\pm$ 2 GPa. This is very satisfactory since it is closer to the elastic modulus of bone than conventional biomaterials, i.e. bone, E = 17 GPa; stainless steel, E = 210 GPa; high density alumina, E = 400 GPa.

Four-point bend tests were conducted on three types of samples: a) quenched; b) annealed and, c) annealed + sandblasted. For the quenched specimens, glass was cast into a cold boron nitride mold, which resulted in rapid freezing of the molten glass. For the annealed samples, the glass was poured into a preheated (560 ^{o}C) boron nitride mold followed by careful annealing at the same temperature for 10 minutes. In addition, a number (10) of the annealed specimens were sandblasted prior to testing. Calibrated silica sand was used; its size distribution is given in Figure 28.

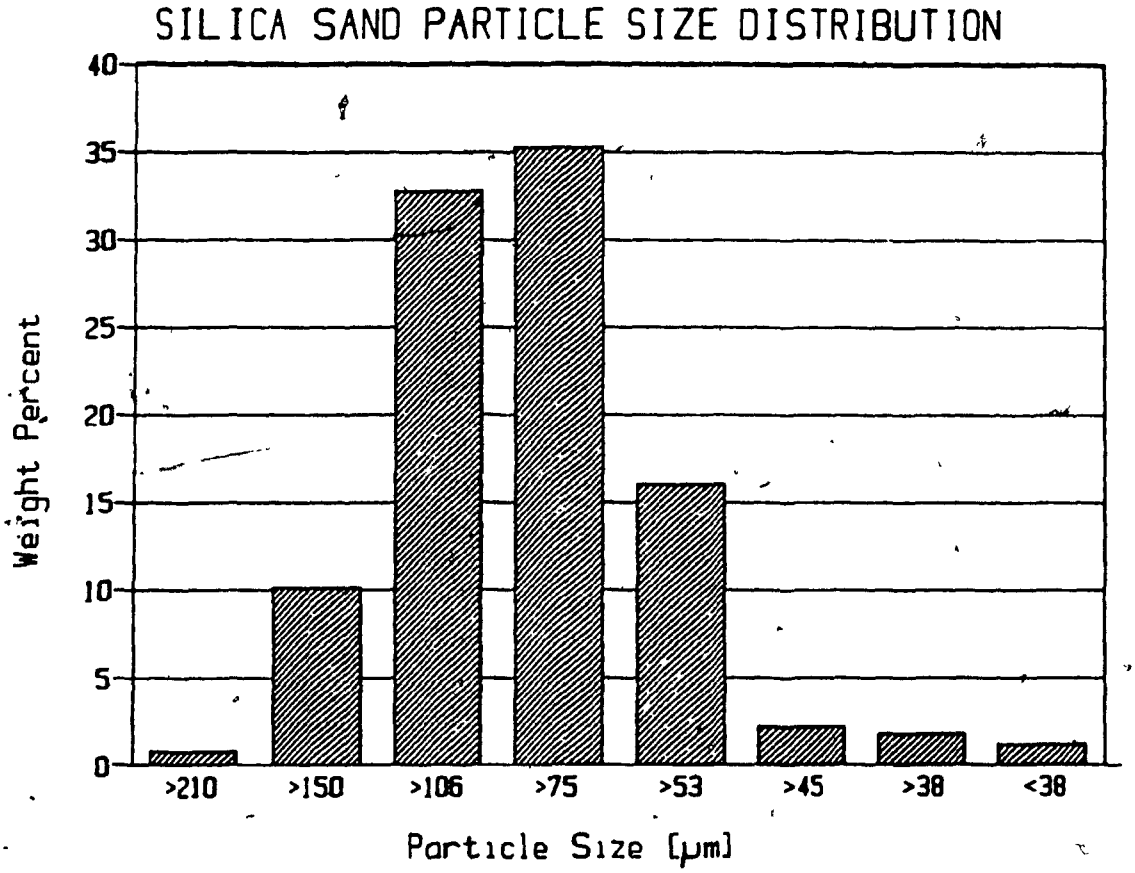

Figure 28: Particle size distribution of silica sand used for sandblasting specimens.

Table XIII gives the number of specimens tested, the modulus of rupture with its standard deviation and the Weibull modulus. Examples of the plots to determine the Weibull moduli are given in Figure 29.

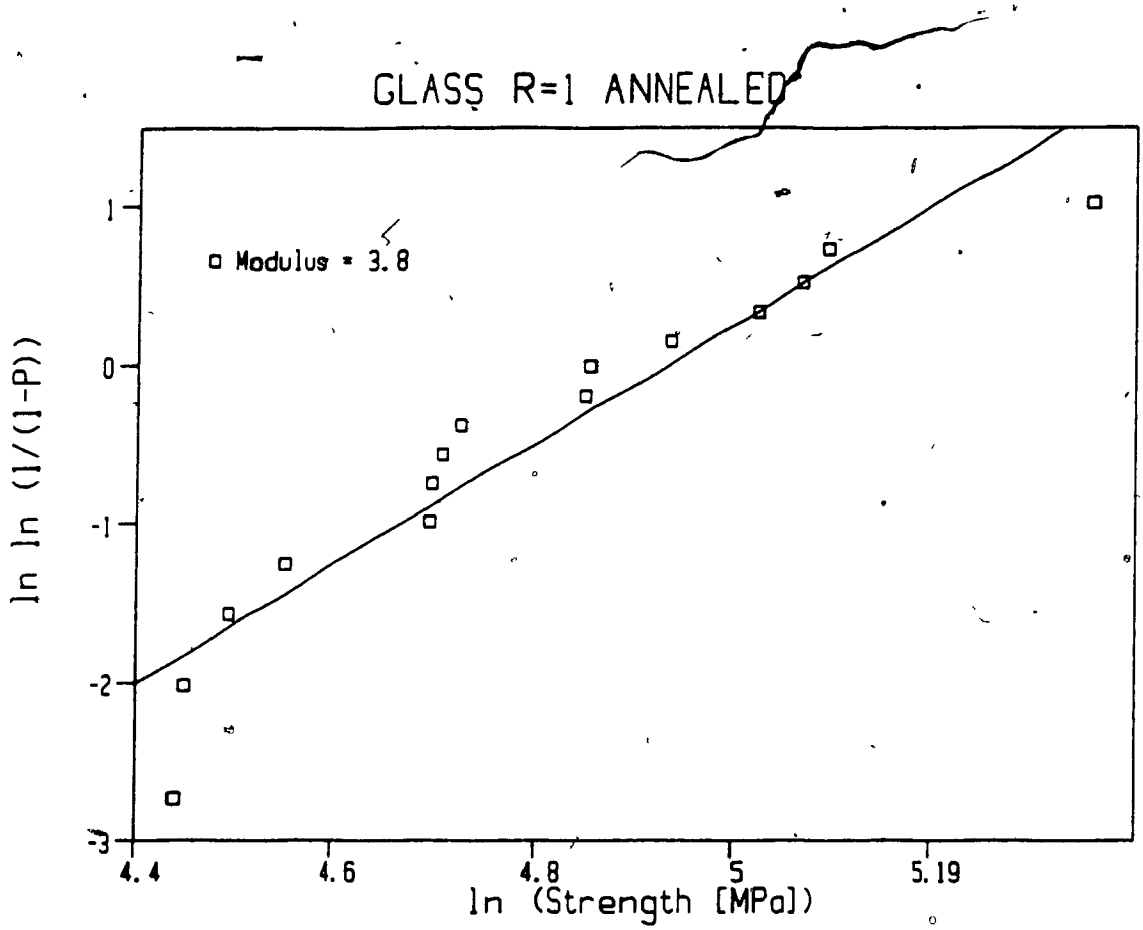

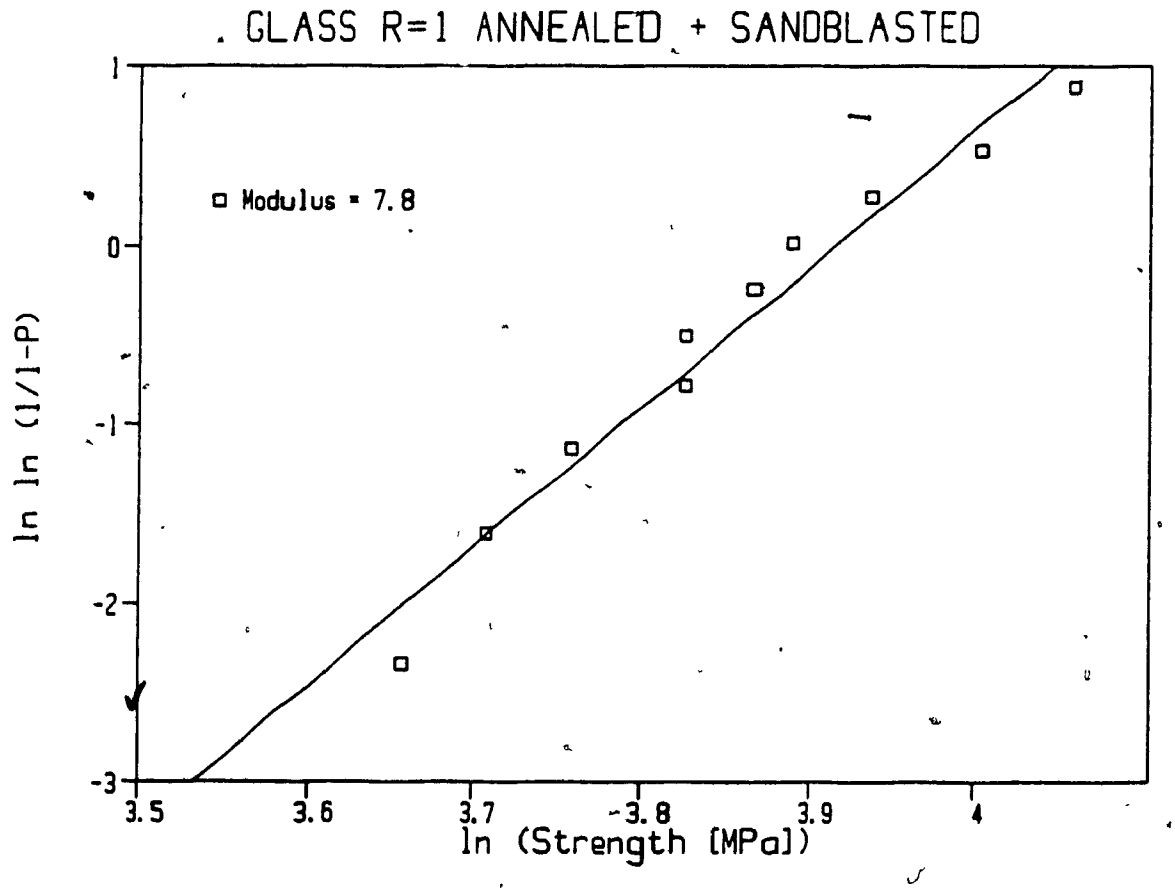

Figure 29: Weibull moduli determination for the a) annealed specimens and b) annealed + sandblasted specimens.

Table XIII: Flexural Strength and Weibull Modulus for Calcium Phosphate Glass Specimens.

Specimen	Number of Tests	MOR [MPa]	Weibull Modulus
Quenched	3	217 ± 46	-
Annealed	15	125 ± 35	3.8
Annealed + Sandblasted	10	47 ± 6	7.8

As can be seen from Table XIII, the results obtained for the MOR are strongly dependent on specimen preparation. The values can be decreased by a factor of 5 by generating flaws at the surface of the specimen.

The high flexural strength for the quenched specimens arises from the surface compression generated during the fast cooling. The first layer of glass coming into contact with the cold mold solidifies immediately, resulting in a low density glass layer. The centre of the specimen solidifies more slowly resulting in a higher density. Since the outer layer is already too viscous to deform, the shrinkage resulting from the higher density at the sample centre induces a high compressive stress at the surface. Therefore, during the bending of the specimens, this compressive stress has to be overcome before the material starts to undergo a tensile stress. The increase in flexural strength is, hence, proportional to the amount of compressive stress induced by

the fast cooling rate. However, the large scatter of the data should be noted, i.e. ± 21%. This arises from the large amount of energy stored in the sample and the uncontrolled flaw distribution. Therefore, once a crack begins to grow, it will lead to catastrophic failure since energy to grow the crack is readily available.

Casting the glass into a preheated mold and annealing allowed for stress relaxation to occur and eliminated the surface compression stresses. The specimen was, therefore, subjected to tensile stress from the start of the test, which explains the lower value for the flexural strength. The large scatter of the data, i.e. ± 28 %, as well as the low Weibull modulus of 3.8, indicates that the flaws are distributed over a wide range of sizes.

Sandblasting generates surface flaws of a specific size distribution. Ninety nine weight percent of the sand particles are smaller than 210 μm. Since ten percent of the particles are between 150 and 210 μm, it is reasonable to assume that on the surface under maximum tension during testing of each specimen there is at least one flaw with a size of the order of 200 μm. These large flaws are responsible for the drastic decrease in flexural strength. The small scatter of the data, i.e. ± 12 %, and the higher Weibull modulus of 7.8 are due to the homogeneity and reproducability of the flaw size distribution.

5.2.2 Glass-Ceramic Strength

Pure calcium phosphate glass specimens were crystallized at temperature just above T_g, i.e. 570 °C. Three samples were tested as-crystallized and six were sandblasted prior to testing. Ten supplementary samples were crystallized at 650 °C. The results are listed in Table XIV. At this temperature, both high nucleation and crystallization rates are expected.

Table XIV: Flexural Strength and Weibull Modulus for Calcium Phosphate Glass-Ceramic Specimens.

Specimen	Number of Tests	MOR [MPa]	Weibull Modulus
Crystallized at 650 °C	10	35 ± 3	11.2
Crystallized at 570 °C	3	70 ± 7	-
Sandblasted	6	38 ± 3	11.6

The low flexural strengths for the specimens crystallized at 570 °C are due to the mode of crystallization. Since only surface nucleation occurs, the crystal fibres grow perpendicular to the surface. Although the crystal fibres themselves are very strong along their length, the bonding between them is relatively weak. Therefore, where crystal fibres cross the complete cross-sectional area of the specimen, a plane of weakness is generated. Fracture usually

originates at a nucleation site and follows one of these planes of weakness; this is illustrated in Figure 30. The low scatter of the order of $\pm$ 9 % and the high Weibull modulus of 11.2 are due ot the consistent fracture initiation mechanism, i.e. failure is thought to originate at a surface defect which is a nucleation site.

Sandblasting has the same effect on the glass-ceramic as it does on the glass; large surface flaws are generated which decrease the flexural strength. However, the Weibull modulus is still relatively high (11.7), since the mode and the reproducibility of the failure origin are likely to be similar in both cases, i.e. whether they are due to a calibrated flaw size distribution or if they originate at a nucleation site.

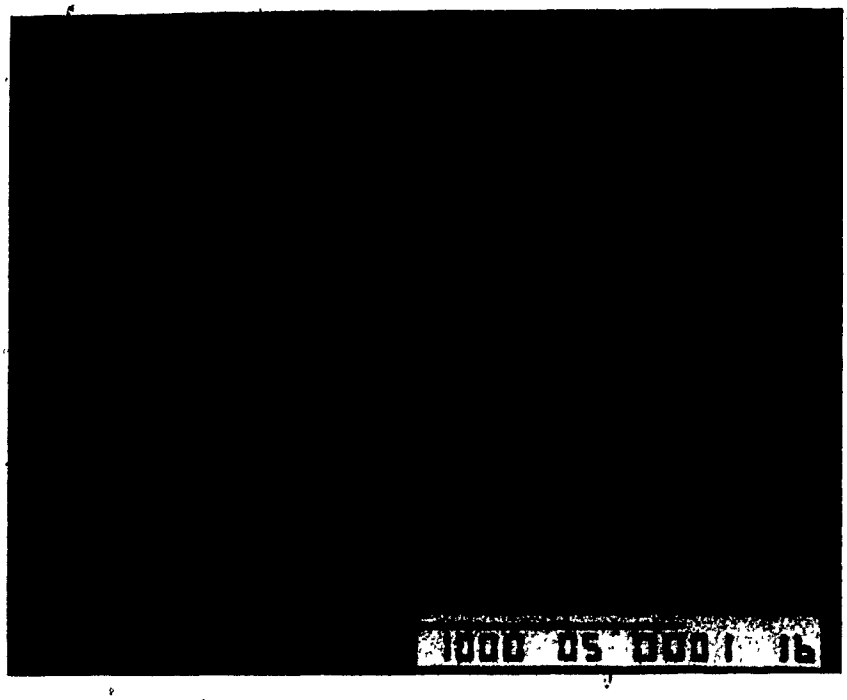

Figure 30: Fracture surface of a calcium phosphate glass-ceramic bending specimen showing the interfibre fracture behavior (T_c = 570 ^{o}C)

Glass-ceramics crystallized at 650 °C exhibit a much lower strength than those crystallized at 570 °C. This is due to the porosity induced during crystallization at this temperature. The bonding between the fibres is reduced, since the bonded surface area is decreased by the porosity. Furthermore, the strength of each fibre is drastically decreased, since pores act as stress-raisers and reduce the fibre cross-sectional surface area. Figure 31 shows that, instead of only following the crystal fibres, the cracks are capable of growing perpendicular to the fibre growth axis. The obtained Weibull modulus of 11.2 is satisfactory, since fracture originates at pores having approximately the same size range resulting in a low data scatter, i.e. ± 10 %.

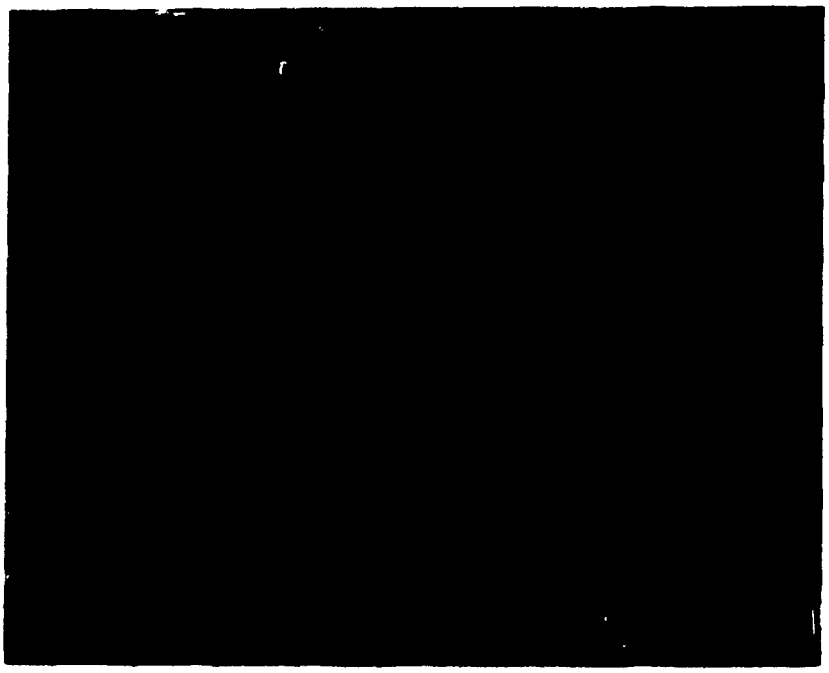

Figure 31: Crack progressing perpendicular to the fibre axis in a calcium phosphate glass-ceramic crystallized at 650 °C.

5.2.3 Bulk Nucleated Glass-Ceramics

Addition of 1% of zirconia (ZrO_2) affected the nucleation behavior of calcium phosphate glass. Instead of surface nucleation, ZrO_2 promotes bulk nucleation. The characteristic fibrous structure of surface nucleation is shown in Figure 32 and completely disappeared when a nucleating agent was used (see Figure 33). The fact that a glassy layer remained at the surface of the specimens and on the surface of the pores (Figure 34) seems to indicate that although bulk nucleation was achieved, the crystallization mechanism is the same as for pure calcium phosphate glasses, i.e. stress induced crystallization.

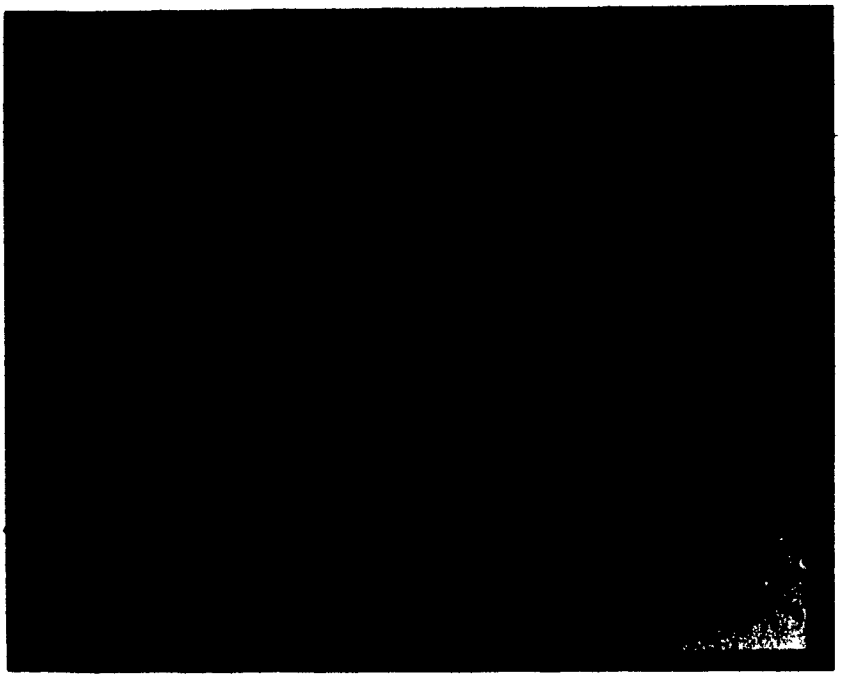

Figure 32: Characteristic fibrous structure of surface nucleation in pure calcium phosphate glass (fracture surface, T_c = 570 ^{o}C).

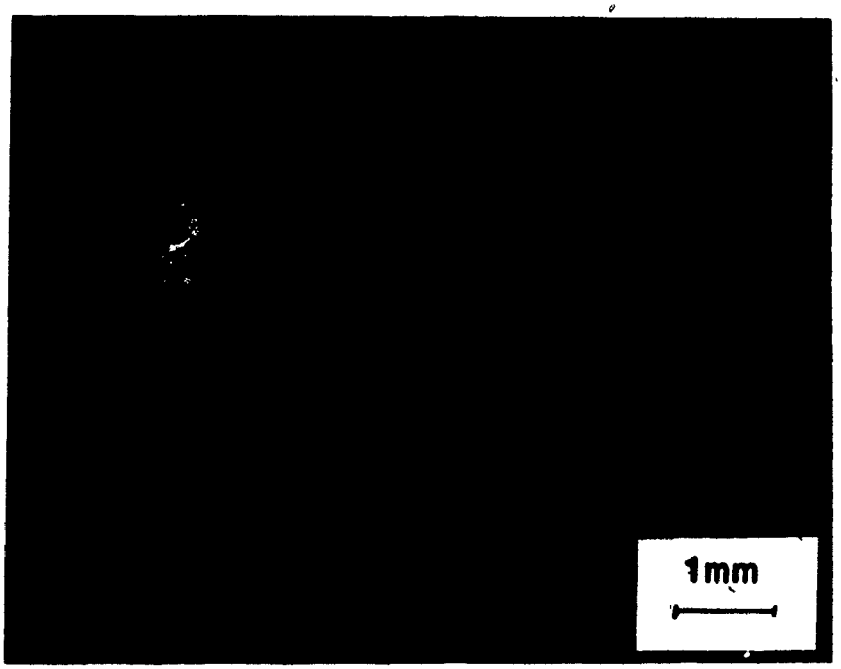

Figure 33: Addition of 1% zirconia enhanced bulk rather than surface nucleation (fracture surface, T_c = 570 °C).

Figure 34: 1% zirconia calcium phosphate glass showing a glassy layer on the crystallization defect surface (fracture surface, T_c = 570 °C).

A comparison of the strength data for both the glasses and glass-ceramics with 1% ZrO_2 addition are given in Table XV. The high strength for the quenched glass arises from the surface compression induced during the fast cooling of the specimens on casting. Annealing the sample results in relaxation of these surface stresses, thus decreasing, at the same time, the bend strength. Although additions of 1% ZrO_2 to calcium phosphate glass do not affect the mean MOR (see Table X), i.e. 125 MPa, there is a significant improvement in the Weibull modulus, i.e. from 3.8 to 7.2.

Table XV: Flexural Strength and Weibull Modulus for Calcium Phosphate Glass and Glass-Ceramic Samples with 1% ZrO_2 Addition.

Specimen	Number of Tests	MOR [MPa]	Weibull Modulus
Quenched glass	3	268 ± 44	-
Annealed glass	11	125 ± 17	7.2
Crystallized at 570 °C	3	73 ± 9	-
Crystallized at 650 °C	9	18 ± 13	1.4

Glass-ceramic samples crystallized close to T_g (570 °C) have a higher strength than those crystallized at 650 °C. Once again, the porosity is the determining factor: The former contains very little or no porosity (Figure 34), whereas the

latter has a very uneven microstructure (Figures 35 and 36). Some parts of the same specimen are densely crystallized (see Figure 35), while other areas exhibit substantial microporosity as illustrated in Figure 36. This inhomogeneity could be the result of a poor mixing of the zirconia powder. The existance of two different microstructural constituents in the specimens can explain the large scatter of data, i.e. $\pm$ 72 %.

Figure 35: 1% zirconia calcium phosphate glass-ceramic densely crystallized (fracture surface, T_c = 650°C).

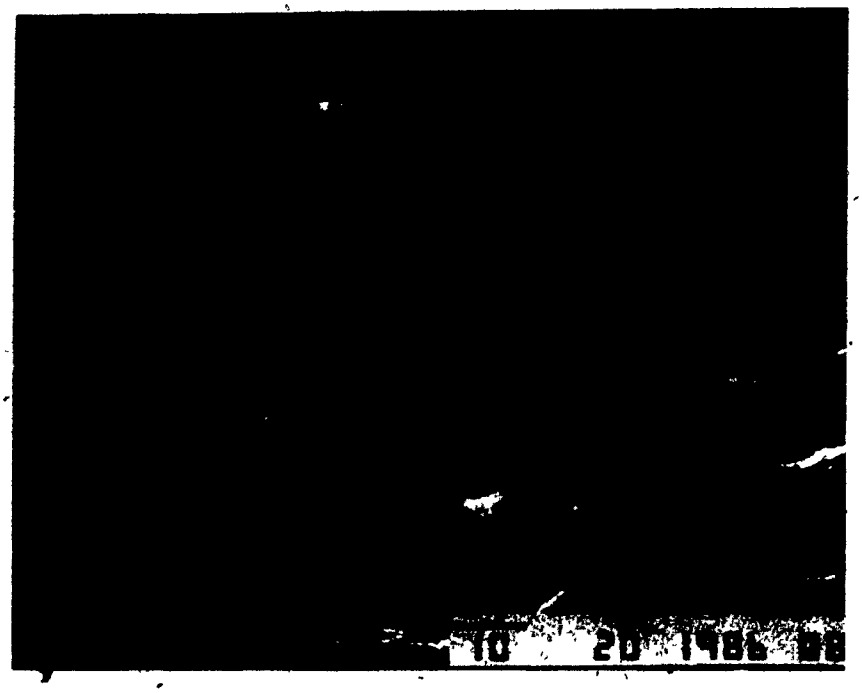

Figure 36: 1% zirconia calcium phosphate glass-ceramic showing micropores of approximatly 0.5 μm in size (fracture surface, T_c = 650 °C).

5.2.3 Strengthening Agent

The bend strength for both the glasses and the glass-ceramics with 2% Al_2O_3 addition are listed in Table XVI. Additions of alumina to calcium phosphate glass does not affect the bend strength in the expected way. Although the values of MOR are of the same order, considering the scatter of the measurements, calcium phosphate glasses with 2% alumina exhibit lower bend strengths, 94 MPa compared with 125 MPa for pure calcium phosphate glasses. However, the scatter of the data is decreased, i.e. ± 16 %.

Table XVI: Flexural Strength and Weibull Modulus for 2% Alumina Calcium Phosphate Glass and Glass-Ceramic Samples.

Specimen	Number of Tests	MOR [MPa]	Weibull Modulus
Annealed Glass	10	94 ± 15	5.8
Annealed Glass + Sandblasted	6	52 ± 22	2.2
Crystallized at 700 °C	5	43 ± 8	9

Alumina is a network former in silicate glasses and has the effect of increasing their strength. This may not be the case in calcium phosphate glasses. However, there is evidence of some structural modification in these glasses because there is an increase in (a) the crystallization peak temperature, i.e. from 665 °C for pure calcium phosphate glass to 712 °C for 2% alumina containing glass, and (b) the fracture toughness, i.e. from 4.56 to 5.35 MPa $m^{1/2}$ (see section 5.3.1). The hardness of the glass does not change significantly, i.e HV = 3.41 ± 0.06 GPa and HV = 3.33 ± 0.3 GPa, respectively. The decrease in MOR cannot be explained, since it seems to be inconsistent with the other observation. Further investigation in this area would be required, but this is beyond the scope of the present study.

The increase in data scatter for the sandblasted specimens, i.e. ± 42%, is also inconsistent with the results discussed earlier. Sandblasting samples prior to testing

should decrease the data scatter and, so increase the Weibull modulus, since it generates reproducible flaws at the surface of the specimens. The decrease in Weibull modulus, from 7.8 for the pure calcium phosphate glass to 2.2 for the alumina containing glass, could be explained by the inhomogeneity of the samples tested, i.e. since some of the samples might contain more network modifying ions than others, they would exhibit higher strength. However, this is unlikely since no difference in refractive index in the as-cast glass was observed; this being characteristic of heterogeneity in translucent glasses.

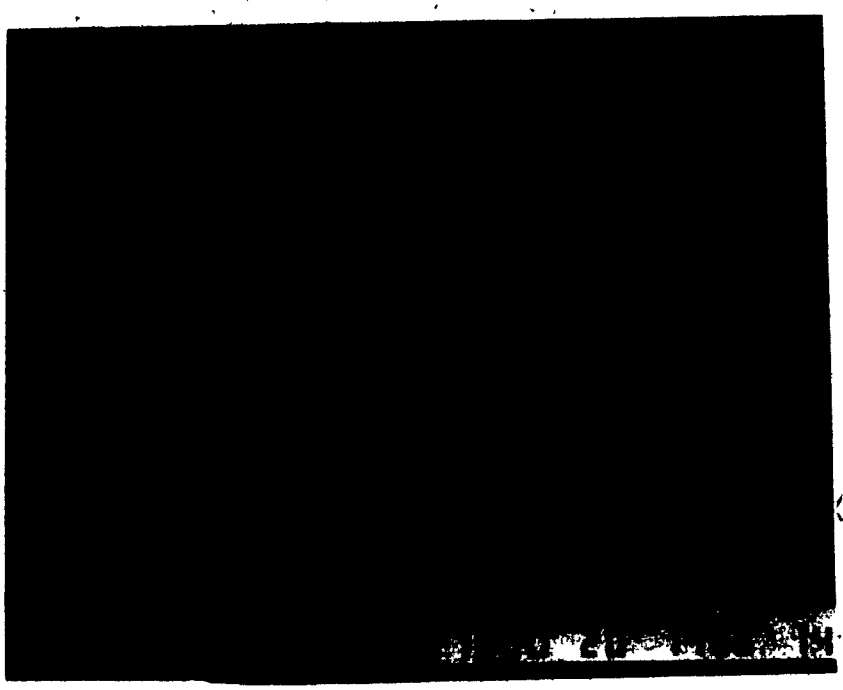

Figure 37: 2% alumina calcium phosphate glass-ceramic showing crystal fibres grown from the surface towards the centre of the specimen (fracture suface, T_c = 700 ^{o}C).

The low bend strength for the glass-ceramic is due to the fact that only surface nucleation occurs. In this case, however, the nuclei are numerous enough so that crystal fibres grow from every point of the surface towards the centre of the specimen, as shown in Figure 37. Although it is still a fibrous structure, the bonds between fibres appear to be more numerous and so, it is more difficult to resolve them (see Figure 38). As a result, there might be an increase in the strength of the glass-ceramic which is counteracted by the presence of microporosity, evident in Figure 39.

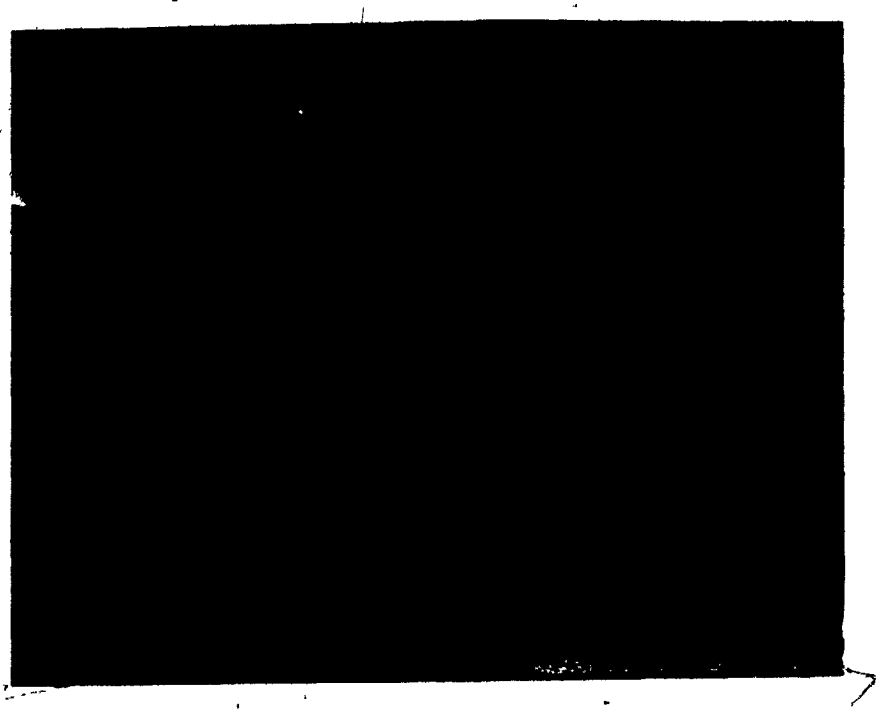

Figure 38: 2% alumina calcium phosphate glass-ceramic fibres (fracture surface, T_c = 700 ^{o}C).

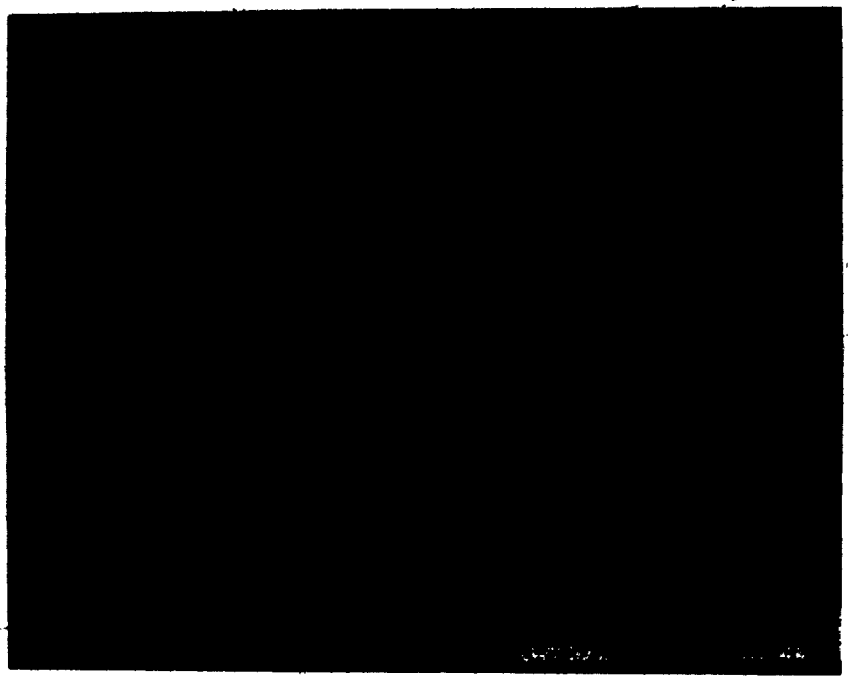

Figure 39: Microporosity in 2% alumina calcium phosphate glass-ceramic (fracture surface, T_c = 700 ^{o}C).

5.3 Fracture Toughness

5.3.1 Vickers Indention Technique

Fracture toughness determination using the Vickers indentation technique was only performed on the glass, since it was not suitable for the glass-ceramic. Instead of developing half-penny like cracks initiating at the indentation corners, the cracks in the glass-ceramics tended to propagate along the fibre bundles, perpendicular to the surface, as may be seen in Figure 40. Therefore, the crack geometry was fundamentally different from that used in the Vickers indentation theory.

Figure 40: Vickers indentation in a calcium phosphate glass-ceramic (load 20 kg).

On the other hand, the geometry of the cracks developed in each of the calcium phosphate glasses tested was similar to the crack geometry discussed in the theory (see Section 4.5.1). A crack was initiated at each corner of the indentation (see Figure 41) and usually grew to a greater length than the indentation diagonal. Figure 42 shows that a half-penny crack has developed beneath the indentation. However, it is obvious that the geometry of the crack is more complex than a simple half-penny since some radial cracks have also formed; one even extended 2.5 times beyond the half-penny radius. Since the energy to grow these radial cracks is not used to propagate the half-penny cracks (the measured cracks), it will lead to an overestimate of the fracture toughness, K_{1c}.

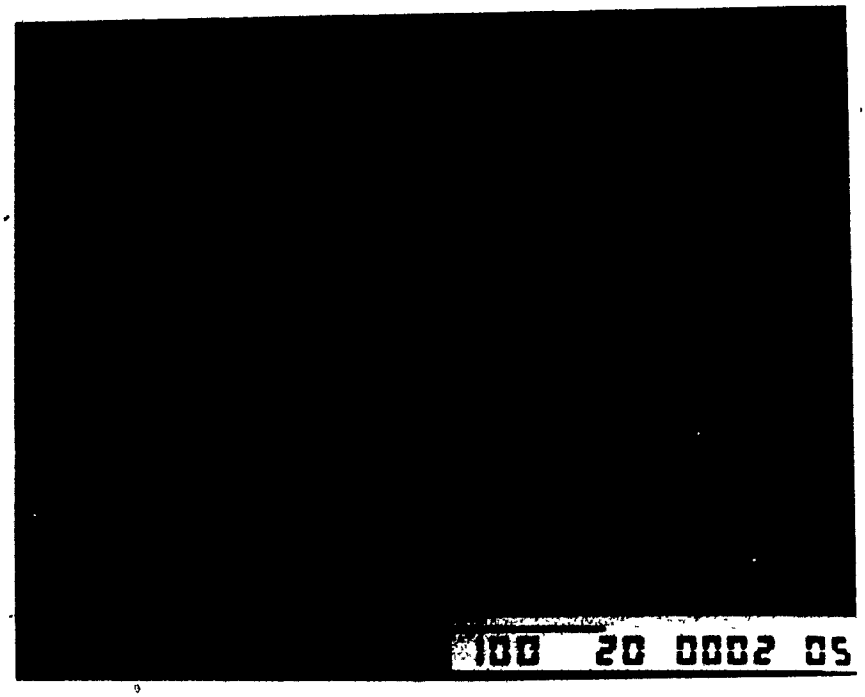

Figure 41: Vickers indentation in a calcium phophate glass showing a well-developed crack system (load 2 kg).

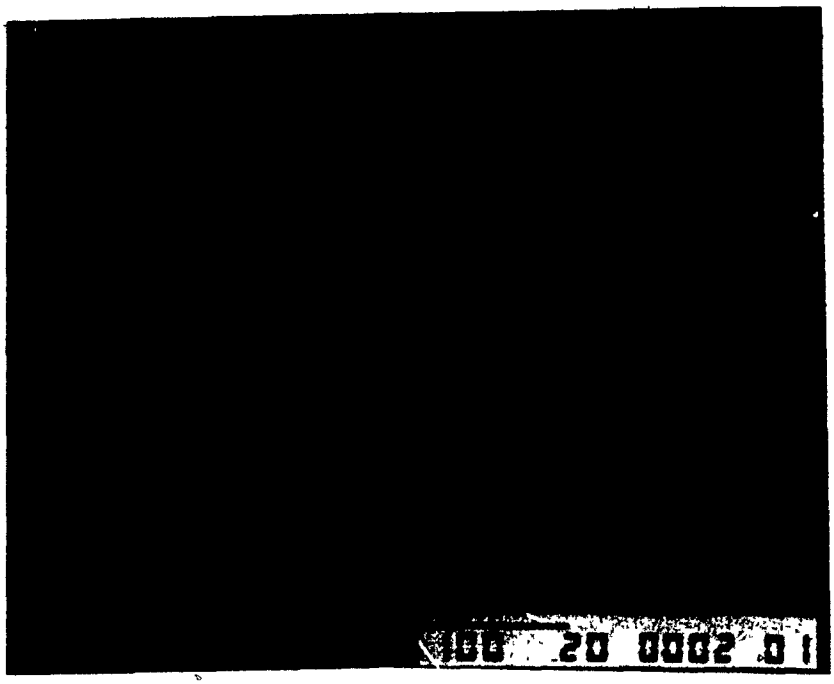

Figure 42: Fracture surface below a Vickers indentation illustrating the half-penny like crack (load 2 kg).

5.3.1.1 Effect of the Indenter Load

The influence of the indenter load on the fracture toughness was first investigated. A calcium phosphate glass with 1 % zirconia was tested with an applied load varying from 2 to 20 kg. The variation of the fracture toughness is shown in Figure 43.

The fracture toughness increases with an increasing indenter load; this is due to the crack geometry. When loads larger than 3 kg are used, multi-branched cracks are developed and, furthermore, lateral vents start to appear as shown in Figure 44. The energy used to create these extra cracks is not

taken into account during the measurement of the median crack lengths and so the values of fracture toughness are overestimated. The large data scatter is due to the difficulty in differentiating, in many cases, between the end of the median crack and the beginning of the lateral vent. Therefore, 2 kg was chosen as the optimium load for the measurements of K_{1c}.

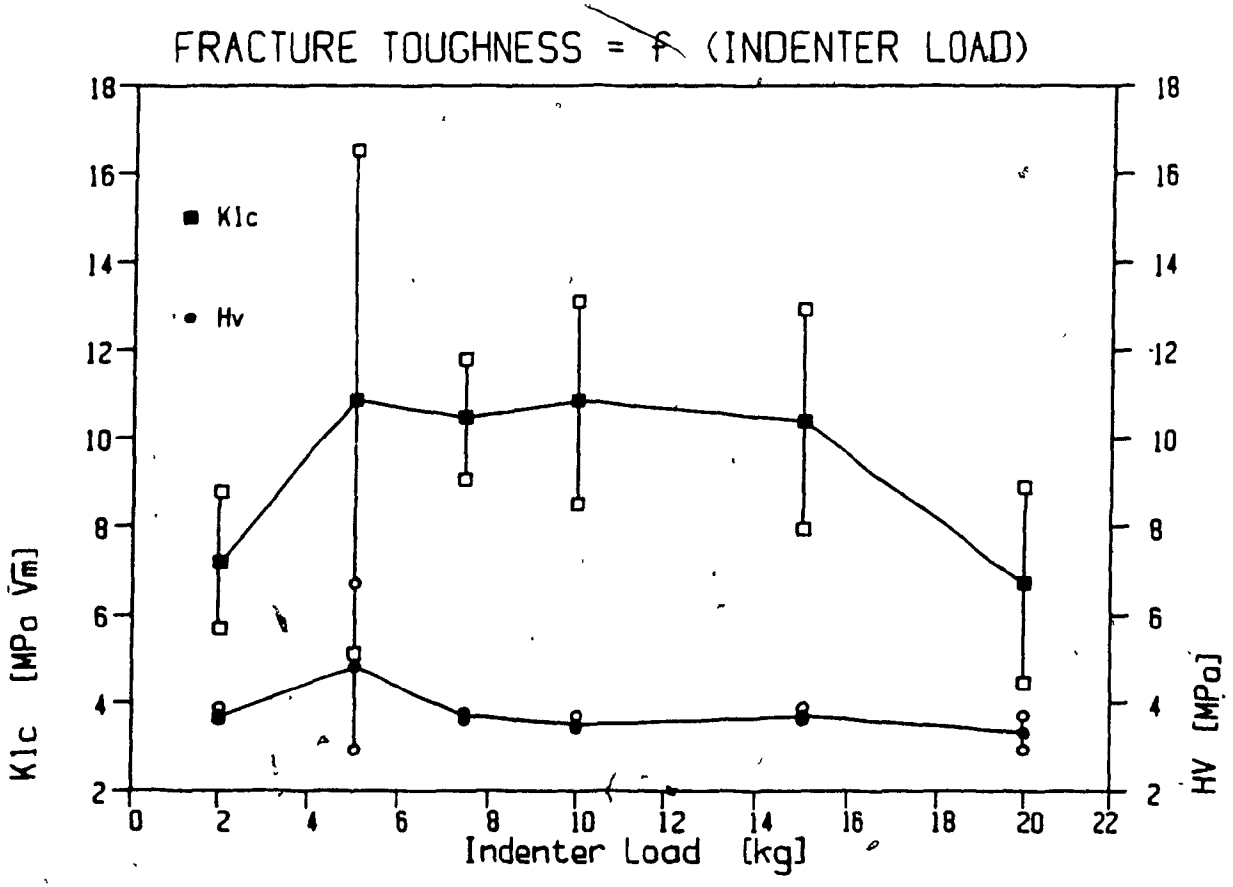

Figure 43: Variation of fracture toughness with indenter load for a 1% zirconia calcium phosphate glass.

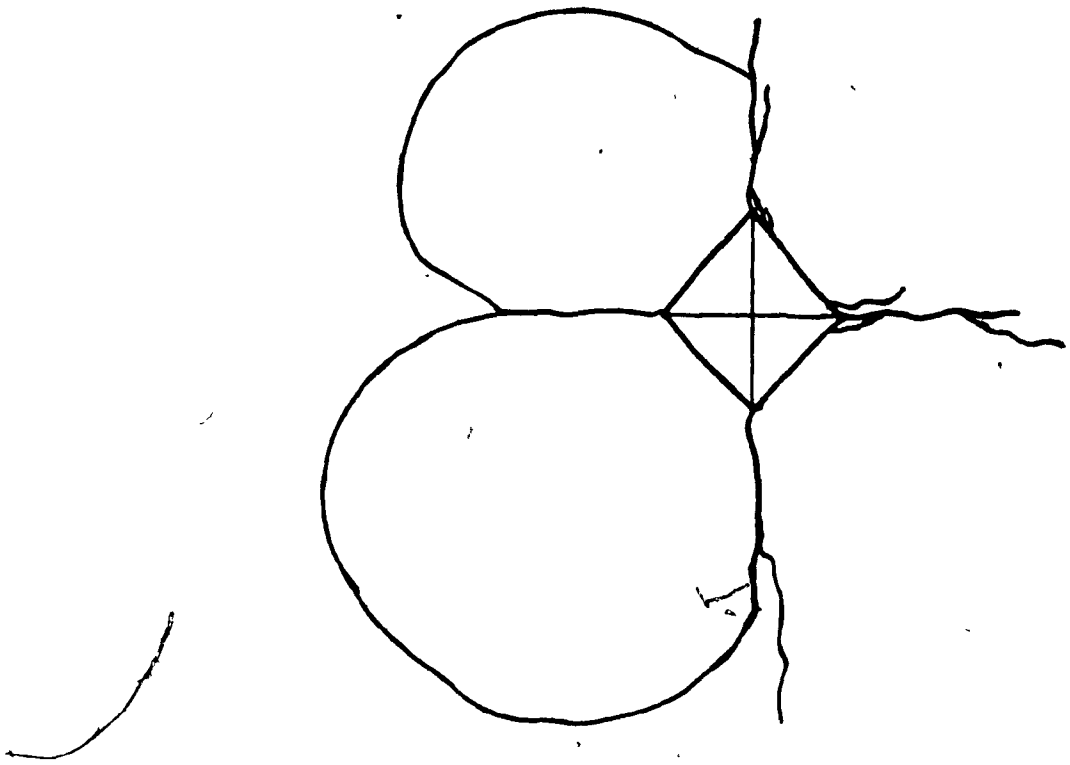

Figure 44: Typical crack geometry for indenter loads >= 3 kg.

5.3.1.2 Fracture Toughness Measurements

The fracture toughness (K_{1c}) was determined twice on the same set of samples: a) pure calcium phosphate glass (CaO / P_2O_5 = 1), b) glass with addition of 1% of zirconia and c) glass with addition of 2% of alumina. In Table XVII, the results measured on the as-polished samples are given and the measurements performed on the same samples after a subsequent annealing heat treatment are listed in Table XVIII. Each fracture toughness value is the average of the measurements from four indentations, i.e. 16 crack lengths.

Comparison between Table XVI and XVII indicates that the

surface stresses induced by the polishing have a significant effect on the fracture toughness values since, on annealing, they were reduced by 13%, 48% and 34% for the pure glass, the 1% ZrO_2 containing glass and the 2% Al_2O_3 containing glass samples respectively. The explanation for this is that polishing induces surface compression which tend to prevent crack propagation. Since the fracture toughness is inversely proportional to the crack length, surface compression leads to an overestimate of K_{1c}. The fracture toughness determined

Table XVII: Fracture Toughness Determined by Vickers Indentation Technique on As-Polished Glass Samples (load 2 kg).

Specimen	Fracture Toughness [MPa $m^{1/2}$]	Hardness [GPa]
Glass	4.56 ± 0.23	3.47 ± 0.07
1% ZrO_2	7.20 ± 1.54	3.71 ± 0.15
2% AL_2O_3	5.35 ± 0.65	3.33 ± 0.3

Table XVIII: Fracture Toughness Determined by Vickers Indentation Technique on Annealed Glass Samples (load 2 kg).

Specimen	Fracture Toughness [MPa $m^{1/2}$]	Hardness [GPa]
Glass	3.96 ± 0.23	3.41 ± 0.06
1% ZrO_2	3.69 ± 0.22	3.56 ± 0.09
2% Al_2O_3	3.54 ± 0.35	3.27 ± 0.49

by the Vickers indentation technique is a local fracture toughness, e.g. in this case, the typical half-penny radius varied from 0.1 to 0.2 mm. Therefore, the condition of the surface should be representative of the bulk material if the Vickers indentation technique is to be used with any degree of confidence. On the other hand, the hardness readings were not significantly affected by the surface compression.

The effect that the addition of alumina to calcium phosphate glass has on the fracture toughness was investigated. Samples with 1, 2, 3, 4, and 5 % alumina were tested. Results for the as polished samples are given in Figure 45.

Additions of alumina increases the fracture toughness and the hardness of calcium phosphate glass, i.e. from 4.56 to 7.75 MPA $m^{1/2}$ and from 3.41 to 4.07 GPa respectively, for an addition of 5 wt % Al_2O_3. Although these values were measured on as-polished samples, and thus not absolute values, they are still representative of the trend. It is very unlikely that this fracture toughness increase is due only to increasing surface compression since this increase would not be so constant. An illustration of the effect of poor polishing on the fracture toughness is the value obtained for 1% alumina (see Figure 45). Here, the high value measured, i.e. K_{1c} = 8.01 MPa $m^{1/2}$, is certainly only due to the surface compression induced by poor polishing.

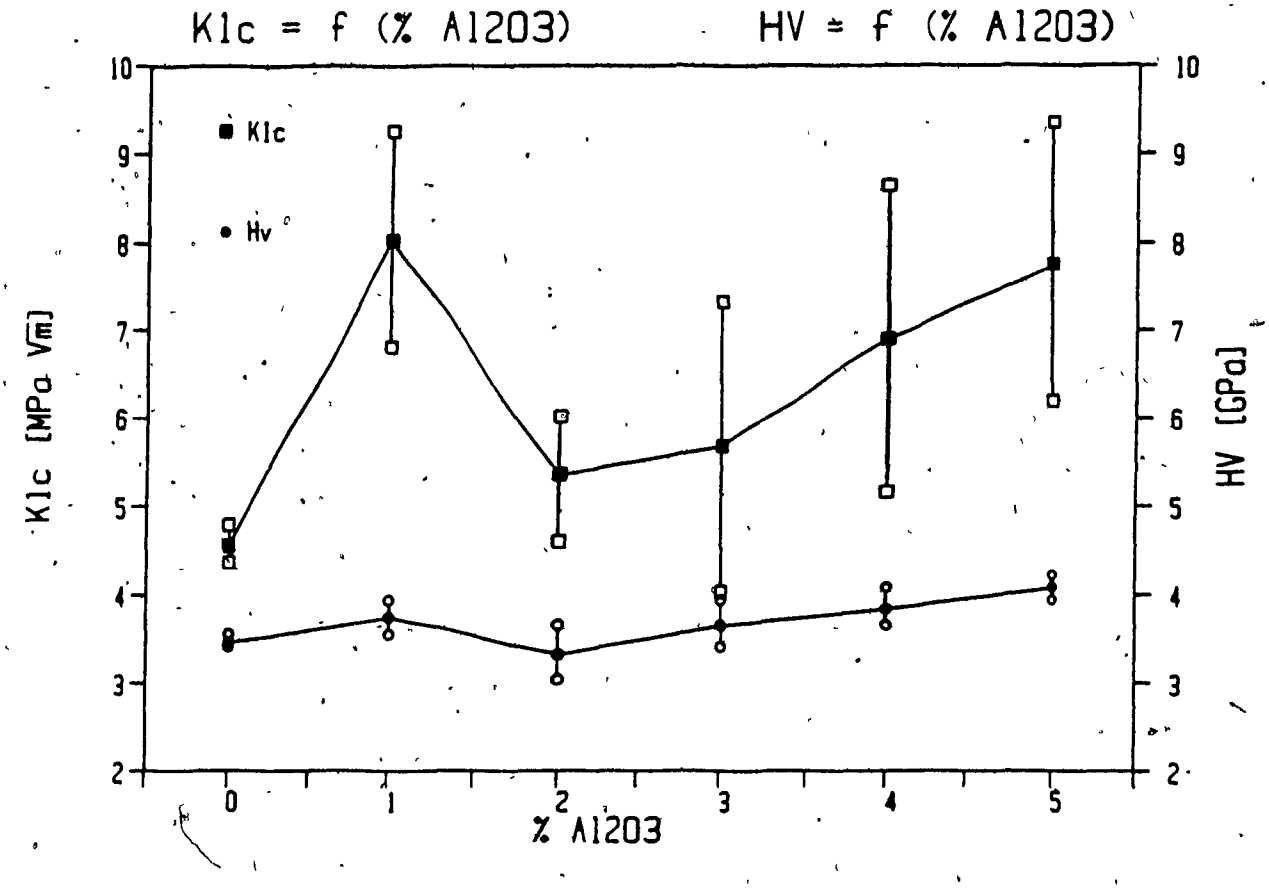

Figure 45: Effect of additions of alumina to calcium phosphate glass on the fracture toughness and the hardness.

The fracture toughness measured for the different calcium phosphate glasses are relatively high, e.g. K_{1c} = 3.96 MPa $m^{1/2}$ for glass having a ratio CaO / P_2O_5 = 1, since normal K_{1c} values for silicate glasses lie between 0.6 and 1 MPa $m^{1/2}$. However, since there are some uncertainties as to the validity of the fracture toughness determination by the Vickers indentation technique because of crack geometry and surface compression, the values obtained were double-checked by a more conventional method as discussed below.

5.3.2 Single Edge Notched Beam Technique

Fracture toughness determinations using the single edge notched beam technique were carried out on pure calcium phosphate specimens. Since it was not possible to precrack the specimens, the notch was made as sharp as possible using a razor blade. However, this generated small cracks in the glass samples which, eventually, grew through the complete section by slow, subcritical crack growth. Only one glass sample and three glass-ceramic samples were tested (Table XIX).

Table XIX: Single Edge Notched Beam Fracture Toughness for Pure Calcium Phosphate Materials.

Material	K_{1c} [MPa $m^{1/2}$]
Glass	4.3
Glass-Ceramic	16.7 $\pm$ 7.8

Although a fracture toughness value determined from only one sample does not allow for any statistical variation, the value for the glass given in Table XIX is considered reliable. However, the use of a sharp razor blade did not generate a uniform crack along the complete width of the specimen. Therefore, the fracture toughness is overestimated since the energy, and hence the load, used to initiate a crack is higher than that used to propagate the crack. However, both the notched beam and the Vickers indentation techniques lead to

similar values for the glass, i.e. 4.3 MPa $m^{1/2}$ and 4 MPa $m^{1/2}$ respectively. Therefore, it is possible to conclude that the Vickers indentation technique for the glass specimens is a satisfactory technique since it is very easy to perform and gives reasonably accurate results.

Figure 46: Fracture surface of a calcium phosphate glass-ceramic notched beam.

For the glass-ceramic specimens, the use of a sharp razor blade led to other problems. The crack did not always initiate only at the bottom of the groove, but also at the side of the notch. This is due to the fibrous structure of the crystals, shown in Figure 46, since it is easier for a crack to initiate at a fibre joint than in the middle of a fibre.

Therefore, if the bottom of the notch is in a fibre, the crack will initiate on the side of the notch at the closest fibre joint. The very large data scatter, i.e. $\pm$ 47 %, is also due to this crack initiation problem. However, the high fracture toughness measured seems to be promising although it has to be viewed with caution, since precracking was not successful and only three specimens were tested.

5.4 Tribological Study

The wear behavior of three material combinations was assessed: UHMWPE-Vitallium, UHMWPE-Alumina and UHMWPE-calcium phosphate glass. Every combination was tested once for up to 7×10^5 cycles with the stress on the UHMWPE pin being 9 MPa; results are ploted in Figure 47.

This preliminary wear behavior study indicated that the Vitallium combination exhibits a steady increase in wear debris. This is consistent with clinical experience where it was noted that the wear rate keps increasing after only a few months in service [3]. This characteristic is obviously not favorable because of a) the possible adverse biological response and b) the early "wearing out" of the polyethylene part.

Both the alumina and the calcium phosphate glass combinations exhibit similar wear behaviors. After a very short "run-in" period, the wear rate becomes negligible and

remains so for the duration of the test. The UHMWPE-calcium phosphate test was stopped earlier than that involving Vitallium because the fluid level dropped below the conterface level. However, it was still concluded that the wear rate of the UHMWPE-calcium phosphate combination was much more satisfactory than that of the conventional UHMWPE-Vitallium combination.

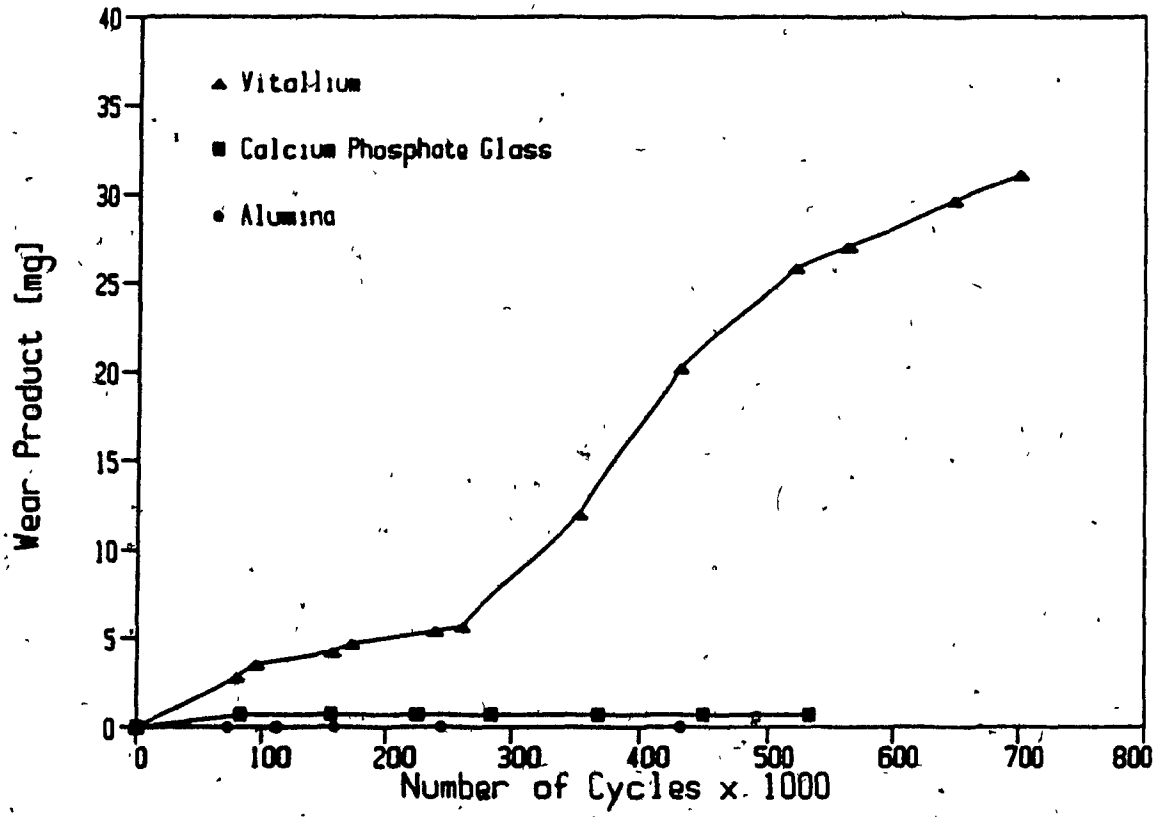

Figure 47: Wear behavior of UHMWPE pins tested on Vitallium, alumina and calcium phosphate glass under a 9 MPa stress and in saline solution.

The wear behavior of calcium phosphate glass - polyethylene combination is considered to be excellent since the wear of the polyethylene pin (the softer material) was very small. However, this result has to be considered with caution for two reasons: a) only one sample was tested and b) the experiment was not carried out in biologicaly active solution. Since calcium phosphate glass is a bioactive material, the natural lubricating fluid in joints (the synovial fluid) may affect the glass by physio-chemical reaction with the surface. This may lead to the degradation of the highly polished surface and hence, drasticaly increase the wear rate.

Chapter 6

CONCLUSION

6.1 Calcium Phosphate Glass-Ceramics

1. The poor strength of calcium phosphate glass-ceramic samples, i.e. MOR = 70 MPa, crystallized at temperatures close to T_g (570 ^{o}C) arises from the crystallization mode. Since nucleation takes place only at the surface of the material, the crystals grow in a fibrous form perpendicular to the surface. The bonds between the fibers are weak and planes of weakness where cracks can easily propagate are generated. At higher crystallization temperatures (650 ^{o}C), the large difference in density between the glass and the crystal, as well as the low glass viscosity, promotes pore formation, further decreasing the strength of the glass-ceramic, i.e. MOR = 35 MPa. However, with a value of 16 MPa $m^{1/2}$, the fracture toughness is satisfactory.

2. According to the literature, unidirectional crystallization substantially increases the glass-ceramic strength, i.e. MOR = 640 MPa. However, the sensitivity of this process to experimental conditions made it impossible to grow crystals longer than 40 mm, i.e. suitable for strength measurements.

3. The addition of zirconium oxide to calcium phosphate glass promotes bulk nucleation. However, the strength of the glass-ceramic crystallized at temperatures close to T_g (570 ^{o}C) is not improved significantly, i.e. MOR = 73 MPa. Furthermore, higher crystallization temperatures (650 ^{o}C) result in very uneven structures further lowering the

glass-ceramic strength, i.e. MOR = 18 MPa.

4. Alumina modifies the structure of calcium phosphate glass-ceramics by promoting the formation of strong Al_2O_3-P_2O_5 bonds. This tends to decrease the fibrous nature of the crystals. However, the expected increase in strength is counteracted once more by the porosity, thus leading to low bulk strength values, i.e. MOR = 43 MPa.

5. Therefore, calcium phosphate glass-ceramics, in the form presented in this study, do not appear to be particularly promising candidates as biomaterials for applications in the highly stressed environment of the locomotor system of the human body.

6.2 Calcium Phosphate Glasses

1. The strength of calcium phosphate glass (CaO / P_2O_5 = 1) is affected by the cooling rate after casting. Annealed calcium phosphate glass has a flexural strength of 125 MPa. However, increasing the cooling rate generates surface compression, and significantly improves the flexural strength, i.e. MOR = 213 MPa.

2. The strength of the glass is not changed by the addition of zirconium oxide, but the scatter of the data is decreased significantly, i.e. the Weibull modulus is increased from 3.8, for calcium phosphate glass, to 7.2 for the 1% zirconia containing glass.

3. Despite the fact that alumina additions do not have a pronounced effect on the glass strength, they do modify its fracture behavior, i.e. additions of 5 wt % of Al_2O_3 increase the fracture toughness of the glass by 70%.

4. The preliminary study of wear behavior indicates that ultra high molecular weight polyethylene used in conjunction with calcium phosphate glass results in a) much lower wear rates than that of the conventional biomaterial combination, UHMWPE-Vitallium and b) similar wear rates to that quoted for the UHMWPE-alumina combination.

5. Since calcium phosphate glasses have satisfactory bend strength, good fracture toughness, good tribological properties and excellent biocompatibility, it is concluded that they are very promising biomaterials. However, before they could be used in a clinical environment, their long term in vitro and in vivo behavior should be assessed (see Chapter 7).

Chapter 7

SUGGESTIONS FOR FURTHER STUDY

1. The fracture toughness values reported in this thesis were measured using the Vickers indentation and the single edge notched beam techniques. There are still a number of uncertainties related to the indentation technique and it was not possible to precrack the SENB samples. Therefore, a more rigorous fracture toughness determination should be carried out with samples that are easier to precrack, e.g. by double torsion or compact specimen testing.

2. Dramatic slow subcritical crack growth was noticed in one of the glass SENB specimens. A scientific evaluation of this problem is paramount for the determination of the suitability of these materials for highly stressed medical applications. Subcritical crack growth is related to the static fatigue behavior of the material.

3. The effects of the addition of higher percentages of zirconia to calcium phosphate glasses and glass-ceramics could be promising. This would involve the use of a zirconium based powder that can be dissolved in larger quantities and at lower temperatures than zirconia.

4. A technique that would allow for very fast cooling rates after the casting of the glas,s but maintain smooth surfaces, should be developed. This would toughen the glass and might limit the slow crack growth problem.

5. The characterisation of the mechanical properties, i.e. strength, fracture toughness, slow subcritical crack growth and fatigue, of the glass under in vitro conditions would

be essential to determine its suitability for long term use in vivo applications.

6. Although the glass has satisfactory mechanical properties, it is doubtful whether it could be used as a prosthesis material on its own. The study of its joining to metallic alloys and to other ceramics would be a first step towards developing a composite prosthesis.

REFERENCES

1. H. Zitter, "The Suitability of Metals for Surgical Implants", Advances in Artificial Hip and Knee Joint Technology, M. Schaldach ed., 1976, 227-241.

2. J. Charnley, "Total Hip Replacement by Low-Friction Arthroplasty", Clinical Orthopaedics, 2, 1970,72.

3. B.W. Sauer, J. Klawitter, A. Weinstein and M. Spector, "The Use of Polymers in High Load Bearing Joints in the Locomotor System", Advances in Artificial Hip and Knee Joint Technology, M. Schaldach ed., 1976, 273-286

4. D. Geduldig, R. Lade, P. Prussner, H. Willert, L. Zichner and E. Doerre, "Experimental Investigations of Dense Alumina Ceramic for Hip and Knee Joint Replacements", Advances in Artificial Hip and Knee Joint Technology, M. Schaldach ed., 1976, 435-445.

5. P. Griss, G. Heimke, B. Krempien and G. Jentschura, "Ceramic Hip Joint Replacement - Experimental Results and Early Clinical Experience", Advances in Artificial Hip and Knee Joint Technology, M. Schaldach ed., 1976, 446-455.

6. K. deGroot, "Ceramics Based on Calciumphosphates", Ceramics in Surgery, P. Vincenzini ed., Elsevier Scientific Publishing Company, 1983, 79-90.

7. C. Klein, K. de Groot and A. Driessen, "Biodegradation of Calciumphosphate Ceramics", Lignano-Sabbiadoro, Italy, 1982.

8. S. Kihara, A. Watanabe and Y. Abe, "Calcium Phosphate Glass-Ceramic Crown Prepared by Lost-Wax Technique", J. Am. Ceram. Soc. , 1984, C-100 - C-101

9. D. Hohmann, "Clinical Requirements of Artificial Joints" Advances in Artificial Hip and Knee Joint Technology, M. Schaldach ed., 1976, 211-217.

10. A.H. Huggler and E. Weidmann, "Design Criteria of Total Hip Replacements Fixed with Bone Cement", Advances in Artificial Hip and Knee Joint Technology, M. Schaldach ed., 1976, 361-373.

11. E.M. Evans, M. Freeman, A. Miller and A. Vernon-Roberts, "Metal Sensivity as a Cause of Bone Necrosis and Loosening of the Prosthesis in Total Joint Replacement", J. of Bone and Joint Surgery, 56-B, 1974, 626.

12. E. Morscher, R. Mathys and H. Henche, "Iso-Elastic Endoprostheses - A New Concept in Artificial Joint Replacement", Advances in Artificial Hip and Knee Joint Technology, M. Schaldach ed., 1976, 403-421.

13. B.G. Weber and G. Stuhmer, "The Trunnion Bearing Total Hip Prosthesis", Advances in Artificial Hip and Knee Joint Technology, M. Schaldach ed., 1976, 203-210.

14. H.U. Zwicker and H.J. Schmid, "Mechanical Properties of Metallic Materials for Long Term Use in Highly Stressed Locomotor System", Advances in Artificial Hip and Knee Joint Technology, M. Schaldach ed., 1976, 257-272.

15. M. Salzer, H. Locke, H. Plenk, G. Punzet, N. Stark and K. Zweymuller, "Experience with Bioceramic Endoprostheses of the Hip Joint", Advances in Artificial Hip and Knee Joint Technology, M. Schaldach ed., 1976, 459-474.

16. V.A. Memoly, J. Woodman, R. Urban and J. Galante, "Long Term Biocompatibility of Porous Titanium Fiber Metal Composites", Trans. ORS, 8, 1983, 237.

17. H.U. Debrunner, A. Wettstein and P. Hofer, "The Polymerisation of Self-Curing Acrylic Cements and Problems Due to the Cement Anchorage of Joint Prostheses", Advances in Artificial Hip and Knee Joint Technology, M. Schaldach ed., 1976, 294-324.

18. G. Friedelbald and R. Kolbel, "State of the Art of Hip and Knee Joint Replacement", Advances in Artificial Hip and Knee Joint Technology, M. Schaldach ed., 1976, 3-23.

19. J.J. Klawitter, A. Weinstein, S. Hulbert and B. Sauer, "Tissue Ingrowth and Mechanical Locking for Anchorage of Prostheses in Locomotor System", Advances in Artificial Hip and Knee Joint Technology, M. Schaldach ed., 1976, 422-433.

20. L.L. Hench and H.A Paschall, "Direct Chemical Bond of Bioactive Glass-Ceramic Materials to Bone and Muscle", J. Biomed. Mater. Res. Symposium, 2 - part 1, 1973, 25-42.

21. F. Pernot, J. Zarzycki, F. Bonnel, P. Rabischong and P. Baldet, "New Glass-ceramic Materials for Prosthetic Applications", J. Mater. Sci., 14, 1979, 1694-1706.

22. H. Dreesman, "Ueber Knochenplombierung", Beitr. Klin. Chir., 9, 1894, 200.

23. K. deGroot, "Degradable Ceramics", Biocompatibility of Clinical Implant Materials, 1, D.F. Williams ed., CRC press, 1981, 199-224.

24. G. deWith, H. van Dijk and N. Hattu, "Mechanical Behaviour of Biocompatible Hydroxyapatite Ceramics", Proc. of the British Ceram. Soc., Special Ceramic 7, D. Taylor ed., 31, 1981, 181-189.

25. J.M. van der Zel and K. deGroot, Dutch patent, Prestressed Ceramic Implants.

26. F. Pernot, P. Baldet, F. Bonnel, J. Zarzycki and P. Rabischong, "Phosphate Glass-Ceramics for Bone Implants", Ceramics in Surgery, P. Vincenzini ed., 1983, 177-186.

27. H. Fukui, Y. Taki and Y. Abe, "Implantation of New Calcium Phosphate Glass-Ceramics", J. Dent. Res., 56, 1977, 1260.

28. Y. Abe, "Kinetic Studies on Crystallization of Calcium Metaphosphate Glass", J. Ceram. Soc. of Japan, 81, 1973, 471-475.

29. Y. Abe, T. Arahori and A. Naruse, "Crystallization of $Ca(PO_3)_2$ Glass Below the Glass Transition Temperature", J. Am. Ceram. Soc., 39, [11], 1976, 487-490.

30. Y. Abe, "Abnormal Characteristics in Crystallization of $Ca(PO_3)_2$ Glass", Nature (London), 282, 1979, 55-56.

31. Y. Abe, M. Hosoe, T. Kasuga, H. Ishikawa, N. Shinkai, Y. Suzuki and J. Nakayama, "High-Strength $Ca(PO_3)_2$ Glass-Ceramics Prepared by Unidirectional Crystallization", J. Am. Ceram. Soc., 65 [11], 1982, C189-C190.

32. Y. Abe, T. Kasuga, H. Hosono and K. de Groot, "Preparation of High-Strength Calcium Phosphate Glass-Ceramics by Unidirectional Crystallization", J. Am. Ceram. Soc., 67 [7], 1984, C142-C144.

33. D.W. Richerson, Modern Ceramic Engineering Properties, Processing, and Use in Design, Chap. 3, Dekker ed., N.Y., 1982, 76-100.

34. W. Weibull, "A Statistical Distribution Function of Wide Applicability", J. Appl. Mech., 1951, 293-297.

35. D.W. Richerson, Modern Ceramic Engineering Properties, Processing, and Use in Design, Chap. 11, Dekker ed., N.Y., 1982, 317-324.

36. S. Palmqvist, "Occurence of Crack Formation During Vickers Indentation as a Measure of the Toughness of Hard Metals", Arch. Eisenhuettenwes., 33 [9], 1962, 629-633.

37. A.G. Evans, "Fracture Toughness: The Role of Indentation Techniques", Fracture Mechanics Applied to Brittle Materials, ASTM STP 678, S.W. Freiman ed., 1979, 112-135.

38. B.R. Lawn, A.G. Evans and D.B. Marshall, "Elastic/Plastic Indentation in Ceramics: The Median/Radial Crack System", J. Amer. Ceram. Soc., 63 [9-10], 1980, 574-581.

39. A.G. Evans and E.A. Charles, "Fracture Toughness Determination by Indentation", J. Amer. Ceram. Soc., Disc. and Notes, 59 [7-8], 1976, 371-372.

40. M. Srinivasan and S.G. Seshadri, "The Application of Single Edge Notched Beam and Indentation Techniques to Determine Fracture Toughness of Alpha Silicon Carbide", The Carborundum Compagny, Niagara Falls, N.Y., 1980.

41. A. Yamamoto, "Determination of Characteristic Points on Commercial Glasses by Differential Thermal Analysis", Analyst (Japan), 14, 1965, 692-697.

42. N.H. Ray, "The Transformation Temperature of Inorganic Oxide Glasses", Scientific and Technical Communications, 9th Int. Congress on Glass, Versailles, 1971, 633-653.

43. A. Marotta, A. Buri, F. Branda and S. Saiello, "Nucleation and Crystallization of $Li_2O.2SiO_2$ Glass - a DTA Study", Advances in Ceramics, 4, "Nucleation and Crystallization in Glasses", J.H. Simmons ed., 1981, 146-153.

44. J.E. Ritter, Fracture Mechanics of Ceramics IV, R.C. Bradt, D. Hasselman, F. Lange eds., N.Y., Plenum Press, 1978.

45. K. Wright and J. Scales, " The Use of Hip Joint Simulators for the Evaluation of Wear of Total Hip Prostheses", Evaluation of Biomaterials, G. Winter, J. Leray and K. de Groot eds., Wiley, 1980, 135-146.

46. K. Wright, "Friction and Wear of Materials and Joint Replacement Prostheses", Biocompatibility of Orthopedic Implants, 1, D.F. Williams ed., 1982, 141-195.

47. K. Wright, H. Dobbs and J. Scales, "Wear Studies on Prosthetic Materials Using the Pin-on-Disc Machine", Biomaterials, 3, 1982, 41-48.

48. W.A. Johnson and R.H. Mehl, " Reaction Kineticsin Process of Nucleation and Growth", Trans. AIME, 135, 1939, 416-442.

49. M. Avrami, " Kinetics of Phase Change", J. Chem. Phys., 7, 1939, 1103-1112.

APPENDIX 1

Slow Crack Growth Coefficient

Assuming that the crack velocity, v, is related to the stress intensity factor, K, by the relation (A1):

$$v = A\ K^n \qquad (A1)$$

where A is a constant depending on the crack geometry and on the material tested, it is possible to estimate the slow crack growth exponent, n, from the strain rate dependence of the strength [44], using equation (A2):

$$\ln MOR = (1/(n+1))\ \ln V + const. \qquad (A2)$$

with: MOR, the modulus of rupture at a certain cross head speed, V, of the testing machine.

By measuring the modulus of rupture at different cross head speeds, the value of n may be calculated. Low values of n correspond to high subcritical crack growth.